Importance of S. Cerevisiae Rcf1 and Rcf2 Proteins for the Mitochondrial Protonmotive Force Generation

Vera Strogolova
Marquette University

IMPORTANCE OF *S. CEREVISIAE* RCF1 AND RCF2 PROTEINS FOR THE MITOCHONDRIAL PROTONMOTIVE FORCE GENERATION

by

Vera Strogolova, B.S., M.S.

A dissertation submitted to the Faculty of the Graduate School,
Marquette University,
in Partial Fulfillment of the Requirements for
the Degree of Doctor of Philosophy

Milwaukee, Wisconsin

December 2018

ABSTRACT
IMPORTANCE OF *S. CEREVISIAE* RCF1 AND RCF2 PROTEINS FOR THE MITOCHONDRIAL PROTONMOTIVE FORCE GENERATION

Vera Strogolova, B.S., M.S.

Marquette University, 2018

Mitochondria are the site of oxidative phosphorylation (OXPHOS) pathway, which can supply majority of energy in a eukaryotic cell. OXPHOS enzyme activities generate electrochemical gradient known as mitochondrial protonmotive force (PMF). PMF coordinates OXPHOS enzyme activities and supports essential cell survival functions such as transport of proteins and metabolites in and out of mitochondria. PMF is maintained despite variations in cellular energy demand and oxygen availability.

Mitochondrial proteins belonging to the conserved hypoxia induced gene domain (HIGD) family improve cell survival during the hypoxic and hypoglycemic stress. Their molecular function is not fully understood but they seem to act through regulating OXPHOS enzyme cytochrome *c* oxidase (complex IV). Complex IV activity is important for PMF generation.

Using yeast as a model organism, this study addresses function of HIGD proteins Rcf1 and Rcf2. The data presented here indicate that Rcf1 and Rcf2 support complex IV PMF generation and/or prevent proton leak across the inner membrane of the mitochondria. Deletion of Rcf1 (Δ*rcf1*) causes lower complex IV steady state levels and electron transfer activity. Deletion of Rcf2 in Δ*rcf1* strain (Δ*rcf1;*Δ*rcf2*) does not further decrease complex IV steady state levels and electron transfer activity, yet strongly impairs respiratory growth. Analyses of single mutant strains Δ*rcf1* and Δ*rcf2* indicated that deletion of Rcf1 or Rcf2 lowers OXPHOS efficiency and decreases PMF. These defects become more severe when both Rcf1 and Rcf2 are deleted. The inability to maintain PMF and PMF-dependent functions is proposed to underlie the strong respiratory growth deficiency of Δ*rcf1;*Δ*rcf2* mutant. In addition to this new role of Rcf1 and Rcf2 in PMF maintenance, several pleiotropic phenotypes of Δ*rcf1;*Δ*rcf2* mutant – such as decreased ATP synthase levels, abnormal mitochondrial morphology – suggest that these proteins may have wider impact on OXPHOS function.

ACKNOWLEDGEMENTS

Vera Strogolova, B.S., M.S.

I am immensely thankful for the inspiration and the example of my mentor of eight years, Dr. Rosemary Stuart. Rosemary, your strength and ability to lift others are exceptional. Thank you for believing in me and helping me develop writing skills and elegant confidence. Through a chance meeting with Dr. Jasvinder Kaur at a Cold Spring Harbor conference, I found a position in Stuart lab. I was fortunate to work in a star team of former and current lab members - Jasvinder Kaur, Joshua Garlich, Micaela McGrath, Scott Jensen, Jonathan Scheel, Jodie Box, and Jessica Anderson. What a dear time I have spent with all of you. Thank you for your friendship.

I thank my committee members, Dr. Allison Abbott, Dr. Martin St. Maurice, Dr. Pinfen Yang, for their support and advice. I am grateful to Dr. Dale Noel for being on my committee until his retirement, for many discussions and his encouragement.

I received my M.S. degree at University of Wisconsin-Milwaukee. I owe much gratitude to my exceptional mentors there, Dr. Sergei Kuchin and Dr. Marianna Orlova, who I respect enormously. I thank you for my growth as a scientist and for being as a family to me. I strive to teach as Sergei teaches, making complicated concepts simple. I always approach a new project with a fearlessness of “what would Masha do?”

In a pursuit of the doctoral degree I am fulfilling a dream and a promise to myself. I owe endless debt to my dear family who did everything possible to help. I thank my husband, Slava, for being understanding and supportive. If it wasn’t for my parents, mother-in-law, sister-in-law, and grandparents, in whose care and love our two children were at all times when both of us were working, I wouldn’t complete my audacious journey. Thank you mom for always reading. Thank you Slava for being a dreamer. Thank you Kisha for prayers and love. I will make you proud and be your strength. Justice Ruth Bader Ginsburg gracefully commented on the work-life balance of being in school while having young children: “Each part of my life provided respite from the other and gave me a sense of proportion”. I enthusiastically concur.

Marquette Biological Sciences department is a unique support system of faculty, students and staff who truly care about each other, have common goals, and are passionate about teaching and research excellence. I am thankful for the support and fellowship I received at Marquette. I discovered what I want in a workplace and an institution here.

TABLE OF CONTENTS

LIST OF TABLES

LIST OF FIGURES

LIST OF ABBREVIATIONS

A.U.	arbitrary units
Ap5A	P1,P5-di(adenosine-5')pentaphosphate (Ap5A)
AAC	ADP/ATP carrier protein
ADP	adenosine 5’ diphosphate
ATP	adenosine 5’ triphosphate
BN-PAGE	blue native polyacrylamide gel electrophoresis
BSA	bovine serum albumin
CL	cardiolipin
˚C	degree Celsius
C*c*O	cytochrome *c* oxidase
CCCP	carbonyl cyanide m-chlorophenylhydrazone
Ccp1	cytochrome *c* peroxidase protein
C-terminal	carboxyl terminal
Cyt *a*	cytochrome *a*
Cyt *b*	cytochrome *b*
Cyt *c*	cytochrome *c*
Δψ	mitochondrial membrane potential
ΔpH	proton gradient
DDM	n-dodecyl b-D-maltoside
DIC	differential interference contrast
DMSO	dimethylsulfoxide
DNA	deoxyribonucleic acid
DTT	dithiothreitol
E.U.	enzyme units
ECL	enzyme catalyzed light generation
EDTA	ethylenediaminetetraacetic acid
ETC	electron transport chain
g	gravity
GFP	green fluorescent protein
HEPES	N-(2-hydroxyethyl)-piperazine-N’-2-ethanesulfonic acid
HIGD	hypoxia-induced gene 1 domain
His	histidine
HRP	horseradish peroxidase
IgG	immunoglobulin
IBM	inner boundary membrane, part of inner membrane
IM	inner membrane
IMS	intermembrane space
KCN	potassium cyanide
kDa	kilodalton
KPi	potassium phosphate
L	liter
µg	microgram
µl	microliter
mg	milligram

ml	milliliter
mM	millimolar
mt	mitochondrial
MOPS	(3-(N-morpholino)propanesulfonic acid)
N-terminal	amino terminal
NAD^+	nicotinamide adenine dinucleotide, oxidized form
NADH	nicotinamide adenine dinucleotide, reduced form
NADP	nicotinamide adenine dinucleotide phosphate
Ni-NTA	nickel-nitriloacetic acid
OCR	oxygen consumption rate
OD	optical density
oligo	oligomycin
OM	outer membrane
ORF	open reading frame
OXPHOS	oxidative phosphorylation
PAGE	polyacrylamide gel electrophoresis
PIC	inorganic phosphate carrier protein
PLS	proton loading site
PMF	proton motive force
PMSF	phenylmethylsulphonyl fluoride
PCR	polymerase chain reaction
Rcf1/2	respiratory supercomplex factor protein 1/2
ROI	region of interest
ROS	reactive oxygen species
S	synthetic
SEM	sucrose EDTA mannitol
SH	sorbitol HEPES
SDS	sodium dodecyl sulfate
TBS	Tris buffered saline
TCA	trichloroacetic acid
TE	Tris EDTA buffer
Tim44	translocase of inner membrane protein subunit
TMPD	N,N,N’,N’-tetramethyl-*p*-phenylenediamine
Tris	tris-(hydroxymethyl)-aminomethane
YP	yeast extract and peptone
V	Volts
WT	wild-type

CHAPTER 1. INTRODUCTION

1.1. Overview

Eukaryotic cells contain energy-generating organelles, mitochondria. Mitochondria perform many functions in the cell, one of which is to synthesize the energy molecule adenosine triphosphate (ATP). The extensive cable-like mitochondrial network maintains electrochemical potential, called protonmotive force (PMF), across an energy storing mitochondrial membrane. In a process called oxidative phosphorylation (OXPHOS) mitochondrial PMF transduces energy from (couples) the electron transport (oxidation) reactions to the synthesis of ATP. PMF is generated by membrane-embedded proton-transporting oxidoreductases. The terminal electron transport enzyme cytochrome *c* oxidase (C*c*O, also called complex IV) is central to regulation of electron and proton transport. Proton pumping function of complex IV provides the mechanism for its feedback regulation by PMF and maintaining optimal PMF (Hosler *et al*., 2006).

Mitochondrial proteins belonging to a conserved hypoxia-induced gene 1 domain (HIGD) protein family are proposed to regulate complex IV conformation, stability, and electron transport activity in response to environmental changes such as low oxygen. The mechanism of this regulation is currently unknown. This dissertation characterizes function of yeast HIGD proteins, Rcf1 and Rcf2, and their relationship to regulating the complex IV enzyme. Findings presented in this dissertation indicate that these proteins support not only the electron transport

function, but also proton transport function of complex IV. The absence of Rcf1 and Rcf2 causes mitochondrial defects consistent with PMF maintenance defect. This defect is observed in the absence of only Rcf2, which does not decrease complex IV levels or electron transport. A model for Rcf1 and Rcf2 supporting PMF generation by complex IV is proposed. Additionally, Rcf1 and Rcf2 may support stability and activity of other OXPHOS enzymes.

1.2. Mitochondrial structure

The double membrane structure of mitochondria is vestige of their bacterial origin, as the endosymbiosis theory states that mitochondria originated from proteobacterial symbionts of a eukaryotic progenitor (Martin *et al.,* 2015). An extensive mitochondrial inner membrane (IM) and a less extensive mitochondrial outer membrane (OM) surround the inner compartment, mitochondrial matrix. The portion of the IM that is directly adjacent / parallel to the OM is called inner boundary membrane (IBM). Pocket-like IM folds, called cristae, extend from the IBM into the matrix (a diagram of typical mitochondrial cross-section in Figure 1 illustrates these key features). Specialized ring-like structures - cristae junctions - separate the area of the IM that form cristae from the IBM (van der Laan *et al*., 2016; Harner *et al*., 2016; Hessenberger *et al*., 2017). The cristae IM contains OXPHOS enzymes, which catalyze electron transport, proton transport, and ATP synthesis reactions. The cristae structure is proposed to promote compartmentalization of protons and increase PMF (Song *et al.,* 2013).

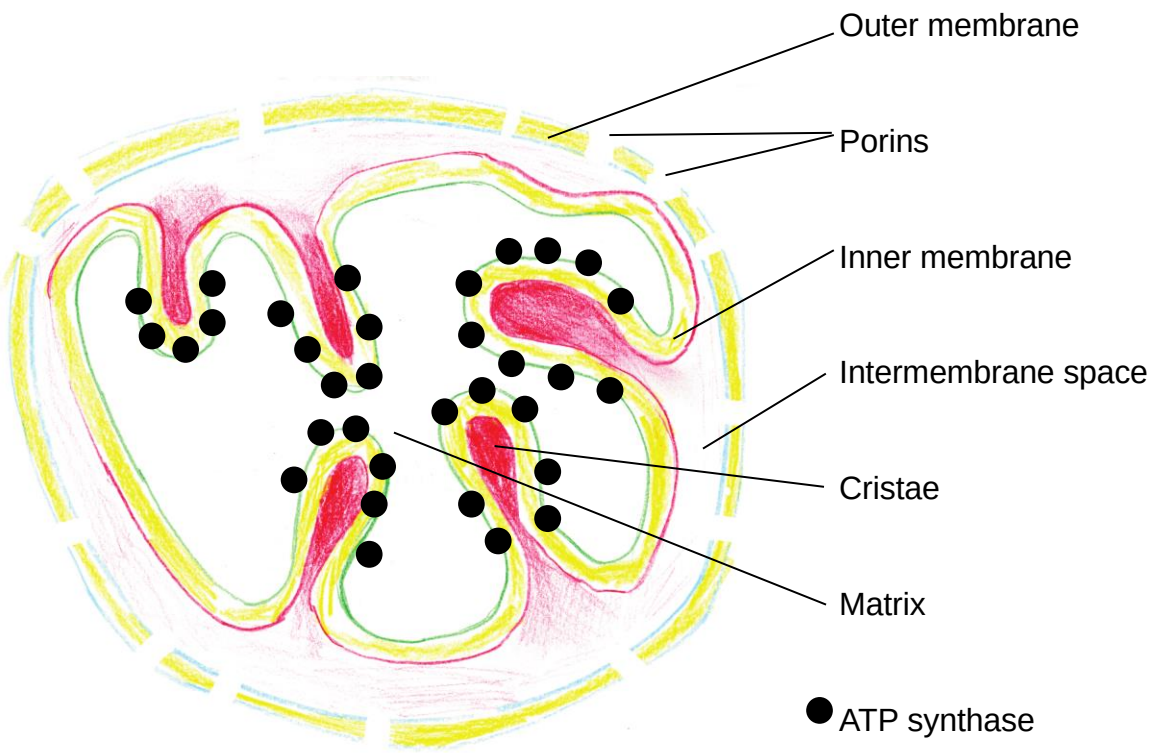

Figure 1. Schematic representation of mitochondria. A typical mitochondrion contains compartments with net positive and negative charges, represented by red and white color, respectively, in the diagram. The shape of cristae is highly variable and the communication between cristae and intermembrane space is sometimes restricted. Proton gradient in the cristae is higher than in the intermembrane space. Many transmembrane and membrane-associated protein complexes densely populating the inner and outer membrane are not shown, but their distribution is represented by the distribution of ATP synthase (circles). Diagram adapted from Nicholls and Ferguson, Bioenergetics, Academic Press, 4th Edition, 2013.

The shapes of the cristae are dynamic and rearrange in response to different respiration levels and PMF levels (Hackenbrock,1966; Cogliati *et al*., 2016).

Mitochondria are not synthesized *de novo*; their content in the cell, maintained by balanced growth, fission and fusion, scales with the size of the cell (Rafelski *et al*., 2012). Mitochondria form a reticular network in the cell which is highly dynamic, continuously undergoing fusion and fission. Fission allows separation and clearance of defective, depolarized mitochondria via process of mitophagy, as well as division of the mitochondrial network during mitosis. The PMF is an indicator of mitochondrial function and represents a regulating factor of mitochondrial fusion, fission, and degradation. PMF positively regulates cristae length (Khalifat *et al.,* 2008), providing positive feedback for mitochondrial biogenesis, morphology, and function.

1.3. Yeast as a model system

Eukaryotic cells can derive energy (ATP) from glycolysis and aerobic respiration, which occur in cytosol and mitochondria, respectively. The balance of glycolysis and respiration is determined by the supply of substrates and the need of the cell. Yeast *Saccharomyces cerevisiae* are well suited to the study of mitochondrial function, as its ability to respire is dispensable for survival. Mitochondrial respiration gives yeast the ability to grow aerobically on non-fermentable carbon sources (e.g. glycerol, ethanol). Defects in respiration are easily detected by slower or absent growth on non-fermentable substrates. Yeast

growth on fermentable (e.g., glucose) carbon sources does not require mitochondrial ATP production, allowing to propagate and study OXPHOS mutations, such as petite mutants caused by loss of mitochondrial DNA. When glucose is present, yeast rely only on glycolysis (fermentation) due to repression of respiration by glucose (Carlson, 1999). However, yeast growing on other fermentable sugars (e.g., galactose) utilize both glycolysis and respiration pathways of energy production.

Importantly, mitochondrial genome, proteome, and function, especially OXPHOS components, are remarkably conserved in yeast and mammalian mitochondria. This, combined with simple genetic manipulation system in yeast, resulted in the great utility of yeast as a model organism to understand assembly and regulation of OXPHOS complexes, and study human mitochondrial diseases. Since this dissertation is focused on mitochondrial function and structure in yeast, primarily yeast enzymes will be described, and yeast gene names and nomenclature will be used unless otherwise noted.

1.4. Mitochondrial function

Mitochondria contain hundreds of proteins and are a site of diverse metabolic reactions within the cell. Mitochondria participate in initiating whole-body responses to hypoxia and other stresses (Nunnari and Suomalainen, 2012). In addition to OXPHOS, mitochondria perform many functions critical to the eukaryotic cell: biosynthesis of heme groups, iron sulfur clusters, amino acids,

fatty acids, generating and metabolizing signaling molecules such as acetyl-CoA and reactive oxygen species (ROS), replenishing NAD^+ for glycolysis; furthermore, mitochondria participate in programmed cell death (apoptosis) (Nunnari and Suomalainen, 2012; Baile and Claypool, 2013).

Mitochondria retain their own mitochondrial genome, and consequently their own mechanisms of transcription, and their own translation machinery. The mitochondrial genome is highly reduced from their bacterial ancestor by genetic transfer to the eukaryotic host nuclear DNA. The mitochondrial genome encodes only a handful of hydrophobic proteins (13 in human, 8 in yeast mitochondrial genome) (Bernardi *et al.*, 1972, Anderson *et al.*,1981). Since so few mitochondrial proteins are encoded by mitochondrial DNA, nuclear genes encode the vast majority of mitochondrial proteins (Nicholls and Ferguson, 2013). Protein import into mitochondria is a process that is essential for life (Baker and Schatz, 1991). Assembly and function of protein translocases, and IMM insertion of positively charged polypeptide sequences, requires PMF (Martin *et al*., 1991).

The mitochondrially encoded proteins are essential for assembly and function of critical OXPHOS enzymes (including complex III, complex IV, and complex V). These complex OXPHOS enzymes each contain more than ten protein subunits and are mosaic in origin, meaning that the rest of their subunits are encoded by nuclear genome, and the assembly of nuclear and mitochondrial subunits is intricately coordinated.

1.4.a. Mitochondrial electron transport chain (ETC)

Mitochondrial OXPHOS is the best-known function of the organelle and provides eukaryotic cells the most productive way to regenerate ATP. The OXPHOS enzymes of the IM are multi-subunit molecular machines commonly referred to as OXPHOS complexes I-V, diagrammed in Figure 2A. The citric acid cycle in mitochondrial matrix completes metabolism of glycolysis and fermentation products, such as pyruvate, ethanol, acetate, lactate. Breakdown of these non-fermentable compounds is coupled to reduction of NAD^+ and FAD^{2+}. NADH and $FADH_2$ are oxidized with reduction of oxygen by the enzymes of electron transport chain (ETC). The ETC is the chain of OXPHOS complexes I-IV. NADH dehydrogenase and succinate dehydrogenase are the alternative beginnings of the ETC. NADH:ubiquinone oxidoreductase (NADH dehydrogenase) reduces lipid-soluble electron carrier ubiquinone to form ubiquinol (reduced form). NADH dehydrogenase in plant and mammalian mitochondria is the largest OXPHOS enzyme complex (complex I). In yeast, complex I is replaced by one-subunit NADH dehydrogenase enzyme. Yeast NADH dehydrogenase isoforms have active sites on the matrix side of the IM (Ndi1) and on the IMS side of the IM (Nde1 and Nde2); in contrast to complex I, Ndi1, Nde1, Nde2 do not contribute to the PMF (do not pump protons) (Rigoulet *et al*., 2004). Despite their relative simplicity, yeast NADH dehydrogenases are functionally similar to mammalian mitochondrial complex I with respect to oxidation of NADH and reduction of ubiquinone; expression of

A

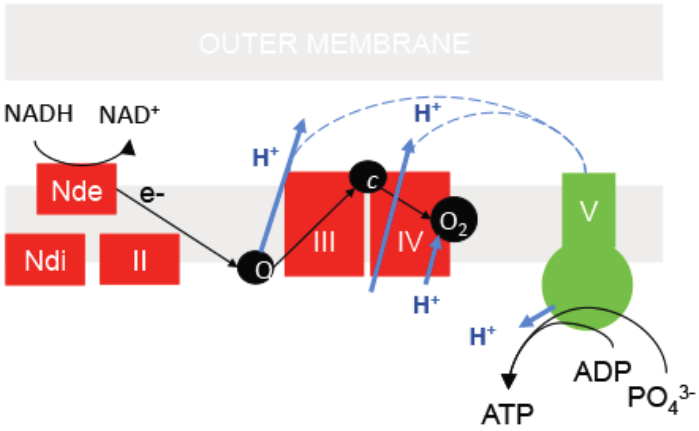

B

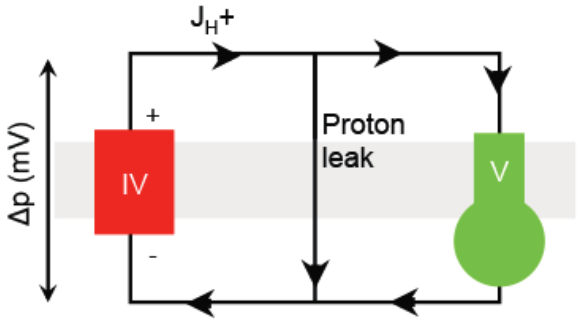

Figure 2. OXPHOS enzymes and the proton circuit. (A) OXPHOS enzymes NADH dehydrogenases (Nde and Ndi), complex II, III, IV are represented by red rectangles; complex V is in green; electron carriers ubiquinone (Q) and cytochrome *c*, as well as oxygen are represented by black circles; gray stripes represent phospholipid bilayers; electron flow is depicted with black arrows, and the flow of protons with blue arrows. **(B)** The flow of protons in a proton circuit formed by OXPHOS complex IV and ATP synthase (V) is diagrammed by black arrows. Diagram adapted from Nicholls and Ferguson, Bioenergetics, Academic Press, 4th Edition, 2013.

yeast Ndi1 in mammalian cells remedies respiratory deficiency caused by complex I defects (Yagi *et al.,* 2006). Succinate dehydrogenase (complex II) is IM-associated enzyme of the citric acid cycle that is conserved on gene and protein level, in yeast and mammalian mitochondria. Complex II transfers electrons from its cofactor $FADH_2$ to ubiquinone on the matrix side of the membrane (Rigoulet *et al.,* 2004).

Electrons from ubiquinol are transferred to cytochrome *c* reductase, complex III (ubiquinol-cytochrome bc_1 oxidoreductase). Complex III transfers the electrons to a soluble IMS carrier cytochrome *c*, simultaneously releasing ubiquinone and protons at the IMS side of the membrane. By cycling the electron carrier ubiquinone across the IM, Complex III translocates protons by "loop" mechanism (Saraste*,* 1999). The final reaction of ETC is oxidation of cytochrome *c* by cytochrome *c* oxidase, complex IV (C*c*O). Transport of electrons by complex IV results in the reduction of molecular oxygen (O_2) to form water. In addition, complex IV translocates protons across the IM by active pumping mechanism (described in detail in section 1.4.c.).

In yeast mitochondria, complexes III and IV form supercomplexes of III_2IV_{1-2} stoichiometric composition (Schägger and Pfeiffer 2000). A subpopulation of the III-IV supercomplexes contains also ADP/ATP carrier (AAC) (Dienhart and Stuart, 2008). AAC is thought to directly assist the assembly and activity of the III-IV supercomplexes. Supercomplexes containing III and IV are found across taxa and reflect coordinated assembly of protein and lipid subunits of complex III and complex IV (Lenaz and Genova, 2009). In mammalian mitochondria, III-IV

supercomplexes can also contain complex I; the resulting supercomplexes are referred to as “respirasomes”. Functionally, respirasomes are proposed to facilitate electron transport to optimize the use of ETC substrates and prevent formation of reactive intermediates (Cruciat *et al.,* 2000; Lapuente-Brun *et al.,* 2013; Barrientos and Ugalde, 2013).

1.4.b. PMF powers ATP synthesis

Catalytic activity of electron transporting enzymes enables transport of protons against concentration gradient from the matrix to the IMS by OXPHOS complexes III and IV. The IM is relatively impermeable to protons, insulating the flow of a proton current through the chemiosmotic circuit in a manner analogous to an electrical circuit (Figure 2B). The proton current powers the synthesis of ATP by the F_1F_O ATP synthase (OXPHOS complex V). The protons from the IMS are transported back into the matrix though the F_O portion; the energy of proton translocation rotates the F_1F_O ATP synthase, inducing conformational changes necessary for catalytic phosphorylation of ADP in the F_1 sector. Under ideal conditions, the insulated proton circuit conserves energy cycling between the OXPHOS enzymes in the form of the PMF; this energy conservation is referred to as coupling of oxidation and phosphorylation.

The coupling can be empirically evaluated as the number of ATP molecules formed per atom of oxygen (O), called P/O (phosphorylation/oxidation) ratio. Each oxygen atom is reduced by two electrons. A transfer of two electrons

by complex III moves four protons from the matrix to the IMS ($4H^+/2e^-$); complex IV pumps two protons, and removes two more protons from the matrix, which are combined with the oxygen atom to form water ($4H^+/2e^-$). Complex V stoichiometry is determined by the number of subunits that make up the rotating F_O portion of the enzyme (subunit c, encoded by yeast gene *ATP9*). Binding of one proton to every Atp9 subunit results in rotation of the F_O portion of the enzyme, catalyzing three ADP phosphorylation reactions in the F_1 portion of the enzyme. Yeast complex V has ten Atp9 subunits (Devenish *et al*., 2000), yielding the 10 H^+/3 ATP =3.33 H^+/ATP stoichiometry. Finally, the AAC exchange of ATP for ADP and inorganic phosphate causes the influx of one additional H^+/ATP in addition to those required for ATP synthase rotation (Nicholls and Ferguson, 2013). Yeast mitochondria can generate up to 1.8 ATP molecules for every atom of oxygen (O) reduced by transfer of two electrons (Hinkle, 2005); the calculated P/O ratio:

$$4\ H^+_{III} + 4\ H^+_{IV}) / (\ 3.33\ H^+_V + 1\ H^+_{ADP/ATP\ exchange}) = 1.84$$

Experimentally determined stoichiometries of the proton translocation by isolated complexes III, IV and V agree with thermodynamic predictions; however, considerable and variable proton leak both *in vivo* and in isolated mitochondria lowers the OXPHOS coupling.

Transport of protons against the concentration gradient generates proton (ΔpH) and charge (Δψ) gradients. The contribution of the Δψ and ΔpH gradients to the PMF which is measured as electrical charge expressed in millivolts (mV) can be calculated as follows:

$$PMF = \Delta\psi - 61\ \Delta pH$$

Due to low capacitance of biological membranes, transfer of only a few protons across a spherical membrane is sufficient to generate considerable Δψ (Bashford and Thayer, 1977; Nicholls and Ferguson, 2013; Björck and Brzezinski, 2018). Therefore, charge component to the voltage expression of PMF is greater than that of the ΔpH component (Perry *et al.,* 2011). Typical PMF values range from 180 to 220 mV, with Δψ contributing 150-180 mV, and ΔpH of 0.5-1.0 units contributing the remaining 30-60 mV (Nicholls and Ferguson, 2013). The relative contribution of Δψ and ΔpH to the PMF is variable and depends on the activity of the ETC, concentration of other cations (Ca^{2+}, K^{+}, Na^{+}, etc.), and buffering capacity of the mitochondrial matrix.

In addition to ATP synthesis, PMF supports redox homeostasis, import of proteins across mitochondrial membranes, and activity of mitochondrial solute carriers. PMF is an indicator of healthy mitochondria and regulates mitochondrial fission, fusion, and degradation (Nunnari and Suomalainen, 2012).

1.4.c. Proton pumping by complex IV (C*c*O)

The terminal electron transporting enzyme, complex IV (C*c*O), confirmed as a true proton pump in 1970s, performs two coupled reactions: transfer of electrons from cytochrome *c* to oxygen and active transport of protons from the matrix to the IMS (Wikström 1977, Nicholls and Ferguson, 2013). Complex IV contains two heme groups and two copper atoms and belongs to A-type heme-

copper oxidase (HCO) family (Sharma and Wikström, 2014; Rauhamaki and Wikström, 2014). A-type HCOs are the only HCOs containing third subunit Cox3, the presence of which corelates with proton pumping D channel (Wikström *et al.,* 2015). Bacterial A-type HCOs are composed of 3 subunits, while mitochondrial complex IV have more (10-12) subunits (Soto *et al*., 2012). The three core subunits of mitochondrial complex IV - Cox1, Cox2, and Cox3 are encoded in the mitochondrial genome and are remarkably conserved with the bacterial A-type HCOs. Cox1 and Cox2 are directly involved in the catalysis. Cox3 is not directly involved in catalysis and it is thought to play a regulatory role (Hosler *et al*., 2006). The nuclear genome encodes complex IV subunits Cox4, Cox5a/b, Cox6, Cox7, Cox8, Cox9, Cox12, Cox13, and Cox26. These subunits are less conserved and serve structural or regulatory roles (Fontanesi *et al*., 2006).

Subunits Cox1 and Cox2 are directly involved in transport of electrons from cytochrome *c* to oxygen. Cox1 coordinates hemes *a* and a_3 and copper Cu_B and Cox2 coordinates copper Cu_A. Heme a_3 and Cu_B form a binuclear reactive center (BNC). BNC catalyzes electron transport to oxygen to form water. Cox2, aided by subunit Cox12, a peripheral subunit in the IMS which makes a “soft and specific” contact with reduced cytochrome *c*. The cytochrome *c* contact site allows cytochrome *c* to undergo structural changes without losing the contact with the enzyme (Shimada *et al.,* 2017). Time-resolved studies demonstrate that the transfer of electrons proceeds from cytochrome *c* to Cu_A to cytochrome aa_3 and Cu_B and finally to oxygen (Nicholls and Ferguson, 2013).

In every catalytic cycle, complex IV uptakes eight protons, four of which combine with oxygen to form water, and four more are pumped from the matrix into the IMS. The current understanding of the mechanism of proton pumping by complex IV is incomplete. Proton pumping is powered by the electron transfer: approximately 545 mV is produced per electron spanning the redox potential difference, ΔE_h, between heme *a* and the BNC: $\Delta E_h = E_{h(\text{heme a})} - E_{h(\text{BNC})}$. This energy is sufficient for the pumping of one proton per electron transferred (Blomberg and Siegbahn, 2014; Wikström *et al.,* 2015). Heme redox potentials are strongly influenced by the PMF (Kim *et al.,* 2012). High PMF lowers redox differential of the enzyme, making proton pumping less thermodynamically favorable.

Uptake of protons occurs at proton loading sites (PLS) on the matrix side of the enzyme. PLS are proton wells, where the local microenvironment (e.g., matrix pH and electrostatic interactions) influences the pK_a of key amino acid residues to promote their protonation (Wikström *et al.,* 2015). The two entry points for the protons involve amino acids Asp(D)92 and Lys(K)315 of the Cox1 subunit. The protons travel via transmembrane ion channels formed by the transmembrane domains of Cox1 and Cox2; protonation of key residues of these two subunits creates a proton “wire” across the membrane. Two universally acknowledged proton pathways are named D and K channels after the conserved Asp(D)92 and Lys(K)315 residues (Blomberg and Siegbahn, 2014). Pumping protons across the membrane occurs exclusively by the D channel (Wikström *et al.,* 2015). The K channel is used for uptake of substrate protons.

Mutation of conserved K-channel lysine demonstrated K-channel importance for proton pumping ability of bacterial cytochrome *c* oxidases. Protonation of K channel Lys(K)315 decreases the redox potential of the BNC by approximately 30 mV, increasing the redox differential of the enzyme, which is necessary for pumping protons at high PMF (Sharma and Wikström 2016).

The levels of complex IV enzyme limit the maximal ETC activity. In intact mitochondria, ETC is operating below its maximal capacity due to negative regulation of complex IV activity by the PMF. The excess complex IV capacity is reserved to respond to rapid changes in PMF. The complex IV activity remains limited by the PMF because of the coupling of electron and proton transport activities by the enzyme (complex IV coupling). Numerous gating mechanisms preventing the backflow of the protons through the complex IV proton channels are proposed (Blomberg and Siegbahn, 2012; Wikström et al., 2015). Multiple lines of evidence indicate that proton-pumping efficiency of mitochondrial complex IV can be altered or a subpopulation of the enzyme can develop elevated proton leak (Kadenbach 2003; Bloch *et al.,* 2004; Bloch *et al.*; 2009, Blomberg and Siegbahn, 2012; Siegbahn and Blomberg, 2014). The existence of proton leak was also reported in enzyme homologous to mitochondrial complex IV, *E.coli* cytochrome bo_3 (Li *et al.,* 2015). Proton leak in small subpopulations of HCOs was postulated to alleviate respiratory pressure and ROS production (Li *et al.,* 2015). The role of the many complex IV subunits and associated proteins, in regulating redox potential of the hemes, dielectric channels and wells, proton leak, and proton pumping rates, remains to be discovered.

1.4.d. Function of the Cox3 subunit

The Cox3 subunit does not directly channel protons or electrons and is thought to play a regulatory or supporting role in complex IV catalysis (Hosler *et al*., 2006). Cox3 importance for proton pumping and mediating the PMF regulation of complex IV activity was recently revealed, providing an example of cooperative action of complex IV protein and lipid constituents during catalysis. Evolutionary comparisons indicate that Cox3 is found only in A-type HCOs (Wikström *et al.,* 2015) and Cox3 presence correlates with improved proton pumping ability of HCOs. This suggests that Cox3 supports proton pumping. Bacterial cytochrome *c* oxidase enzyme depleted of Cox3 displays diminished proton pumping, thus confirming the role of Cox3, and specifically the Cox3 amino terminal region, in proton pumping (Varanasi *et al.,* 2012; Alnajjar *et al.,* 2014). The presence of Cox3 is thought to stabilize the D-channel by increasing pK_a of protonated PLS residues. Cox3 also plays a specific role supporting proton pumping at high PMF, which requires the K channel. Thus, Cox3 has the potential to influence both proton uptake pathways. Proton uptake and pumping are critical for the stability of the BNC and of the enzyme.

Cox3 subunit dissociates when purified bovine complex IV is subjected to alkaline conditions (pH 9.5), or detergent (1 mM DDM), or elevated temperature (Kadenbach and Hüttemann, 2015). Removal of Cox3 accelerates destabilization of BNC, loss of enzyme activity and degradation of the enzyme. This indicates that Cox3 interactions with the other subunits are critical for enzyme activity and

stability. Key interface of Cox3 with complex IV is alongside Cox1 subunit. The Cox1-Cox3 interface is lined with phospholipid molecules that form an oxygen delivery pathway to the active site of the enzyme (Shinzawa-Itoh *et al.,* 2007). Dynamics of Cox3 conformations within the enzyme during catalytic activity or inactivity, are unknown. While the biogenesis and assembly of complex IV protein subunits have been extensively studied, it is unknown how and whether subunit switching occurs (e.g. when condition specific isoforms are synthesized or when peripheral subunits dissociate). Similarly, no mechanisms are known for assembly of repair of the enzyme's lipids, even as lipids in the vicinity of the oxygen delivery pathway are at risk of oxidative damage.

1.4.e. OXPHOS coupling and efficiency

OXPHOS coupling is the relationship between ATP synthesis and oxygen consumption by the ETC system (P/O ratio). OXPHOS coupling depends on the degree of insulation of the proton current, or PMF. Non-productive proton leaks occur across the energized phospholipid bilayer and through transmembrane protein and protein complexes. The phospholipid bilayer is a source of constant proton leak and becomes more permeable to protons at higher PMF in a non-linear manner (Jastroch *et al.,* 2010). Transport-independent proton leak through the ADP/ATP carrier (AAC) is another source of proton leak (Nicholls and Ferguson, 2013). It is estimated that such proton leaks dissipate 20-30% PMF *in vivo* (Jastroch *et al.,* 2010).

OXPHOS coupling and the “reserve” capacity of the ETC enzymes both contribute to respiration efficiency, or the ability of the mitochondria to maintain optimal P/O ratio in response to varying ATP demand (Gnaiger *et al.,* 1998). The amount and activity of the ETC enzymes relative to ATP synthase influences the degree by which the ETC activity is limited by the PMF and the “reserve” capacity needed to rapidly ramp up the ATP synthesis in response to ATP demand (Quarato *et al.,* 2011). Proton pumping by complex IV is a regulatory point for the regulation of the ETC activity by the PMF.

Empirical measurements of ATP production and oxygen consumption in whole cells and in isolated mitochondria showed that the P/O ratio is optimized to different ATP synthesis rates in different tissues (i.e., different cell types have different respiration efficiency). For example, mitochondria in skeletal muscle are better prepared to support rapid ATP production, while mitochondria liver have lower P/O ratio and lower apparent affinity for ADP phosphorylation (Gouspillou *et al.,* 2011). P/O ratio and respiration efficiency are influenced by stress, aging, diet (Ocampo *et al.,* 2012, Gouspillou *et al.,* 2011, Salin *et al.,* 2018). Differences in respiration efficiency are a determining factor in survival and fitness of cells, tissues, and organisms (Stefano and Kream, 2016).

1.4.f. Hypoxia survival adaptation depends on better respiration efficiency

Selective expression of alternative OXPHOS protein subunit isoforms leads to tissue and condition specific differences in respiration efficiency; the

mechanism(s) of this phenomenon are currently debated. One such mechanism, where two different isoforms of Cox5 are expressed (Cox5a, which is expressed constitutively, and Cox5b, which is induced by low oxygen concentration (hypoxia)) is proposed to be acting through regulation of complex IV activity (Kadenbach and Hüttemann; 2015, Sinkler *et al.,* 2017). Hypoxia limits complex IV activity and leads to oxidative stress and energy depletion. Adaptation to hypoxia depends on oxygen sensing pathways in mammalian and yeast cells, that induce expression of hypoxic isoforms of cytochrome *c* (Cyc7), complex IV (Cox5b, and equivalent Cox4-2 in mammals) and AAC (Aac3) (Ziello *et al.,* 2007; Liu and Barrientos 2013; Hon *et al.,* 2003). Adaptation to hypoxia in human divers was found to be primarily mediated by lowering ETC capacity and increasing OXPHOS efficiency (Kjeld *et al.,* 2018). The expression of hypoxic isoforms is thought to promote OXPHOS efficiency (Fukuda *et al.,* 2007; Hwang *et al.,* 2015) by increasing complex IV affinity for oxygen, thus lowering incomplete electron transfer events that lead to oxidative stress (Liu and Barrientos 2013; Waterland *et al.,* 1991). A non-conservative substitution of Cox3 Trp(W)116 to Arg(R) in the bar-headed geese, is postulated to alter Cox1-Cox3 interaction and complex IV activity and endow the geese with a unique ability to fly at high-altitude, hypoxic conditions, for long periods (Scott *et al*., 2011). Overall, complex IV is central to adaptation to hypoxia.

Mitochondrial dysfunctions present in many pathological conditions (cancer, neuropathies, myopathies, and ischemia/reperfusion injury) can lower respiration efficiency by altering OXPHOS enzyme levels, activity and kinetics

(Rak *et al.,* 2016). The changes in the mitochondrial proteome that take place during short hypoxic preconditioning are protective and can prevent damage from subsequent hypoxia/ ischemia (Russel *et al.,* 2014; Dumke *et al.,* 2009; Villani *et al.*, 1998). Recently, it was demonstrated that a mitochondrial disease (Leigh syndrome) mouse model benefited from hypoxia induced adaptive response (Jain *et al.,* 2016). Therefore, understanding hypoxia-induced adaptive response has clinical significance since this response can counteract pathological changes associated with mitochondrial disease.

1.4.g. OXPHOS associated lipids

Mitochondrial structure and function are influenced by its membrane lipids, especially non-bilayer phospholipids phosphatidylethanolamine (PE) and cardiolipin (CL), which support membrane curvature and surround large dynamic transmembrane enzyme complexes (Ball *et al.,* 2018). CL is a highly charged lipid only found in mitochondrial IM (Hoch, 1992). CL in artificial lipid bilayer membranes promotes tubulation and self-maintaining cristae-like shape in response to local pH gradient *in vitro* (Khalifat *et al.,* 2008). Thus, CL participates in feedback regulation of IM morphology by the PMF.

The proximity of the OXPHOS enzymes and lipid environment in the cristae is proposed to support the lateral proton diffusion from the enzymes of electron transport chain (ETC) such as complex IV to the ATP-generating enzyme, F_1F_O ATP synthase (Sjöholm *et al.,* 2017); CL patches are proposed to

be especially important for this process (Haines and Dencher, 2002). Membrane proteins can play a role in modulating organization of lipids in the mitochondrial membranes, for example by sequestering lipid molecules from circulation (Chen *et al.,* 2018). Crystallized OXPHOS enzymes have demonstrated that lipids are integral conserved components of all OXPHOS enzymes. Three CL molecules bind strongly to the periphery of each AAC molecule, stabilizing it (Klingenberg, 2009). CL is important for the formation and/or stability of the III-IV supercomplexes. Structural CL molecules of the complex III support enzyme structural integrity and proton translocation (Pöyry *et al*., 2013; Arnarez *et al.*, 2013; Xia *et al.,* 2013). Complex IV contains 13 lipid molecules, of which three are associated with Cox3 and two are CL molecules (Shinzawa-Itoh *et al.,* 2007). Phospholipid molecules at the interface of Cox3 and Cox1 play a crucial role in oxygen delivery pathway to the core of the complex IV enzyme and prevent loss of Cox3 (Shinzawa-Itoh *et al.,* 2007). Finally, CL promotes assembly, stability, and smooth rotation of the F_1F_O ATP synthase (complex V) required for its catalytic function. CL binding involves a conserved lysine of the Atp9 subunit (Duncan *et al.,* 2016). Specific yet transient (on-and-off) interactions with CL prevent proton leaks through the F_O (Duncan *et al.,* 2016; Mehdipour and Hummer, 2016).

CL is postulated to regulate many aspects of OXPHOS, but many reports contradict the benefit of CL for OXPHOS efficiency. In liver mitochondria, increased CL content increases non-productive oxygen consumption, but does not increase ATP synthesis, therefore lowering OXPHOS efficiency (Bobyleva *et*

al., 1997; Julienne *et al.*, 2014; Peyta *et al.,* 2016). Therefore, it appears that CL levels need to be coordinated with the OXPHOS protein levels for optimal OXPHOS efficiency.

The pool of mitochondrial phospholipids is regulated by lipid degrading and remodeling enzymes. CL is synthesized in mitochondria and undergoes acyl chain remodeling after synthesis. CL remodeling is thought to be a repair mechanism of CL molecules sustaining oxidative damage of component acyl chains (Baile *et al.,* 2013; Schlame and Greenberg, 2017). Without remodeling, CL degradation is increased but how turnover and degradation is regulated is not known (Xu *et al.*, 2016). CL is essential for viability of the mammalian cells. Deficient CL remodeling causes human mitochondrial disease (Barth syndrome). Importantly, loss of CL decreases mitochondrial DNA stability, viability, and respiration efficiency, but has a mild effect on respiration-based growth in yeast (Zhong *et al.,* 2004).

1.5. Rcf1 and Rcf2

This dissertation focuses on the yeast respiratory supercomplex associated factors Rcf1 and Rcf2. These proteins are thought to support respiration by regulating complex IV (cytochrome *c* oxidase), yet a possibility that these proteins influence activity of other OXPHOS enzymes has not been ruled out. Whether Rcf1 and Rcf2 regulate complex IV proton transport or coupling is not known.

Many genes in *S. cerevisiae* have paralogs arising from an ancient genome duplication event (Kellis *et al*., 2004; Dujon *et al*., 2004). *RCF1* (*YML030W*) and *RCF2* (*YNR018C*) are paralogs; both genes are constitutively expressed, and encode transmembrane proteins located in the IM. Rcf1 and Rcf2 were identified as novel proteins interacting with the III-IV supercomplex in a proteomic screen (Helbig *et al*., 2009; Hess *et al*., 2009). These interactions were confirmed by co-purification of His-tagged Rcf1 and Rcf2 proteins with almost all subunits of complex III and complex IV (Chen *et al.,* 2012; Strogolova *et al.,* 2012; Vukotic *et al.,* 2012), with the exception of peripheral subunits Cox12 and Cox13, which were absent in $Rcf1_{HIS}$-associated complex IV (Strogolova *et al.,* 2012; Vukotic *et al.,* 2012). Rcf1 and Rcf2 interact with the III-IV supercomplex independently (Strogolova *et al.,* 2012).

Deletion of *RCF1* (Δ*rcf1*) is associated with impaired respiratory growth in the BY4741 yeast genetic background (Chen *et al*., 2012) but near-normal respiratory growth is observed in the W303 genetic background (the genetic background used in this study) (Strogolova *et al.,* 2012). The *S. cerevisiae* BY4741 genetic background exhibits an elevated rate mtDNA loss, due to several genetic polymorphisms, including one that occurs within the gene encoding transcription factor *HAP1* and negatively affects the expression of complex IV subunits (Dimitrov *et al.,* 2009; Bruder *et al*., 2016). Compared to BY4741, W303 genetic background has more robust complex IV levels and more stable mitochondrial genome and thus is preferred for mitochondrial studies. The deletion of the *RCF2* gene (Δ*rcf2*) does not appear to negatively impact

respiratory growth in BY4741 and W303 genetic backgrounds (Strogolova *et al.,* 2012; Vukotic *et al.,* 2012; Römpler *et al*., 2016). The double mutant (Δr*cf1*;Δ*rcf2*) yeast strain was studied only in W303 genetic background (Strogolova *et al.,* 2012) and never reported in BY4741 genetic background. The double mutant (Δr*cf1*;Δ*rcf2*) in W303 genetic background is characterized by decreased complex IV activity and a strong respiratory growth defect, which can be complemented by either RCF1 or RCF2 expression (Strogolova *et al.,* 2012). The cross-complementation was suggested at the time to indicate that Rcf1 and Rcf2 have a shared function supporting respiration, most likely involving the III-IV supercomplex.

1.5.a. Rcf1 and Rcf2 are members of a conserved HIGD family of proteins

Immunodetection and quantification of epitope and GFP tagged proteome estimated Rcf1 protein abundance to be > 1000 molecules per cell (Ghaemmaghami *et al*. 2003) while Rcf2 protein was estimated to be twice as abundant as Rcf1 (Chong *et al*., 2015); both proteins are constitutively expressed and abundant. Yeast does not have a hypoxic-regulated HIGD protein isoform. Rcf1 and Rcf2 sequences are divergent from each other and share strongest homology near one of their transmembrane domains, where a conserved (Q/I)X3(R/H)XRX3Q motif is found. The (Q/I)X3(R/H)XRX3Q motif is found in the hypoxia-induced gene 1 domain (HIG1D or HIGD), found in a conserved HIGD protein family. HIGD containing proteins are found in yeast, plant, animal

mitochondria, as well as many α-proteobacteria. Based on the sequence of the (Q/I)X3(R/H)XRX3Q motif, HIGD protein isoforms are subdivided into type 1 (V/IHLIHMRX3Q) and type 2 (QX3RXRX3Q) (Figure 3A). Type 1 HIGD proteins are regulated by transcription factor HIF1 and are upregulated during hypoxia and hypoglycemia (Wang *et al.*, 2006; An *et al.*, 2011). Type 2 HIGD proteins are constitutively expressed; Rcf1 and Rcf2 are both type 2 HIGD proteins (Strogolova *et al.*, 2012; Garlich *et al.,* 2017).

Expression of mammalian type 1 HIGD proteins is associated with better adaptation to hypoxia and hypoglycemia resulting in lower cell death (apoptosis) (Wang *et al.,* 2006; Zhang *et al.,* 2012; Ameri *et al.,* 2015; Ameri and Maltepe 2015) as well as improved mitochondrial morphology (An *et al.,* 2013). These characteristics attracted interest to the mechanism of action of HIGD proteins, yet the mechanism of action remains unknown. Mammalian type 1 HIGD protein Higd1a has been shown to interact with complex IV and proposed to promote conformational change and increase the turnover number (electron transport rate) *in vitro* (Hayashi *et al.,* 2015). The function of HIGD type 2 proteins had not been studied.

1.5.b. Rcf1 and Rcf2 function

Rcf1 and Rcf2 interacts transiently with a small sub-population of the supercomplex III-IV and Rcf1 was reported to minimize reactive oxygen species (ROS) levels (Chen *et al.*, 2012; Vukotic *et al.*, 2012; Fischer *et al.,* 2015). In the

A

```
Re          ..MMKGGDANISNKLMQLRVLLQAVAVILIMLTLW.. 59
Bj          ..MMRGGSPNTSQKLMRWRVLLQFVAIVIAMIAVW.. 101
Nw          ..MIRGGNPWRSQYLMQTRVVLQFVAIVMVMMAVW.. 60
Rs          ..RGGEYNRLNANKIMRWRLMAQFVAVVLIAGLAW.. 62
ScRcf2      ..VNKDPIMTKAQKIVQARMYAQFITVGLLLASVG.. 167
ScRcf1      ..NVRLGNKWKAQYYFRWRVGLQAATLVALVAGSF.. 83
SqYGHL1     ..MKNRGDTKMSVHLIHMRVAAQGFVVGAMTVGVL.. 71
HsHIG1-1A   ..LKSRGNTKMSIHLIHMRVAAQGFVVGAMTVGMG.. 94
HgHIG1-1A   ..LKSRGNTKMSIHLIHMRVAAQGFVVGAMTLGMG.. 80
CeM05       ..SSFLGDKVGAQKMMQYRIMAQFFTVTALVAGVT.. 130
HsHIG1-2A   ..SFHRGNSQRSQLMMRTRIAAQGFTVAAILLGLA.. 98
BtHIG1-2A   ..CFHRGQSQRSQLMMRTRIAAQGFTIVAILVGLA.. 98
HgHIG1-2A   ..CFHRGHSQRSQFMMRTRIAAQGFTVAAILFGLA.. 98
                          QRRQ Motif
```

B

```
Bj          ..TSQKLMRWRVLLQFVA.. 92
ScMic60     ...EQIYNRWNLLADDFK.. 442
Rs          ..NANKIMRWRLMAQFVA.. 53
HsMic60     ..EETLRARFYAV-QKL... 641
ScRcf1      ..KAQYYFRWRVGLQAAT.. 74
                     **
```

Figure 3. Conservation and position of the Rcf1 and Rcf2 (Q/I)X_3(R/H)XRX_3Q (QRRQ) motifs. Sequence alignments and proposed topology of Rcf1 and Rcf2 proteins. **(A)** Sequence alignment of the QRRQ motifs from *S. cerevisiae* Rcf1 (ScRcf1), *S. cerevisiae* Rcf2 (ScRcf2), bacterial homologs *Rhizobium etli* WP_011426989.1 (Re), *Bradyrhizobium japonicum* WP_014491643 (Bj), *Nitrobacter winogradskii* WP_041344966.1 (Nw), *Rhodobacter sphaeroides* WP_107672675 (Rs), and animal homologs *C. elegans* NP_001254152 (CeM05), *Seriola quinqueradiata* BAC67703.1 (SqYGHL1), *Homo sapiens* NP_001093138.1 (HsHIG1-1A) and NP_620175 (HsHIG1-2A), *Heterocephalus glaber* XP_021113455.1 (HgHIG1-1A) and XP_004836396.1 (HgHIG1-2A), *Bos taurus* NP_001071329 (BtHIG1-2A). **(B)** Sequence alignment of *S. cerevisiae* Rcf1 (ScRcf1) R67 and W68 residues within the QRRQ motif and Mic60 lipid binding R433 and W434 residues. Sequence alignment includes Rcf1 bacterial homologs *Bradyrhizobium japonicum* WP_014491643 (Bj), *Rhodobacter sphaeroides* WP_107672675 (Rs), *S. cerevisiae* KZV09957.1 (ScMic60), *H. sapiens* NP_006830.2 (HsMic60).

absence of Rcf1, complex IV abundance is decreased, and consequently fewer III-IV supercomplexes can be formed. Based on the observed decrease in supercomplex III-IV levels in absence of Rcf1, Rcf1 and Rcf2 were initially proposed to be promoting and required for respiratory III-IV supercomplex formation (Vukotic *et al.,* 2012; Cui *et al.,* 2014). Despite lower complex IV levels, all of complex IV assembles into the supercomplex in the mitochondria lacking both Rcf1 and Rcf2 (Strogolova *et al.,* 2012). Furthermore, our lab and others have demonstrated that Rcf1 is not a stoichiometric component of the III-IV supercomplexes, as would be expected if it was provided a bridge connecting or stabilizing the supercomplex structurally (Garlich *et al.,* 2017).

Rcf1 interacts with subunit 3 of complex IV immediately following Cox3 synthesis and prior to its assembly into the enzyme. This observation led to the suggestion that Rcf1 may be a Cox3 chaperone mediating its folding and maturation, and possibly lipid modification. Rcf1 can also be found in association with Cyt1*,* Qcr6, and AAC, all lipid (CL) binding OXPHOS proteins, which led to the proposal that Rcf1 may be a lipid (CL) chaperone (Strogolova *et al.,* 2012, Garlich *et al.,* 2017).

Current structural studies of complex IV and supercomplex III-IV did not detect Rcf1, Rcf2 or HIGD protein. Rcf1 is in proximity to complex III subunit cytochrome c_1 and AAC; mutation of the QX3RXRX3Q motif influences these interactions (J.Garlich, PhD disseration, Garlich *et al.*, 2017). The QX3RXRX3Q motif may be involved in lipid-binding. In addition to the OXPHOS proteins, Mic10, a component of MICOS complex, which forms cristae junctions, was

found to co-purify with both Rcf1 and Rcf2 (Alkhaja *et al.*, 2012). Cristae junction formation is thought to be coordinated with the position of OXPHOS supercomplexes (Alkhaja *et al.,* 2012, Friedman *et al.,* 2015). Cristae junction formation is initiated by the lipid remodeling protein Mic60; Mic60 conserved Arg(R)433 and Trp(W)434 amino acid residues are directly involved in binding phospholipid membranes (Hessenberger *et al.,* 2017). Arg65 and Trp66 residues within the Rcf1 QX3RXRX3Q motif are homologous to Mic60 lipid-binding site 1 (LBS1) (Figure 3B), suggesting that Rcf1 may have a lipid binding site.

1.6. Objectives of the research

Despite considerable interest in HIGD proteins, their role in respiration is not clearly understood. HIGD proteins interact with a subpopulation of III-IV supercomplex. HIGD proteins, including yeast Rcf1, regulate abundance and electron transport activity of complex IV, but the mode(s) of regulation are not determined. Whether proton pumping activity of complex IV or OXPHOS efficiency are affected by HIGD proteins has never been addressed.

Rcf1 specifically interacts with respiratory complex IV subunit 3 (Cox3) during its assembly (Strogolova *et al.*, 2012; Su *et al.,* 2014B; Garlich *et al.,* 2017). In the Δ*rcf1* mitochondria, steady state levels of Cox3 and of complex IV are decreased. Despite the decreased OXPHOS complex IV levels, the Δ*rcf1* strain does not display a strong respiratory growth deficiency, and neither does Δ*rcf2* strain. The Δ*rcf1;*Δ*rcf2* double mutant however has a strong respiratory

growth deficiency thought to be due to loss of complex IV levels from the loss of function of Rcf1 and Rcf2. However, previous studies have not indicated a role of Rcf2 in complex IV assembly or stability. Deletion of *RCF2* does not diminish complex IV or III-IV supercomplex steady-state levels. The molecular function of the Rcf2 protein is unclear and respiratory growth deficiency when both Rcf1 and Rcf2 are deleted is not sufficiently explained. As paralogs, Rcf1 and Rcf2 are thought to function similarly, but this is not confirmed. This dissertation explores the molecular function of Rcf1 and Rcf2 in yeast mitochondria and seeks a more complete explanation for the respiratory growth deficiency of the Δ*rcf1;*Δ*rcf2* strain.

My first aim was bioenergetic characterization of the Δ*rcf1;*Δ*rcf2* mitochondria with a specific focus on complex IV, PMF maintenance and OXPHOS efficiency. I determined how the deletion of Rcf1 or Rcf2 affected mitochondrial respiratory complex levels, activity, oxygen consumption rate, and mitochondrial PMF.

Rcf1 and Rcf2 may play a wider role and influence non-COX proteins and functions such as proteolipid interactions or cristae architecture. My second aim was to characterize the consequences of Rcf1 and Rcf2 deletion on the content and activity of critical OXPHOS enzymes AAC and ATP synthase, as well as mitochondrial morphology.

Results presented in this dissertation indicate that both Rcf1 and Rcf2 are necessary for optimal PMF generation. However, Rcf2 contribution to complex IV assembly or stability is minor. Overall, Rcf1 and Rcf2 are proposed to regulate

proton transfer activity of complex IV. This important molecular function of Rcf1 and Rcf2 supports OXPHOS response to ADP, ATP synthesis, mitochondrial morphology, and respiratory growth. Future studies will focus on proton pumping activity of the isolated complex IV and identifying proton translocation defects or proton leaks develop in the absence of Rcf1 and Rcf2.

Additionally, Rcf1 and Rcf2 influence ATP synthase levels and activity, AAC stability, and proteolytic processing of several mitochondrial proteins. These non-COX defects can be a consequence of a lower PMF or may reflect additional functions of Rcf1/2; these explanations are not mutually exclusive and will require future studies of HIGD proteins in yeast and mammalian mitochondria.

CHAPTER 2. MATERIALS AND METHODS

This chapter describes the chemicals and biological reagents as well as molecular biology, cell biology and biochemical methods.

2.1. Materials

2.1.a. Chemical reagents

Chemical reagents used in this study are listed in Table 1.

Table 1. Reagents used in this study.

Source	Name
Alfa Aesar (Haverhill, MA)	Methanol Ethanol
Becton Dickinson (Sparks, MD)	Bacto™ Agar
Calbiochem	ethylenediaminetetraacetic acid (EDTA), sodium salt
ICN biomedicals (Aurora, Ohio)	Geneticin disulfide salt (G418)
Life Technologies (Carlsbad, CA)	4-acetamido-4'maleimidylstilbene-2,2'-disulfonic acid (AMS)
	Acrylamide
	Agarose
	Bisacrylamide
	Digitonin
	n-dodecyl-β-D-maltoside (DDM)
Mallinckrodt Baker (Phillipsburg, KY)	Sodium dodecyl sulfate (SDS)
Roche	Hexokinase / glucose-6-phosphate dehydrogenase
	Proteinase K

Serva (Heidelberg, Germany)	Ponceau S
Sigma (St. Louis, MO)	P1,P5-di(adenosine-5')pentaphosphate (Ap5A)
	Adenine diphosphate (ADP)
	Adenine triphosphate (ATP)
	Ammonium molybdate
	Ascorbic acid
	β-mercaptoethanol
	Bisacrylamide
	Bromophenol blue
	Bovine Serum Albumin (BSA)
	carbonyl cyanide m-chlorophenylhydrazone (CCCP)
	DL-lactic acid
	Dithiothreitol (DTT)
	ferrous sulfate
	Galactose
	Glycerol
	Glycine
	Hydrogen peroxide (H_2O_2)
	KCN
	Lithium dodecyl sulfate (LDS)
	Luminol
	Magnesium Chloride ($MgCl_2$)
	Mannitol
	N-(2-hydroxyethyl)-piperazine-N'-2-ethanesulfonic acid (HEPES)
	nicotinamide adenine dinucleotide, reduced form (NADH)
	NADP, oxidized form
	Nigericin
	N,N,N',N'-tetramethyl-*p*-phenylenediamine (TMPD)
	Oligomycin
	p-coumaric acid
	P1,P5-di(adenosine-5')pentaphosphate (Ap5A)
	phenylmethylsulphonyl fluoride (PMSF)
	Potassium chloride
	Potassium hexacyanoferrate (ferrocyanide)
	Potassium hydroxide
	Potassium phosphate (dibasic)
	Potassium phosphate (monobasic)
	Rhodamine 123
	Sodium dithionite (dithionite)
	Sodium hydroxide (NaOH)
	Sodium taurodeoxycholate (deoxycholate)
	Sorbitol
	Sulfuric acid

	Trichloroacetic acid (TCA)
	Tricine
	Triton X-100
	Trizma Base (Tris)
	Valinomycin
Sunrise Biologicals	Zymolyase
US Biologicals	Dropout mix, synthetic
	Peptone
	Yeast Extract
VWR	Glucose

2.1.b. Oligonucleotides

Oligonucleotides used in this study in polymerase chain reactions (PCR) for generation and verification of yeast strains are listed in Table 2.

Table 2. Oligonucleotides used in this study.

Name	Sequence
ST591 RCF1-FOR	5’-GGTAGCGAATCAAGGAGGGC-3'
ST592 RCF1-REV	5'-GTTTTAAGTGATAGTTATACAAG-3'
ST727 RCF2-FOR	5’- CTTTCTTATTTCCCTTTTAACC-3’
ST728 RCF2-REV	5'-CGAATGAATAGTTTTAGTTG-3'

2.1.c. Plasmids

Plasmid pRS416-mtGFP was a gift of R. Jensen (John Hopkins Medical School, Baltimore, MD). The mtGFP plasmid encodes a fusion of a yeast *COX4* mitochondrially targeted presequence (first 21 amino acids) fused to jellyfish

green fluorescent protein (GFP) and under the control of ADH1 promoter. Plasmid Yip351-His-Aac2 encodes a His-tagged Aac2p, $_{HIS}$Aac2, under the control of GAL10 promoter (Dienhart and Stuart, 2008).

2.1.d. Yeast strains

Saccharomyces cerevisiae (*S. cerevisiae*) strains used in this study are wild-type (WT; W303–1A, Mat a, *leu2, trp1, ura3, his3, ade2*), Δ*rcf1* (W303–1A, Mat a, *leu2, trp1, ura3, ade2, RCF1::HIS3*), Δ*rcf2* (W303–1B, Mat alpha, *leu2, trp1, ura3, his3, ade2, RCF2::KAN),* Δ*rcf1;*Δ*rcf2* (W303–1A, Mat a, *leu2, trp1, ura3, ade2, RCF1::HIS3, RCF2::KAN*) (Strogolova *et al*., 2012).

2.1.e. Antibodies

Antibodies used in this study are listed in Table 3.

Table 3. Antibodies used in this study.

Primary antibodies		
Targeted epitope	**Source**	**Origin**
AAC	Rabbit	Dr. Rosemary A. Stuart
Atp4	Rabbit	Dr. Jasvinder Kaur
Atp9	Rabbit	Dr. Jean Velours (France)

Ccp1	Rabbit	Dr. Rosemary A. Stuart
Cpr3	Rabbit	Dr. Rosemary A. Stuart
Cox1	Mouse	Invitrogen (Carlsbad, CA) # 11D8-B7
Cox2	Rabbit	Dr. Rosemary A. Stuart
Cox3	Mouse	Invitrogen (Carlsbad, CA) # 459300
Cox12	Rabbit	Dr. Klaus Pfanner (Freiburg, Germany)
Cox13	Rabbit	Dr. Klaus Pfanner (Freiburg, Germany)
Cyt *b*	Rabbit	Dr. Rosemary A. Stuart
Cyt b_2	Rabbit	Dr. Rosemary A. Stuart
Cyt *c*	Rabbit	Dr. Carla Koehler (Los Angeles, CA)
Cyt c_1	Rabbit	Dr. Rosemary A. Stuart
F_1 sector of ATP synthase	Chicken	Dr. David Mueller (Chicago, IL)
His tag	Rabbit	Bethyl (Montgomery, TX)
Mgm1	Rabbit	Dr. Rosemary A. Stuart
Mcr1	Rabbit	Dr. Carla Koehler (UCLA, CA)
MrpL32	Rabbit	Dr. Thomas Langer (Cologne, Germany)
Pgk1	Mouse	Dr. Anita Manogaran (Milwaukee, WI)
PIC	Rabbit	Dr. Klaus Pfanner (Freiburg, Germany)
Por1	Rabbit	Dr. Rosemary A. Stuart
Qcr7	Rabbit	Dr. Klaus Pfanner (Freiburg, Germany)
Rcf1	Rabbit	Dr. Rosemary A. Stuart
Rcf2	Rabbit	This study

Su e of ATP synthase	Rabbit	Dr. Rosemary A. Stuart
Tim17	Rabbit	Dr. Rosemary A. Stuart
Tim44	Rabbit	Dr. Carla Koehler (UCLA, CA)
Secondary antibodies		
Anti-rabbit IgG, horseradish peroxidase linked whole antibody	Sheep	Amersham Bioscience (England, UK)
Anti-mouse IgG, horseradish peroxidase linked whole antibody	Goat	Sigma (St. Louis, MO)
Anti-chicken IgG, horseradish peroxidase linked whole antibody	Goat	Sigma (St. Louis, MO)

2.2. Molecular biology methods

The basic molecular biology techniques such as polymerase chain reactions (PCR), restriction enzyme digestion of DNA, DNA precipitation, gel electrophoresis and gel purification of DNA, DNA ligation, preparation of *E.coli* competent cells, transformation of *E.coli*, colony PCR of *E.coli* cells, plasmid DNA extraction, DNA concentration determination, preparation of *S. cerevisiae* competent cells, transformation of the yeast *S. cerevisiae* and genomic DNA isolation were done according to Stuart lab protocols adapted from the book, Molecular Cloning: A Laboratory Manual by Sambrook, Fritsch and Maniatis.

2.2.a. Creating the *RCF1/2* deletion strains

Null Δ*rcf1* and Δ*rcf2* mutants were generated by a homologous recombination technique in the yeast strains W303-1A and W303-1B,

respectively. Briefly, a selective marker was PCR-amplified adding on either side of the marker 50-100 nucleotides shoulders, complementary to the DNA upstream and downstream of the region of interest (ROI). Transformation and recombination of the PCR product into competent yeast cells resulted in recombination and replacement of the ROI. The open reading frame *YML030W* (*RCF1*) on chromosome XIII was replaced with the *HIS3* gene. The open reading frame *YNR018W* (*RCF2*) on chromosome XIV was replaced with the KAN^{MX} , geneticin resistance cassette. Chromosomal deletions were confirmed by PCR.

The Δ*rcf1;*Δ*rcf2* double mutant was created by mating the two single mutant haploid strains, and tetrad dissection of the resulting diploid strain. Haploid segregants were selected based on complementation of histidine auxotrophy and geneticin-resistant growth. The genotype was confirmed by PCR of the chromosomal DNA.

2.3. Cell biology methods

2.3.a. Growth of yeast cultures

Yeast strains were maintained and cultured using standard protocols at 30°C on YP media supplemented with 2% glucose and 20 mg/L adenine hemisulfate (YPAD), Strains were stored in 15% glycerol at -80˚C. YP-0.5% lactate media supplemented with 2% galactose (YPGal), or YP media supplemented with 3% glycerol (YPG), as indicated. Where indicated the YPAD,

YPGal, and YPG agar was supplemented with 1.0 µM nigericin, oligomycin, antimycin A, or cycloheximide, at indicated concentrations.

2.3.b. Growth assays

Yeast strains were streaked fresh from freezer stocks and passaged on YPAD agar no more than 4 times prior to the assay. Yeast cells growing on YPAD agar 24 hours were re-suspended in sterile water to OD_{600nm} =0.1, and 10-fold serial dilutions in sterile water were made. The cell suspensions (3 µl) were spotted on nutrient agar. When the spots dried, the petri dishes were incubated at indicated temperatures.

2.3.c. Petite (rho$^{0/-}$) occurrence assay

The proportion of petite cells in cultures was measured on YPG plates supplemented with 0.1% glucose. Petite colonies appear small and stop growing on this media once the glucose is consumed, and they are unable to use glycerol (Soubannier *et al,* 2002). Even though Δ*rcf1*;Δ*rcf2* cells grow slowly on this media, they do not stop growing, so that after 6 days the Δ*rcf1*;Δ*rcf2* colonies reach the size that the wild-type colonies reach after 3 days. Cultures were grown overnight in YP-Gal, diluted in sterile water, and plated to yield 25-250 colonies per plate. The number of colonies that appear small (petite) after 5-7 days was counted and expressed as a percent of the total colonies (% rho$^{0/-}$).

2.3.d. Microscopy.

Yeast WT and Δ*rcf1* / Δ*rcf2* / Δ*rcf1*;Δ*rcf2* cells were transformed with pRS416-mtGFP plasmid. The transformants were streaked on a selective glucose media lacking uracil (SD-URA), grown for 24-48 hours and inoculated into liquid media containing galactose (SGal-URA). Aliquots of overnight culture (3 µl) on glass slides were imaged at 100X magnification. Three-dimensional (3D) images of mitochondria were taken using Leica DMI6000 B microscope (Dr. Anita Manogaran, Marquette University, Milwaukee, WI) using Z-stack feature. Nomarski differential interference contrast (DIC) channel and green fluorescent protein (GFP) channel were used. The excitation wavelength for GFP was 488 nm, and 470-510 nm emission was detected. Initial analysis and scoring of the images was performed manually using 2D maximal projection setting in the Leica LASX software. 3D images were subsequently analyzed in ImageJ software using the software plugin Yeast_MitoMap (Vowinckel *et al.*, 2015). Yeast_MitoMap automatically identified, traced and counted mitochondrial networks in each individual cell. Number of individual mitochondrial networks in each cell was recorded. Mitochondrial network fragmentation index *f* was calculated for each cell. The fragmentation index *f* is defined as a sum of relative fragment volumes that individually constitute less than 20% of mitochondrial volume of the network. Main mitochondrial network in each cell was selected by excluding fragments with volumes less than 20% of the total. Main mitochondrial

network volume, surface area, and other shape descriptive parameters were automatically calculated using Yeast MitoMap.

2.3.e. Whole cell protein extracts

Cultures were grown in YPGal at 30˚C and OD_{600nm} =0.6 was collected and washed with 0.5 ml of 40 mM potassium phosphate buffer pH 6.0. The cell pellet was resuspended in 75 µl Rodel mix (2.78 M NaOH, 11% β-mercaptoethanol, 15 mM PMSF), immediately 500 µl water was added followed by 575 µl 50% tricarboxylic acid (TCA). The TCA precipitated proteins were pelleted at 15000 g for 10 minutes and washed once with 0.5 ml of 0.5 M Tris (pH not adjusted) and once with water. The protein pellet was resuspended in 1.5X Laemmli buffer (3% SDS, 15% glycerol, 0.015% bromophenol blue, 3.25% β-mercaptoethanol, 90mM Tris, pH 6.8) and loaded on an SDS-PAGE gel.

2.3.f. Whole cell respiration

Whole cell respiration was measured as described previously (Barrientos 2002). Cultures were grown in YPGal at 30˚C to OD_{600nm} =0.6 (1 ml of culture at OD_{600nm} =0.6 corresponds to 1 x 10^7 cells). 2 x 10^7 cells were collected by centrifugation at 2500 rpm, washed with and resuspended in 1 ml buffer (0.3M mannitol, 10 mM KCl, 5 mM $MgCl_2$, 10 mM potassium phosphate, pH 7.4) and placed in an oxygen electrode chamber at 30˚C to measure endogenous

respiration. KCN (0.7 mM) was added to inhibit respiration. KCN-sensitive oxygen consumption is expressed as % of the wild-type.

2.3.g. Isolation of mitochondria

Yeast strains were streaked fresh from freezer stocks and grown to OD_{600nm} 1.5-2 on YPGal at 30˚C. Mitochondria were isolated according to the previously described method (Herrmann et al.,1994). Following isolation, mitochondria were resuspended in SEM buffer (250 mM sucrose, 2 mM EDTA, 10 mM MOPS-KOH pH 7.2) at a protein concentration of 10 mg/ml, flash-frozen in liquid nitrogen in 27 µl aliquots and stored at -80˚C. Aliquots were subsequently thawed on ice and used only once.

2.3.h. Protein concentration

Mitochondrial protein concentration was determined using the Bradford dye binding assay (Bradford, 1976). Bovine gamma globulin IgG (Bio-Rad) was used to generate standard curve.

2.4. Biochemical methods

2.4.a. Spectral analysis of mitochondrial cytochromes

Complex III or complex IV levels in the wild-type or mutant mitochondria were quantified based on dithionite reduced – ferrocyanide oxidized absorption spectra. The absorption spectra depend on the redox state of cytochromes: reduced *c*, *b*, and *a* type cytochromes absorb light at 552, 560, and 603 nm, respectively (absorption maxima). Cytochromes c_1 and *b* are part of complex III, while cytochromes *a* and a_3 are part of complex IV. Mitochondria (1 mg) were resuspended in 50 mM Tris-KCl, pH 7.4 buffer, containing 2% DDM (500 µl), incubated at room temperature with occasional mixing by inversion, and centrifuged 10000 rpm 5 minutes. 450 µl of the clarified supernatant was transferred to a 1 ml, 1 cm path cuvette. A crystal of potassium ferrocyanide was added and dissolved completely to oxidize the cytochromes, and absorbance in the 500 – 700 nm region was read five times. A few grains of sodium dithionite was added to the same sample to reduce mitochondrial cytochromes, and dissolved completely by stirring to reduce the cytochromes. Absorbance of the reduced spectra in the 500 – 700 nm region was recorded five times and the difference between reduced and oxidized spectra was calculated. A hand-drawn baseline from 700 nm to 630 nm was used to measure the height of the peak at 603 nm (Tzagoloff *et al*., 1975).

2.4.b. NADH-cytochrome *c* reductase activity assay

The NADH-cytochrome *c* reductase activity was measured by following the reduction of exogenously added ferro-cytochrome *c* at 550 nm. Mitochondria

were solubilized in 0.4% sodium deoxycholate and kept on ice. Mitochondria (20 µg protein) were added to 10 mM potassium phosphate buffer, pH 7.5, containing 0.1 mM KCN, 66 µM horse heart cytochrome *c.* The reaction was started by the addition of 0.1 mM NADH. Absorbance increase at 550 nm was recorded for 45-60 seconds, the rate cytochrome *c* reduction rate. (Tzagoloff *et al.,* 1975). Relative specific activities of the enzyme were calculated.

2.4.c. Cytochrome *c* oxidase activity assay

Cytochrome *c* oxidase enzyme activity was measured by following the oxidation of exogenously added ferro-cytochrome *c* at 550 nm. Mitochondria were solubilized with 1 mM n-dodecyl-β-D-maltoside (DDM) and kept on ice. Horse heart cytochrome *c* (Sigma) was reduced with 0.5 mM dithiothreitol (DTT) solution 15 minutes prior to the start of the experiment. Mitochondria (4 µg protein) were added to 10 mM Tris-HCl buffer, pH 7.0, containing 120 mM KCl, and 11 µM reduced horse heart cytochrome *c*. The concentration of KCl in the buffer was changed where indicated.

2.4.d. Oxygen consumption measurement in isolated mitochondria

Oxygen consumption rates (OCR) were calculated as the rate of decrease in oxygen concentration measured with a Clark-type oxygen electrode (Rank Brothers Digital Model 10) at 30˚C. Mitochondria (40 µg protein) resuspended in

0.5 ml respiration buffer (0.6 M mannitol, 2 mM $MgCl_2$, 1 mg/ml BSA, 20 mM HEPES-KOH, 1 mM EDTA, 10 mM K_2PO_4 pH 7.2) were added to the oxygen electrode chamber and the suspensions were continuously stirred. Oxygen consumption was recorded for 1 minute after the mitochondria were added to establish baseline. For state 2 measurements, NADH (1 mM) was added. State 2 OCR was recorded for 8-10 minutes. For state 3 measurements, NADH (1 mM) was followed by ADP (50-200 µM, as indicated). For state 2_{oligo} measurements, addition of the mitochondria was immediately followed by oligomycin (20 µM). To measure maximal OCR, NADH (1 mM) was followed by membrane uncoupler carbonyl cyanide m-chlorophenylhydrazone (CCCP) (10 µM in DMSO).

For measurement of oxygen consumption by bioenergetically isolated complex IV, mitochondria (20 µg protein) resuspended in 0.5 ml respiration buffer (0.6 M mannitol, 2 mM $MgCl_2$, 1 mg/ml BSA, 20 mM HEPES-KOH, 1 mM EDTA, 10 mM K_2PO_4 pH 7.2) were added to the oxygen electrode chamber and the suspensions were continuously stirred. Oxygen consumption was recorded for 1 minute after the mitochondria were added to establish baseline. At one minute, TMPD/ascorbate (1.4 mM N,N,N',N'-tetramethyl-p-phenylenediamine (TMPD) and 12.5 mM potassium ascorbate pH 7) were added. OCR was recorded for 1-6 minutes, and initial OCR (1 minute) was calculated. To measure maximal OCR, TMPD/ascorbate was followed by membrane uncoupler carbonyl cyanide m-chlorophenylhydrazone (CCCP) (10 µM in DMSO). A baseline of oxygen consumption in the absence of mitochondria with TMPD/ascorbate was recorded

and subtracted. KCN (0.2 mM) was added to inhibit respiration and confirm the absence of extramitochondrial respiration.

2.4.e. Membrane potential measurements

Rhodamine 123 (R-123) fluorescence at 488/525 nm was recorded using a fluorimeter (Dr. David Mueller, Chicago, Il). Mitochondria (150 µg protein) were resuspended in 2 ml of buffer (0.65M mannitol, 0.3 mM EGTA, 3mM Tris phosphate, 10 mM Tris maleate, pH 6.8) containing 0.5 µM Rhodamine 123 (in methanol). For State 2 measurements, NADH (2 mM) was added. For State 3 measurements, NADH was immediately followed by ADP (45 µM). At the end of each trace, the membrane potential was dissipated by CCCP (10 µM). Fluorescent signal in the presence of NADH+CCCP was set to 100% and changes in the fluorescence were expressed as % quenching relative to that signal. Mitochondrial membrane potential generated by ATP hydrolysis was measured as follows. Mitochondria (150 µg) were resuspended in 2 ml buffer containing 0.5 µM R-123 (in methanol); following the addition of ethanol (68 mM), KCN (0.2 mM), 2 mM ATP, 1 mM $MgCl_2$. R-123 fluorescence was recorded for ~1 minute followed by addition of oligomycin (20 µM), and CCCP (10 µM).

2.4.f. ATP synthesis and ATP export

ATP synthesis and ATP export rate were measured at 30˚C according to published methods (Hamazaki *et al*., 2011; De Marcos Lousa *et al., 2*002) with modifications described here. Mitochondria (40 µg of protein) were resuspended in 0.7 ml of ATP detection buffer (0.6 M mannitol, 0.1 mM EGTA, 2 mM $MgCl_2$, 10 mM potassium phosphate, 5 mM alpha-ketoglutarate, 0.01 mM Ap5A, 2.5 mM glucose, 0.2 mM NADP, 10 mM Tris-HCl, pH 7.4) containing the ATP detection enzymes (hexokinase (1.7 E.U.) / glucose-6-phosphate dehydrogenase (0.85 E.U.). The exchange reaction was initiated by adding oligomycin (20 µM) and ADP (20 µM). The rate of ATP release was monitored as the rate of NADPH formation (increase in NAD(P)H absorbance at 339 nm). The reactions were carried out in quartz cuvettes (Hellma). Absorbance was measured with Beckman Coulter DU800 spectrophotometer.

Endpoint ATP synthesis assays were carried out as follows. ADP was added to the mitochondria (40 µg of protein) resuspended in ATP detection buffer (0.6 M mannitol, 0.1 mM EGTA, 2 mM $MgCl_2$, 10 mM potassium phosphate, 5 mM alpha-ketoglutarate, 0.01 mM Ap5A, 2.5 mM glucose, 0.2 mM NADP, 10 mM Tris-HCl, pH 7.4) without the ATP detection enzymes containing ethanol or succinate in presence of oligomycin (1 µM or lower concentration as indicated in the experiment) or DMSO. After the indicated times, synthesis was stopped and mitochondria removed by 10 minute centrifugation at 10000 rpm, and the supernatant was transferred to a fresh tube. ATP in supernatant was converted to NADPH by adding the ATP detection enzymes and incubating for 5 minutes at

30˚C. Alternatively, mitochondrial membranes were solubilized with deoxycholate (0.2%) and the ATP detection enzymes added to assay total ATP.

2.4.g. ATP hydrolysis

Oligomycin-sensitive F_1F_O ATPase activity was assayed at 30˚C at pH 8.4 according to Velours *et al,* 2001 with following modifications. Mitochondria were diluted to protein concentration 5 mg/ml either with SEM buffer (250 mM sucrose, 2 mM EDTA, 10 mM MOPS-KOH pH 7.2) or with 0.375% Triton X-100, as indicated. Aliquots containing 50 µg mitochondrial protein were incubated for 2 minutes in reaction buffer (0.9 ml, 0.2 M KCl, 3 mM $MgCl_2$, 10 mM Tris-HCl, pH 8.4) in the presence or absence of oligomycin (20 µM, in ethanol). The reaction was started with the addition of 5 mM ATP and stopped after 2 minutes by the addition of tricarboxylic acid (TCA) (0.3 M, final concentration). Following a 10-minute, 10000 rpm, 4˚C centrifugation step, inorganic phosphate in the supernatant was measured using ferrous sulfate / ammonium molybdate method (Sumner 1944). Mitochondrial extract supernatant or known phosphate concentration (0.5 ml) was added to measurement solution (2.5 ml) (0.67% ferrous sulfate, 0.55% ammonium molybdate, 0.75 N sulfuric acid), incubated for 15 minutes at room temperature, and Abs_{610nm} was measured. A standard curve with 0, 50, 100, 150, 200, 300, 400 500 mmol potassium phosphate was used for calibration.

2.4.h. TCA precipitation of proteins

Mitochondria (20 µg of protein) were resuspended in 200 µl of water, and 85 µl of 50% TCA was added. Precipitated proteins were pelleted at 15000 g 10 minutes, washed with 0.5 ml of 0.5 M Tris (pH not adjusted) and with water. Protein pellet was resuspended in 1.5X Laemmli buffer (3% SDS, 15% glycerol, 0.015% bromophenol blue, 3.25 % β-mercaptoethanol, 90mM Tris, pH 6.8) and loaded on an SDS-PAGE gel.

2.4.i. SDS-PAGE

17.5% acrylamide, 0.2% bis-acrylamide sodium dodecyl sulfate polyacrylamide gel electrophoresis (SDS-PAGE) gels were prepared according to Laemmli, 1970. Molecular weight markers (14-116 kDa, ThermoFisher) was used to estimate position and size of the proteins.10-15 µl of sample in 1X Laemmli buffer (2% SDS, 10% glycerol, 0.01% bromophenol blue, 2.5 % β-mercaptoethanol, 60mM Tris, pH 6.8) was loaded on each lane of the gel. SDS-PAGE was performed at 25 mA in 1X electrophoresis buffer (2M glycine, 0.1% SDS, 50 mM Tris) for 2 hours.

2.4.j. BN-PAGE

Mitochondria (30 µg) were solubilized in 10 µl Invitrogen pink buffer (50 mM Bis-Tris, 6N HCl, 50 mM NaCl, 10% w/v glycerol, 0.001% Ponceau S, pH 7.2) with the addition of either 1% digitonin or 0.6% DDM. Samples were incubated 20 minutes on ice and centrifuged for 10 minutes at 15000 rpm, 4˚C. The clarified supernatant was transferred to a new tube and G250 Coomassie added to final concentration of 1.75%. Following sample preparation, mitochondrial respiratory complexes and other proteins were separated on a 3-12% Blue Native PAGE (BN-PAGE). NativeMark™ protein standards were used to estimate the molecular weights of the complexes. Pre-cast 3-12% Bis-Tris mini-gels (8cm x 8cm, 1.0 mM thickness) were ran for 5 hours at 4˚C using Novex® NativePAGE™ Bis-Tris gel system (Invitrogen/ThermoFisher Scientific). The gels were transferred to nitrocellulose membrane (Whatman) using semi-dry blotting system and Western blotting buffer (20% Methanol, 150 mM glycine, 0.02% SDS, 20 mM Tris, pH not adjusted), with the modification of 1 hour transfer time. Blots were prepared for detection by incubating in Western strip buffer (25 mM glycine, 100 mM NaCl, 0.05% Tween-20, pH 2.0) and blocked with 5% milk in TBS solution for 30 minutes.

2.4.k. Two-dimensional electrophoresis

Second-dimension-PAGE separation was performed after the BN-PAGE step. Mitochondria (200 µg protein) were solubilized in lysis buffer (34 mM potassium acetate, 34 mM HEPES-KOH, pH 7.4, 11.4% glycerol, and 1 mM

PMSF) containing 1% digitonin. Samples were incubated on ice 30 minutes and subjected to a clarifying spin for 30 min at 30,000 *g,* 4°C. The supernatant from each sample was analyzed on a BN-PAGE as described (Cruciat *et al.,* 2000; Saddar *et al.,* 2008). Individual lanes of the BN-PAGE were excised with a razor blade gel. Each gel strip was incubated in lithium dodecyl sulfate (LDS) (4X LDS (106 mM Tris-HCl, 14 mM Tris Base, 2% LDS, 10% glycerol, 0.51 mM EDTA, 0.22 mM G250 Coomassie, 0.175 phenol red, pH 8.5). Strips were incubated for 30 minutes in each, LDS-DTT (50 mM dithiothreitol (DTT), 1 X LDS), LDS-DMA (N,N-dimethylacrylamide) (50 mM DMA, 1X LDS), and LDS-Ethanol-DTT (5 mM DTT, 20% ethanol, 1X LDS). Each strip was inserted on top of a denaturing NuPAGE™ Bis-Tris gel, and electrophoresis was performed at 100 V for 1.5-2 hours. NativeMark™ and protein standards were used in the first dimension to estimate the molecular weights of the complexes. 14-166 kDa molecular weight markers (ThermoFisher) were used in the second dimension to determine the sizes of protein subunits.

2.4.I. Western blot analysis

Proteins were transferred from polyacrylamide gels to nitrocellulose membrane (Whatman) using semi-dry blotting method for 1.5 hours (unless otherwise specified) at 250 mA in transfer buffer (20% Methanol, 150 mM glycine, 0.02% SDS, 20 mM Tris) (Kyhse-Andersen, 1984). Membranes were stained with Ponceau S solution to visualize molecular weight markers, then

rinsed completely with water. Membrane was then used for autoradiography, or blocked in 5% milk in 1X TBS (150 mM NaCl, 10 mM Tris-HCl pH 7.5) for 1 hour before immunodetection. Membranes were incubated in primary antibody solution. Signal generation was then achieved using secondary antibodies conjugated with horseradish peroxidase (HRP) via chemiluminescence in a buffer containing 100 mM Tris pH 8.5, 0.23 mM p-coumaric acid, 1.25 mM luminol, 0.00015% [v/v] H_2O_2 as previously described (Roswell and White, 1978). Films were developed using an automated developing machine (AGFA CP1000).

2.4.m. Ni NTA affinity purification

Mitochondria from the wild-type and Δ*rcf1*;Δ*rcf2* cells expressing $_{HIS}$Aac2 were subjected to Ni-nitrilotriacetic acid (Ni-NTA) affinity purification. His-tagged protein and their interacting partners were purified from isolated mitochondria (200 µg total protein) solubilized in 300 µl of lysis buffer (31 mM HEPES, 80 mM potassium acetate, 10% glycerol, 1mM PMSF and 0.6% Digitonin) for 30 min on ice. After a clarifying spin (10000 rpm, 10 min at 4˚C), the supernatant was collected, supplemented with imidazole (30 mM final concentration) and incubated with Ni-NTA beads (pre-equilibrated in lysis buffer) for 1 hour at 4˚C. The beads were then washed three times with lysis buffer containing imidazole and the bound proteins were eluted with SDS-sample buffer containing 5% β-mercaptoethanol and 450mM Imidazole. Samples were analyzed by SDS-PAGE and Western blotting.

2.4.n. Mitochondrial translation

Translation *in organello* with [^{35}S] methionine labeling was performed for as described in Hell *et al*., 2001. Briefly, translation was carried out for 20 mintues at 30˚C in presence of [^{35}S] methionine. Translation was stopped by addition of puromycin and excess unlabeled methionine, followed by 5-minute incubation. The mitochondria were collected by centrifugation and subjected to SDS-PAGE.

2.4.o. Quantitation of Western blot band intensities.

Exposed films were scanned in 600 dpi transmission mode on Epson V750 PRO scanner and band density was quantified using ImageJ Gel Analysis method (Gassmann *et al*, 2009). Relative density was adjusted to loading control.

2.4.p. Statistical analysis.

Data were collected and analyzed using GraphPad Prism software version 7 (La Jolla, CA). Mean and standard error of mean (SEM) values (McDonald, 2014) are derived from at least 3 experiments unless otherwise noted. Where applicable, statistical significance between two experimental variables was evaluated using Student’s t-test ($p<0.05$ was considered significant).

CHAPTER 3. Deletion of Rcf1 and Rcf2 cumulatively impairs OXPHOS coupling, evidenced by elevated oxygen consumption and lowered membrane potential

Introduction

The *RCF1* and *RCF2* genes are needed for optimal yeast growth on non-fermentable carbon sources. Utilization of non-fermentable carbon sources (glycerol, ethanol, lactate) for energy requires activity of the electron transport chain (ETC) of the yeast mitochondria, including the activities of the cytochrome bc_1 reductase (complex III) and the cytochrome *c* oxidase (C*c*O, complex IV) enzymes.

In yeast mitochondria, all complex IV molecules are assembled into supercomplexes of III_2IV_2 or III_2IV_1 composition. Prior studies identified Rcf1 involvement in chaperoning Cox3 prior to its assembly into the supercomplex III-IV and supporting assembly and enzyme activity of complex IV (Strogolova *et al*., 2012; Garlich *et al*., 2017). The role of Rcf2 in complex IV assembly or enzyme activity, or III-IV supercomplex content is not apparent (Strogolova *et al*., 2012; Römpler *et al*., 2016; Fischer *et al*., 2015). Deletion of Rcf1 or Rcf2 (Δ*rcf1* and Δ*rcf2* strains) does not strongly influence respiratory growth, but the combined deletion of Rcf1 and Rcf2 together leads to a respiratory growth defect.

In this chapter, the consequences of Rcf1 and Rcf2 deletion on mitochondrial respiration was evaluated by growth and respiration assays and measuring the steady-state levels and catalytic activities of complex III and complex IV. Previous studies focused only on electron transfer (oxygen

consumption) capacity of complex IV enzyme. In particular, this study investigated whether Rcf1 or Rcf2 regulate proton transport function of complex IV. Direct measurement of proton transport by complex IV is not trivial since it requires purified enzyme inserted in phospholipid vesicles. Detergent purified enzyme tends to lose stability, activity, and proteolipid context. Alternatively, complex IV proton transport activity can be accurately inferred from ETC response to ADP or CCCP, obtained from the oxygen consumption rates (OCR) measurements in isolated mitochondria (Barrientos 2002; Brand and Nicholls, 2011; Gouspillou *et al*., 2011). Protonmotive force (PMF) also can be measured in respiring mitochondria using membrane-potential dye Rhodamine 123 (R123). In order to dissect the bioenergetic consequences of Rcf1 and/or Rcf2 removal, measurements of OCR and PMF in intact mitochondria in response to controlled substrates are presented in this chapter.

Results

3.1. *RCF1* or *RCF2* can independently support respiratory growth.

In order to understand the bioenergetic consequences of Rcf1 and/or Rcf2 removal, respiratory growth phenotypes of Δ*rcf1* and Δ*rcf2* mutants (Δ*rcf1::HIS3* and Δ*rcf2::KAN*^{MX}) in the yeast strain W303-1A were studied. Deletion of *RCF1* slightly hindered respiration-based growth (Figure 4A, second column in each panel). We conclude therefore that deletion of RCF1 does not severely

compromise the ability of the cell to grow by aerobic respiration in the genetic background (W303) used in this study.

The deletion of the *RCF2* gene by homologous recombination (Materials and Methods) did not impair growth on non-fermentable carbon sources such as glycerol (YPG) or lactate (YPL) (Figure 4A, third column in each panel). This is consistent with the Δ*rcf2* phenotypes reported in the BY4741 genetic background (Vukotic *et al.*, 2012, Römpler *et al.*, 2016). In contrast to growth on solid agar, respiration-based growth of Δ*rcf2* mutant in liquid media was slower than the wild type and Δ*rcf1* strains (Figure 4B). The slower respiration-based growth in liquid media was not linked to slower glucose de-repression, since this phenotype was the same whether cultures were pre-grown in YPD or YPG or YPL. Stress, such as growth in liquid culture or elevated temperature conditions, can enhance subtle respiratory deficiencies, such as that of the Δ*coa6* mutant (Ghosh *et al.*, 2014). This indicates that the Δ*rcf2* strain, which otherwise has been described as showing normal respiration-based growth, has a modest but measurable respiratory deficiency.

It is possible that slower Δ*rcf2* respiration-based growth in liquid media is resulting from the lower concentration of dissolved oxygen compared to that available on the surface of agar (Somerville and Proctor, 2013). If this was the case, limiting oxygen levels would decrease Δ*rcf2* growth solid agar media. To test this, respiratory growth on solid media was assayed in a hypoxic chamber (2% oxygen). In contrast to normoxia (21% oxygen), Δ*rcf2* grew slower than wild type in a hypoxic chamber (Figure 4C, right panel). This result confirms the sub-

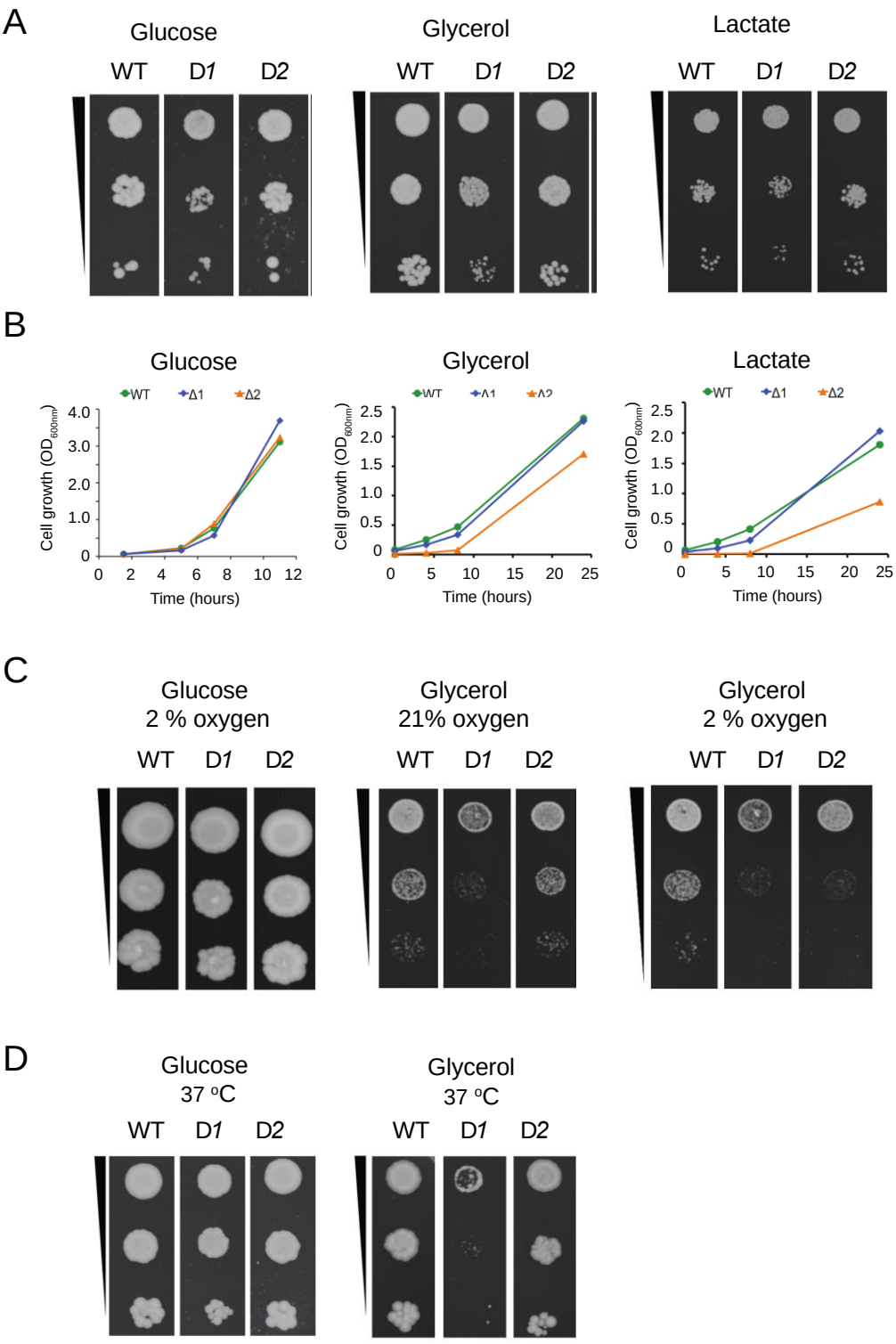

Figure 4. Respiratory growth of single mutants. (A) Serial dilutions of wild type, Δ*rcf1*, Δ*rcf2* yeast cells were spotted on YP media containing 2% glucose, 3% glycerol, or 2% lactate and

incubated at 30˚C for 3 days. In these and subsequent growth assays, the relative cell concentration is indicated by the black wedges. **(B)** Overnight wild type (green), Δ*rcf1* (blue) and Δ*rcf2* (orange) liquid cultures were inoculated in fresh liquid YP media containing 2% glucose, 3% glycerol, or 2% lactate at 30˚C with a starting OD_{600} of 0.1. OD_{600} was measured at indicated times. **(C)** Serial dilutions of wild type (WT), Δ*rcf1* (Δ*1*), Δ*rcf2* (Δ*2*) were spotted on YP media containing 2% glucose or 3% glycerol and incubated at 21˚C for 5 days under normoxia (21% oxygen) or hypoxia (2.5% oxygen). **(D)** Serial dilutions done as in **(A)** and incubated at elevated temperature (37˚C) for 5 days. In this and subsequent figures, the wild type, Δ*rcf1*, and Δ*rcf2* mutants are denoted as WT, Δ*1*, Δ*2*, respectively.

threshold respiration defect in Δ*rcf2* strain that was enhanced by limiting oxygen.

Respiration-based growth of Δ*rcf1* on glycerol was slowed down by decreased (21˚C) (Figure 4C, second panel) or increased temperature (37˚C) (Figure 4D, second panel), compared with optimal temperature (Figure 4A, second panel). This is consistent with the presence of respiratory growth defect in Δ*rcf1* strain that can be exacerbated by suboptimal temperature conditions.

In summary, Rcf1 or Rcf2 alone (as in the Δ*rcf2* and Δ*rcf1* strains, respectively) are sufficient for *S. cerevisiae* respiratory growth under optimal conditions. Stress conditions such as hypoxia or suboptimal temperature reveal that the removal of Rcf1 or Rcf2 caused a subthreshold respiratory growth inefficiency.

3.2. Deletion of RCF1 and RCF2 together impairs respiratory growth.

The Δ*rcf1;*Δ*rcf2* double mutant was created by mating the single mutant haploid strains (Δ*rcf1::HIS3; MAT A* and Δ*rcf2::KAN^{MX}; MAT α*) to generate a diploid (*RCF1/*Δ*rcf1::HIS3; RCF2/*Δ*rcf2::KAN^{MX}*). The diploid was subjected to

sporulation (meiosis) and tetrad dissection to generate double mutant haploid strains (Δ*rcf1::HIS3;* Δ*rcf2::KAN*^{MX}). Respiratory growth of four independently isolated Δ*rcf1;*Δ*rcf2* double mutant haploids was analyzed, and all showed identical growth defect on non-fermentable carbon sources. The Δ*rcf1;*Δ*rcf2* respiratory growth was slow on glycerol, lactate (Figure 5), methanol, acetate, succinate, ethanol, as carbon sources (not shown); thus, the respiratory defect was not linked to inability to utilize a specific carbon source. Some OXPHOS mutants display increased loss of mitochondrial DNA (rho), resulting in formation of spontaneous rho^0/rho$^-$ petite colonies. *RCF1* and *RCF2* genes were identified in a genomic screen for alleles associated with abnormal inheritance of mitochondrial DNA (AIM) (Hess *et al*., 2009); deletion of these genes individually decreased the rate of spontaneous rho^0/rho$^-$ petite colonies. To test whether accumulating rho^0/rho$^-$ petite cells was responsible for respiratory deficiency of the Δ*rcf1;*Δ*rcf2* strain, the rate of spontaneous rho^0/rho$^-$ petite colonies was assessed by colony count on YPG plates supplemented with 0.1% glucose (see Materials and Methods). The rate of rho^0/rho$^-$ petite formation was not increased in Δ*rcf1;*Δ*rcf2* (0.6 ± 0.8%) compared to wild type (3.3 ± 1.6%).

In summary, the Δ*rcf1;* Δrcf2 mutant strain (but not the Δ*rcf1* or Δ*rcf2* single mutants) displays a robust, reproducible growth defect on non-fermentable carbon sources. No increase in rho^0/rho$^-$ petite formation was detected in the mutant. Our lab previously showed that the Δ*rcf1;*Δ*rcf2* respiratory growth could be restored by ectopic expression of Rcf1 or Rcf2 protein with C-terminal His_{12} tag (Strogolova *et al*., 2012). This is consistent with the *RCF1* and *RCF2* gene

products having partially redundant or overlapping function(s) that support respiration-based growth.

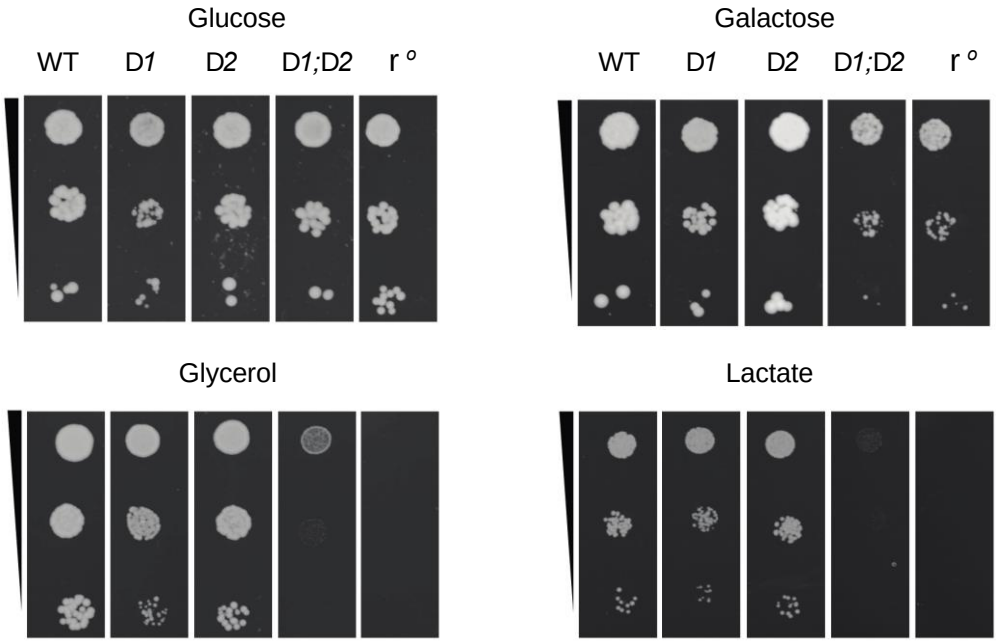

Figure 5. Respiratory growth of Δ*rcf1;*Δ*rcf2* mutant. Serial dilutions wild type , Δ*rcf1*, Δ*rcf2*, and the Δ*rcf1;*Δ*rcf2* (Δ*1*;Δ*2*) cultures were spotted on rich (YP) agar containing glucose (2%), galactose (3%), or non-fermentable substrates glycerol (3%), lactate (2%), and incubated for 3 days at 30˚C. A wild type petite control strain (ρ^0) is shown for comparison.

3.3. Deletion of RCF2 increased endogenous cell respiration.

To further explore whether the observed growth defect of the Δ*rcf1;*Δ*rcf2* cells was due to decreased mitochondrial content of these cells and/or decreased mitochondrial oxygen consumption, levels of mitochondrial proteins in

whole cell extracts and respiration in whole cells were measured. Whole cell oxygen consumption was measured in cultures in liquid galactose containing media. Galactose can be used as a fermentable or non-fermentable carbon and energy source (Lagunas 1986; Herrero *et al*., 1985; Fendt and Sauer, 2010). Mitochondrial dysfunction leads to enhanced galactose fermentation (Jelicić *et al.,* 2005), and the Δ*rcf1;*Δ*rcf2* grew slower than wild type on galactose, but not as slow as on glycerol (Figure 5). Despite their respiration-based growth defect, oxygen consumption in the Δ*rcf1;*Δ*rcf2* cells was ~90% of the wild type cells (Figure 6A, Table 4). A similar oxygen consumption rate was measured for the Δ*rcf1* cells. Surprisingly, the oxygen consumption rate in Δ*rcf2* cells was even increased and was ~140% of that in wild type control. This result is in agreement with previously reported increased oxygen consumption by Rcf2-deficient mitochondria with various respiration substrates (pyruvate/malate, succinate, TMPD/ascorbate, and ADP) (Römpler *et al*., 2016). The nearly normal or enhanced oxygen consumption rates indicate that the respiration-based growth defect observed in the absence of Rcf1 and Rcf2 is not merely due to the inability of the cells to consume oxygen.

To determine whether cell mitochondrial content was altered (or even increased) in the absence of Rcf1 and/or Rcf2, levels of mitochondrial proteins in the cell were analyzed. Whole cell protein extracts were prepared from cultures grown in galactose and were analyzed by SDS-PAGE and Western blotting (Figure 6B). Mitochondrial content was determined by measuring the levels of the mitochondrial outer membrane protein (Por1) and was found to be similar

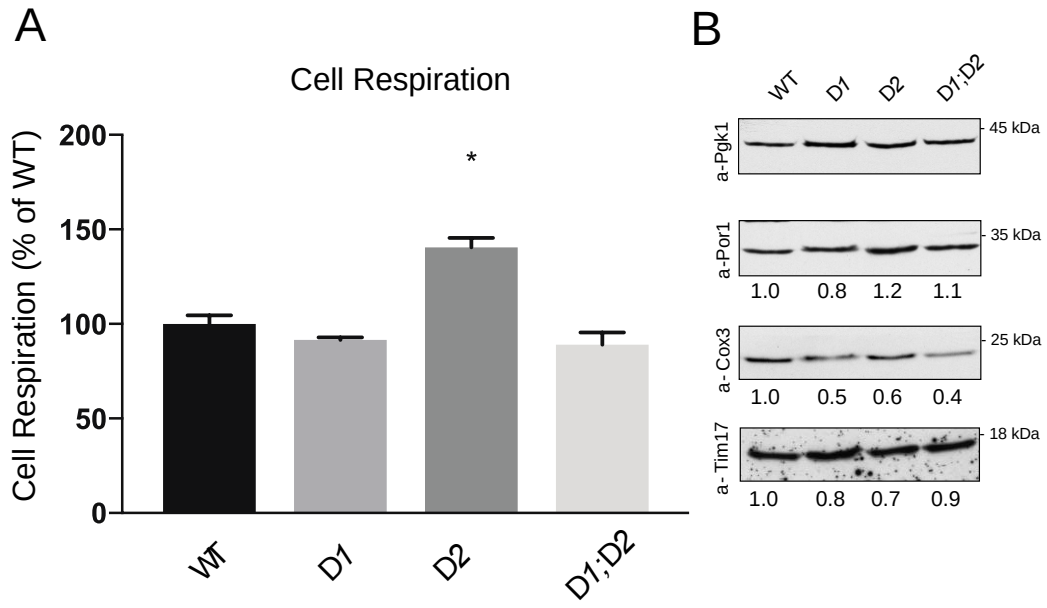

Figure 6. Whole cell respiration and mitochondrial content from the Δ*rcf1*, Δ*rcf2*, and Δ*rcf1*;Δ*rcf2* mutants. Indicated strains were grown on YPGal to exponential phase and harvested at an OD_{600nm}=0.6. **(A)** Endogenous respiration was measured in YPGal grown cells. KCN-sensitive oxygen consumption rate (OCR) was expressed as % of the wild type. Average ± SEM is shown and statistical significance (Student's t-test) $p<0.05$ denoted by asterisk. **(B)** Whole cell protein extracts were analyzed by SDS-PAGE and Western blotting using antibodies to 3-phosphoglycerokinase (Pgk1), mitochondrial outer membrane porin (Por1), mitochondrial inner membrane Tim17, and complex IV subunit 3 (Cox3). Relative band intensity adjusted to Pgk1 is indicated below each band. The positions of the molecular mass standards are indicated on the right (in kilodaltons).

Table 4. Whole cell respiration of the Δ*rcf1*, Δ*rcf2*, and Δ*rcf1*;Δ*rcf2* mutants.

Summary of oxygen consumption data represented in Figure 6A.

Strain	Cell endogenous respiration % of WT
WT	100
Δ*1*	92 ± 3
Δ*2*	141 ± 7
Δ*1*;Δ*2*	89 ± 13

between all cell types. The ratio of Por1 to the cytoplasmic protein 3-phosphoglycerate kinase (Pgk1) was not affected by the absence of Rcf1 or Rcf2 (Por1/Pgk1 signal in wild type= 1.0, Δ*rcf1* = 0.8, Δ*rcf2* =1.2, Δ*rcf1;*Δ*rcf2* = 1.1) (Figure 6B). Similar result was obtained for the levels of the inner membrane translocase subunit protein Tim17. Tim17 and Por1 are proteins that are constutively expressed and frequently used to evaluate mitochondrial levels. We conclude therefore that the absence of Rcf1 and Rcf2 did not alter the cell's mitochondrial levels. In contrast, the levels of complex IV marker, subunit 3 (Cox3) were decreased in Δ*rcf1*, Δ*rcf2* and Δ*rcf1;*Δ*rcf2* cells compared to the wild type cells, indicating a decrease in complex IV (Figure 6B). This indicates decrease in complex IV steady state levels relative to other mitochondrial membrane proteins (see section 3.4.).

In summary, the analysis of whole cell respiration and mitochondrial content established that the observed impaired growth of the Δ*rcf1;*Δ*rcf2* strain on non-fermentable carbon sources is not due to limiting mitochondrial levels or the ability of these mitochondria to consume O_2. Moreover, the enhanced O_2 consumption rate of the Δ*rcf2* strain may suggest an inefficiency of the ETC system to generate and/or maintain a PMF, and thus require an elevated O_2 consumption rate to maintain the PMF at levels required to sustain OXPHOS-based ATP synthesis.

3.4. Deletion of Rcf1 and Rcf2 lower complex IV steady-state levels, but deletion of Rcf1 is epistatic to deletion of Rcf2.

Both complexes III and IV contribute to the establishment of the PMF. To gain more insight into the possible problem with establishing or maintaining the PMF in the absence of Rcf2 (and possibly Rcf1), the content and activities of these enzymes in isolated mitochondria were initially analyzed.

The cytochromes of the OXPHOS complexes within the mitochondria are heme-containing proteins, whose spectral properties can be used to quantify their content. The complex III (cytochrome bc_1) and complex IV (cytochrome aa_3) levels were initially quantified in the wild type or mutant mitochondria by recordings of the dithionite reduced – ferrocyanide oxidized spectra (Figure 7A, Table 5). In Δ*rcf2*, complex IV cytochrome aa_3 levels were moderately decreased to 69% of the wild type levels. In Δ*rcf1*, the cytochrome aa_3 levels were decreased more substantially (52% of wild type). The cytochrome aa_3 levels in the Δ*rcf1;*Δ*rcf2* mitochondria (49% of wild type) were similar to those measured in the Δ*rcf1* mitochondria (Table 5).

Table 5. Quantification of mitochondrial cytochromes

The absorption bands corresponding to cytochromes (aa_3, *b*, and cc_1) were quantified using A603 nm (to account for sloping baseline, a baseline was hand-drawn through A700 and A630 and extended to 603 nm), A560 nm (baseline at A575 was subtracted) and A550 nm (baseline at A575 was subtracted). Average and S.E.M. values are reported, expressed as % of wild type control.

Strain	aa_3	*b*	cc_1
WT	100 ± 4	100 ± 6	100 ± 5
Δ*1*	52 ± 15	116 ± 4	92 ± 7
Δ*2*	69 ± 10	122 ± 2	92 ± 6
Δ*1*;Δ*2*	49 ± 7	155 ± 12	129 ± 11

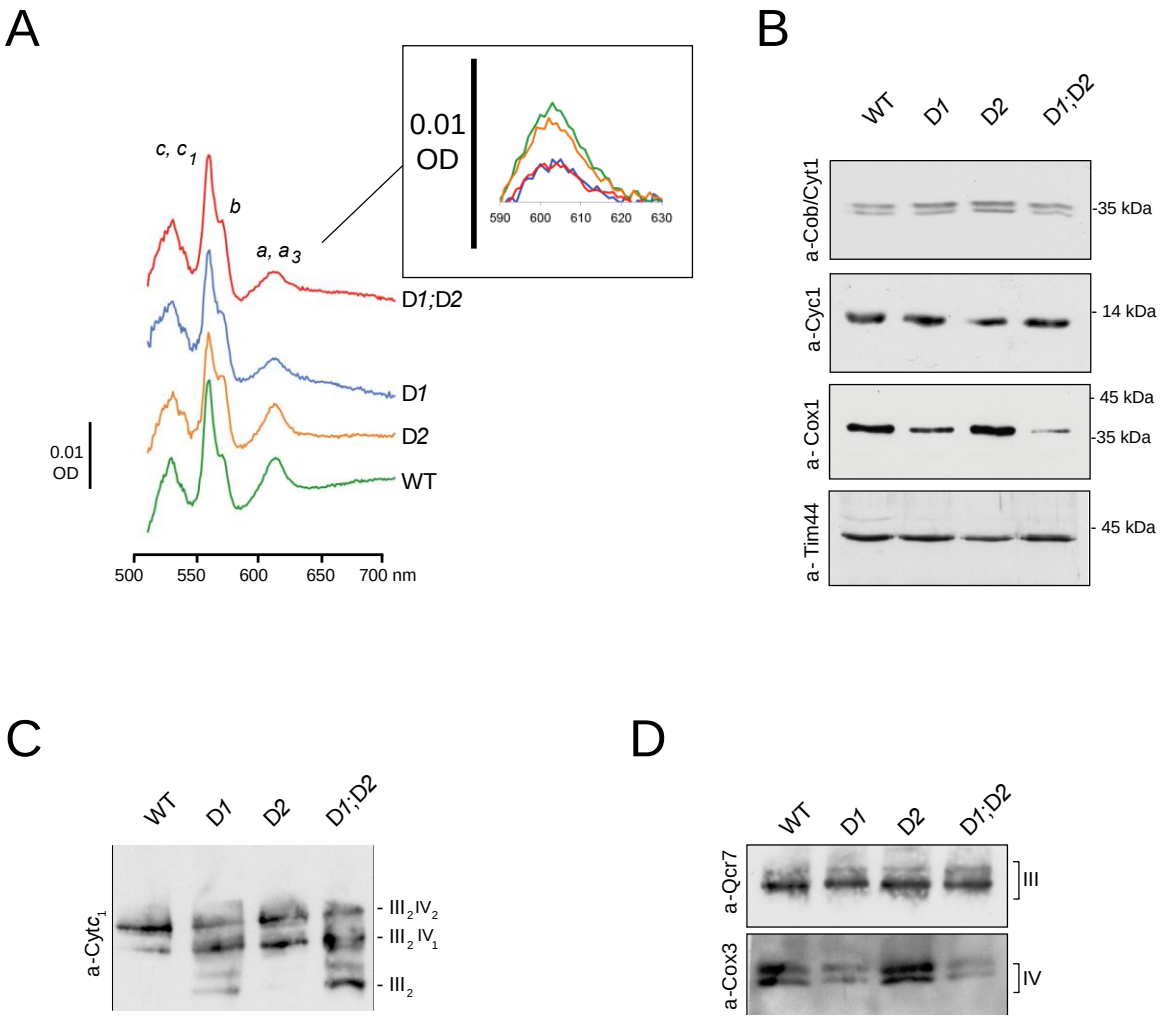

Figure 7. Levels of mitochondrial cytochromes and OXPHOS complexes III and IV. (A) Dithionite reduced – ferrocyanide oxidized spectra of mitochondrial cytochromes. 1 mg of mitochondria was solubilized in 50 mM Tris-KCl, 2% DDM, pH 7.4 for the analysis. Spectra of complex IV core cytochromes *a*, a_3 (603 nm peak) in wild type (green), Δ*rcf1* (blue), Δ*rcf2* (orange), and the Δ*rcf1;*Δ*rcf2* (red) mitochondria are enlarged in the inset to show detail. **(B)** Steady-state levels of supercomplexes components from wild type, Δ*rcf1*, Δ*rcf2*, and the Δ*rcf1;*Δ*rcf2* mitochondria (25 µg protein) analyzed by SDS-PAGE, Western blotting and immunodecoration with the antibodies to: α-Cob/Cytc1 for cytochromes *b* (upper band) and c_1 (lower band), α-Cyc1 for cytochrome *c*, α-Cox1, and α-Tim44 as indicated). Tim44 was used as a loading control. **(C)** Mitochondria (30 µg protein) isolated from wild type, Δ*rcf1*, Δ*rcf2*, and the Δ*rcf1;*Δ*rcf2* strains were solubilized in 1% digitonin and subjected to BN-PAGE analysis, Western blotting, and immunodecoration with antibodies α-Cytc_1 for complex III component cytochrome c_1. **(D)** BN-PAGE analysis performed as in **(C)** except 0.6% DDM was used instead of digitonin, and antibodies α-Qcr7 for complex III component Qcr7 *c*, α-Cox3 for complex IV component Cox3, were used as indicated.

The levels of complex III cytochromes *b* and c_1, and soluble electron carrier cytochrome *c* were not negatively affected in the absence of Rcf1 or Rcf2. An increase in spectral signal corresponding to reduced *b* type cytochromes without a corresponding increase in the signal corresponding to the *c* type cytochromes, was observed in Δ*rcf1*, Δ*rcf2*, and Δ*rcf1;*Δ*rcf2* mitochondria without a corresponding increase in the signal corresponding to the *c* type cytochromes, thus resulting in an increase in the apparent ratio of $b{:}cc_1$ (Table 5).

Immunodetection of complex III components cytochrome *b* and cytochrome c_1 with Cob (cytochrome *b*) and Cyc1 (cytochrome c_1) specific antibodies indicated that complex III components were not affected by the *RCF1/2* deletion (Fig 7B). Cytochrome *c* levels were also found not to be compromised. Increased levels of other cytochrome *b*-containing proteins, such as cytochrome *c* peroxidase, cytochrome b_2, catalase, or yeast flavohemoglobin (Yhb1) may be contributing to the increased cytochrome *b* signal. Reduced levels of the Cox1 protein (containing cytochromes a,a_3) were observed in the Δ*rcf1* and Δ*rcf1;*Δ*rcf2* mitochondria, a result which is consistent with the measured cytochrome aa_3 spectral content (Figure 7B).

Spectral quantification of complex III and complex IV cytochromes operates under an assumption that extinction coefficient properties of the cytochromes are not altered by the deletion of Rcf1 or Rcf2. While the spectral absorption maxima of the cytochromes was not altered, not sufficient evidence is available to validate this assumption. Therefore, steady state levels of the III and IV complexes were assayed using an independent method, BN-PAGE followed

by Western blotting. BN-PAGE can be used to detect the level and assembly state of the III-IV supercomplex populations (when mitochondria are solubilized with the mild detergent, digitonin), or for the individual complexes III and IV (when mitochondria are solubilized with a stronger detergent, dodecylmaltoside (DDM)). Using an antibody against cytochrome c_1 (of complex III), in wild type mitochondria majority of the supercomplex III-IV was observed to be present in the III_2-IV_2 form, whereas in the absence of Rcf1, an increase in the levels of III_2-IV_2 and III_2 forms relative to III_2-IV_2 supercomplex form was observed. A similar result was obtained with the Δ*rcf1;*Δ*rcf2* mitochondria, whereas the absence of Rcf2 had not great effect on the III_2-IV_2 supercomplex organization, which largely mirrored that of the wild type control. Thus, it appears that slightly lower cytochrome aa_3 content in the Δ*rcf2* mutant does not noticeably alter the level of the III_2-$IV_{(1-2)}$ supercomplex assembly.

Analysis of the levels of the individual III and IV complexes following DDM solubilization confirmed the levels of complex III in the Δ*rcf1*, Δ*rcf2*, and Δ*rcf1;*Δ*rcf2* mitochondria levels were similar to those of the wild type control, a result which is consistent with the spectral analysis (Figure 7B). Antibody to complex IV Cox3 subunit detected the previously described two forms of complex IV in DDM solubilized mitochondria (Figure 7B). The two forms, designated IV and IV*, differ in the association of subunit Cox13 and Cox12 (Vukotic *et al.,* 2012, Garlich *et al.,* 2017). As reported previously, when *RCF1* is deleted, there was a decrease in both the IV and IV* populations (Figure 7B). A similar decrease in IV and IV* was observed in Δ*rcf1;*Δ*rcf2* mitochondria, indicating that

the levels of the IV and IV* were not further adversely impacted when Rcf2 in addition to Rcf1 was absent. The qualitative nature of BN-PAGE analysis precludes complete certainty, yet the levels of IV and IV* in the Δ*rcf2* mitochondria appeared similar to wild type levels.

To summarize, complex IV (cytochrome aa_3) is decreased to a similar extent in the Δ*rcf1* and Δ*rcf1;*Δ*rcf2* mitochondria, indicating that the deletion of *RCF2* in the Δ*rcf1* background does not further decrease complex IV steady state levels. Thus, despite having similar reduced levels of complex IV the Δ*rcf1;*Δ*rcf2* mutant displays a strong respiratory growth defect, whereas the single Δ*rcf1* mutant does not. As the growth defect of the Δ*rcf1;*Δ*rcf2* mutant cannot be solely attributed to a reduced content of complex IV, this result prompted us to investigate complex III and IV enzymatic activities to explain the respiratory growth deficiency of the Δ*rcf1;*Δ*rcf2* mutant.

3.5. Rcf1 and Rcf2 support complex IV electron transport activity, but deletion of Rcf1 is epistatic to deletion of Rcf2.

Complex III and IV relative specific enzyme activities in the absence of Rcf1 and/or Rcf2 were determined by spectrally monitoring the rate of exogenous cytochrome *c* reduction or oxidation, respectively. The cytochrome *c* reduction assay indicated that the activity of detergent solubilized complex III in wild type, Δ*rcf1*, and Δ*rcf2* was similar, while in Δ*rcf1;*Δ*rcf2* mitochondria it was even increased (Figure 8A, Table 6 first column). The cytochrome *c* oxidation assay indicated that the activity of detergent-solubilized complex IV was substantially

Table 6. Complex III and complex IV activity in mitochondria from the Δ*rcf1*, Δ*rcf2*, and Δ*rcf1;*Δ*rcf2* mutants.

Reduction (complex III activity, WT (n=9), Δ*1* (n=9), Δ*2* (n=9), Δ*1*;Δ*2* (n=9)) or oxidation (complex IV activity, WT (n=23), Δ*1* (n=9), Δ*2* (n=4), Δ*1*;Δ*2* (n=21)) of exogenous cytochrome *c* was measured spectrophotometrically (Materials and Methods), and expressed as % of the wild type. Complex IV activity was also measured as oxygen consumption rate (OCR, nmol O_2 / minute / mg protein). OCR was recorded at 30˚C upon the addition of complex IV specific substrate TMPD with ascorbate (Asc/TMPD, 12.5 mM ascorbate/1.4 mM TMPD) to mitochondria (20 µg) in presence (WT (n=11), Δ*1* (n=3), Δ*2* (n=6), Δ*1*;Δ*2* (n=5)) and absence (WT (n=11), Δ*1* (n=6), Δ*2* (n=6), Δ*1*;Δ*2* (n=5)) of uncoupler CCCP (10µM). Auto-oxidation of Asc/TMPD substrate measured without mitochondria was subtracted from the OCR. Average and S.E.M. values are reported; **, *p* value < 0.01; *, *p* value < 0.05.

	NADH - cytochrome *c* reductase (complex III) % of WT	Cytochrome *c* oxidase (complex IV) % of WT
WT	100 ± 14	100 ± 6
Δ*rcf1*	83 ± 6	** 31 ± 3
Δ*rcf2*	105 ± 12	** 62 ± 2
Δ*rcf1*;Δ*rcf2*	**126 ± 14	** 28 ± 2

	Asc/TMPD OCR (complex IV) nmol O_2/min/mg	Asc/TMPD + CCCP OCR (complex IV) nmol O_2/min/mg	+/- CCCP ratio (effect of PMF)
WT	620 ± 30	1419 ± 62	2.3
Δ*rcf1*	**338 ± 30	** 527 ± 12	1.6
Δ*rcf2*	*486 ± 28	** 999 ± 26	2.1
Δ*rcf1*;Δ*rcf2*	** 278 ± 12	** 404 ± 19	1.5

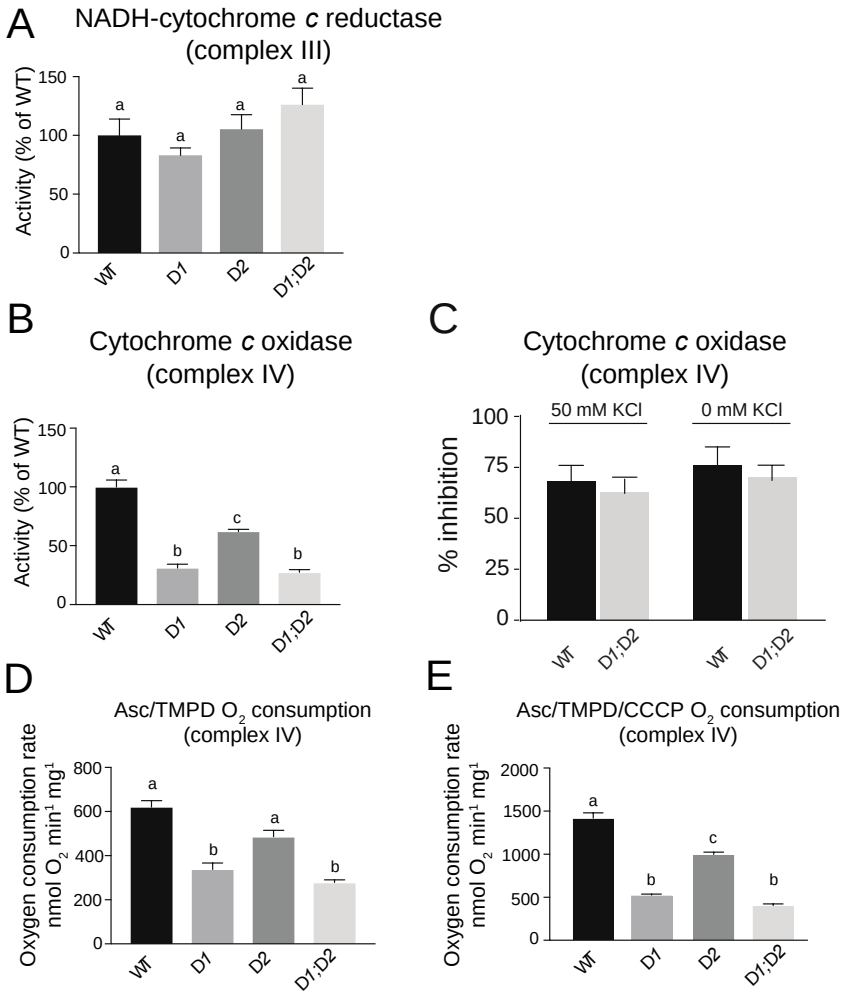

Figure 8. Activity of complex III and complex IV in Δ*rcf1*, Δ*rcf2*, and Δ*rcf1;*Δ*rcf2* mitochondria. (A) Complex III activity. Mitochondria (20 µg protein) were solubilized as described in Materials and Methods. Reduction of cytochrome *c* (initial rate) was measured spectrally. **(B)** Complex IV activity. Mitochondria (4 µg protein) were solubilized as described in Materials and Methods. Oxidation cytochrome *c* (initial rate) was measured spectrally. **(C)** Effect of buffer salt concentration on complex IV activity, measured as in **(B)** except the KCl concentration was changed to 50 mM or 0 mM. The % inhibition is the rate of cytochrome *c* oxidation relative to the control (wild type or Δ*rcf1;*Δ*rcf2* sample measured with 120 mM KCl). **(D)** Complex IV oxygen consumption rate (OCR) in intact mitochondria. Mitochondria (40 µg protein) were resuspended in 0.5 ml respiration buffer (Materials and Methods). OCR was measured upon addition of TMPD/ascorbate. KCN (0.2 mM) was added to inhibit respiration and confirm the absence of extramitochondrial respiration. **(E)** Complex IV maximal OCR in intact mitochondria was measured as in **(D)** except TMPD/ascorbate was followed by CCCP (10 µM in DMSO). In all panels, average ± SEM is shown, and values that are statistically different ($p<0.05$) from each other are denoted by different subscripts.

decreased in Δ*rcf1* mitochondria (31% of the wild type levels) while it was decreased to a lesser extent in Δ*rcf2* mitochondria (62% of the wild type) (Figure 8B, Table 6 second column). The cytochrome *c* oxidation rate in Δ*rcf1;*Δ*rcf2* mitochondria (27% of the wild type) was not significantly different from that of the Δ*rcf1* mitochondria, allowing us to conclude that removal of Rcf2 does not further impair electron transport activity of complex IV in the Δ*rcf1* background.

The cytochrome *c* reduction and oxidation assays are normally performed at the physiological conditions of high ionic strength (*I*=120 mM) (Cortese *et al.,* 1995), which support the electrostatic interaction of cytochrome *c* with the IM. Electrostatic interactions support cytochrome *c* binding to complex IV distant low-affinity binding site (Moreno-Beltrán *et al.,* 2015) from which site it is channeled to the site of its oxidation formed by complex IV subunits Cox2, Cox12, and Cox13 (Shimada *et al.,* 2017). A previous study (Rydström Lundin *et al.,* 2016) found that Δ*rcf1* mitochondria display different oxidation kinetics with exogenously added horse heart cytochrome *c* than with the yeast cytochrome *c*, and proposed a role for Rcf1 in recruiting or coordinating cytochrome *c* to the supercomplex. Additionally, affinity between mammalian HIGD1A protein and cytochrome *c* was reported (Guerra-Castellano *et al.,* 2018). If Rcf1 and Rcf2 are necessary for recruiting cytochrome *c*, the complex IV activity in Δ*rcf1;*Δ*rcf2* and mitochondria may be sensitive to disruption of the electrostatic interactions. To test this possibility, sensitivity of cytochrome *c* oxidation to lower buffer ionic strength was assayed. Lowering buffer ionic strength decreases electrostatic interactions that support cytochrome *c* availability and oxidation by complex IV.

The cytochrome *c* oxidation activities in wild type and Δ*rcf1;*Δ*rcf2* mitochondria were equally sensitive to inhibition by lower salt concentration (Figure 8C). This result indicates that the absence of Rcf1 and Rcf2 did not negatively affect cytochrome *c* binding or recruitment to complex IV.

The cytochrome *c* reduction and oxidation assays are performed with detergent-solubilized mitochondria in the presence of excess cytochrome *c*. This is necessary to quantify changes in cytochrome *c* redox spectra. A second independent approach was used to compare the rate of complex IV specific oxygen consumption in intact mitochondria, and compare complex IV electron transport activity in Δ*rcf1* and Δ*rcf1;*Δ*rcf2* mutants. Oxygen consumption rate (OCR) was calculated as the change in oxygen concentration over time, measured using an oxygen electrode. TMPD/ascorbate, complex IV specific substrate was used to supply electrons to endogenous cytochrome *c*. The use of TMPD bypasses the upstream ETC complexes, bioenergetically isolating complex IV activity. This allows us to measure the oxygen consumption capacity of the complex IV enzyme.

Complex IV specific OCR's were decreased in Δ*rcf1*, Δ*rcf2,* and in Δ*rcf1;* Δrcf2 mitochondria (Δ*rcf1* = 55%, Δ*rcf2* = 78%, Δ*rcf1;*Δ*rcf2* = 45% of the wild type control) (Figure 8D and Table 6 third column). The decrease in the complex IV activity was less in intact mitochondria than the aforementioned cytochrome aa_3 levels and in the cytochrome *c* oxidation assays. This could be due to complex IV activity being less constrained by the PMF.

PMF was completely dissipated by the addition of an uncoupling ionophore CCCP, stimulating maximal oxygen consumption since complex IV was no longer controlled by the PMF. Maximal complex IV OCR in the presence of CCCP was determined to be strongly decreased in Δ*rcf1* (37% of the wild type) while it was reduced to a lesser extent in *Δrcf2* mitochondria (70% of the wild type); and was not significantly less in Δ*rcf1;*Δ*rcf2* mitochondria (28% of the wild type) than in Δ*rcf1* (Figure 8D, Table 6 fourth column). This maximal complex IV OCR was consistent with complex IV activity levels determined by other assays, and indicated that Rcf1 and Rcf2 functionally overlap with respect to complex IV electron transport activity.

Complex IV oxygen consumption was stimulated by the addition of CCCP in all mitochondrial samples (Table 6). This indicates the extent of the constraint imposed by the PMF. CCCP stimulation was smaller in the absence of Rcf1 or Rcf2 compared to wild type control (Table 6 last column). This indicates that PMF maintenance requires greater utilization of complex IV oxygen consumption capacity in mitochondria lacking Rcf1 and/or Rcf2. These results are consistent with uncoupling, or partial loss of PMF in the mutant mitochondria and are consistent with elevated whole cell respiration in the absence of Rcf2.

To summarize, the absence of Rcf2 in the Δ*rcf1* background does not further decrease complex IV content or electron transport from cytochrome *c* to oxygen. The cytochrome *c* reduction and oxidation rates were not significantly different in Δ*rcf1;*Δ*rcf2* mitochondria from those of the Δ*rcf1* mitochondria. Therefore, decreased electron transport activity due to decreased complex IV

levels cannot explain respiratory growth defect of the Δ*rcf1;*Δ*rcf2* strain which is not as pronounced as in the Δ*rcf1* strain. Decreased CCCP-dependent stimulation of oxygen consumption by the mutant mitochondria suggests that the Δ*rcf1;*Δ*rcf2* uses more of its complex IV capacity to maintain PMF. Similar to elevated cellular oxygen consumption in the absence of Rcf2 (Figure 6), these results are consistent with the uncoupling, or loss of PMF in the Δ*rcf2* strain. If the capacity to maintain the PMF is worse in the Δ*rcf1;*Δ*rcf2* than in the single mutants, it would likely result in respiratory growth defect, because the PMF supports the F_1F_O ATP synthase-driven ATP synthesis and other mitochondrial functions.

3.6. Elevated state 2 and lowered state 3 respiration indicated that deletion of Rcf1 and Rcf2 impairs OXPHOS coupling.

To further investigate the nature of OXPHOS uncoupling in Δ*rcf1;*Δ*rcf2* mitochondria, we performed oxygen consumption and membrane potential measurements. Respiration measurements in intact mitochondria with controlled substrates are a powerful bioenergetic tool that reveal many aspects of mitochondrial function: oxygen consumption is proportional to the total proton current flowing in mitochondria. The activity of the individual ETC complexes, ATP synthase activity, and the magnitude of proton leak, could be inferred from the OCR's because of a tight coupling between electron and proton transfer and the requirement of the PMF established by the ETC to support the ATP synthesis activity of the F_1F_O ATP synthase enzyme.

Isolated mitochondria from the wild type, Δ*rcf1*, Δ*rcf2*, and Δ*rcf1*;Δ*rcf2* strains were subjected to bioenergetic profiling. In the presence of a respiratory substrate, such as NADH, mitochondria respire at a steady low rate (state 2). State 2 oxygen consumption counteracts intrinsic proton leak across phospholipid membranes in the absence of ongoing ATP synthesis. Elevated state 2 oxygen consumption was observed in Δ*rcf2* and in Δ*rcf1;*Δ*rcf2* mitochondria (Figure 9A, Table 7 first column), despite the reduced levels of cytochrome aa_3 and complex IV. This result suggests the Δ*rcf2* mitochondria exhibit difficulty in maintaining an optimal PMF. Elevated state 2 oxygen consumption in Δ*rcf2* mitochondria from BY4741 strain was previously reported but not further investigated (Römpler *et al.*, 2016). Interestingly, state 2 OCR was not just elevated in Δ*rcf1;*Δ*rcf2* mitochondria, but it increased during the time of the assay, in contrast to the state 2 OCR of the wild type control (Figure 9B). This increase in OCR was observed in Δ*rcf1;*Δ*rcf2* mitochondria did not appear to be linked to PMF consumption by the F_1F_O ATP synthase since it was still observed in the presence of the F_1F_O ATP synthase inhibitor oligomycin (Figure 9C).

When ADP is added to mitochondria (condition known as state 3), oxygen consumption accelerates since ATP synthesis consumes PMF. Following ADP addition, OCR peaks and then returns to pre-ADP level. State 3 OCR peak in the Δ*rcf1* and Δ*rcf1;*Δ*rcf2* mitochondria was lower than wild type; state 3 OCR peak in the Δ*rcf2* mitochondria was similar to wild type (Figure 10A, Table 7 second column). The OCR peak associated with ATP synthesis was not observed in Δ*rcf1;*Δ*rcf2* mitochondria; the increase in OCR was stunted and only slightly

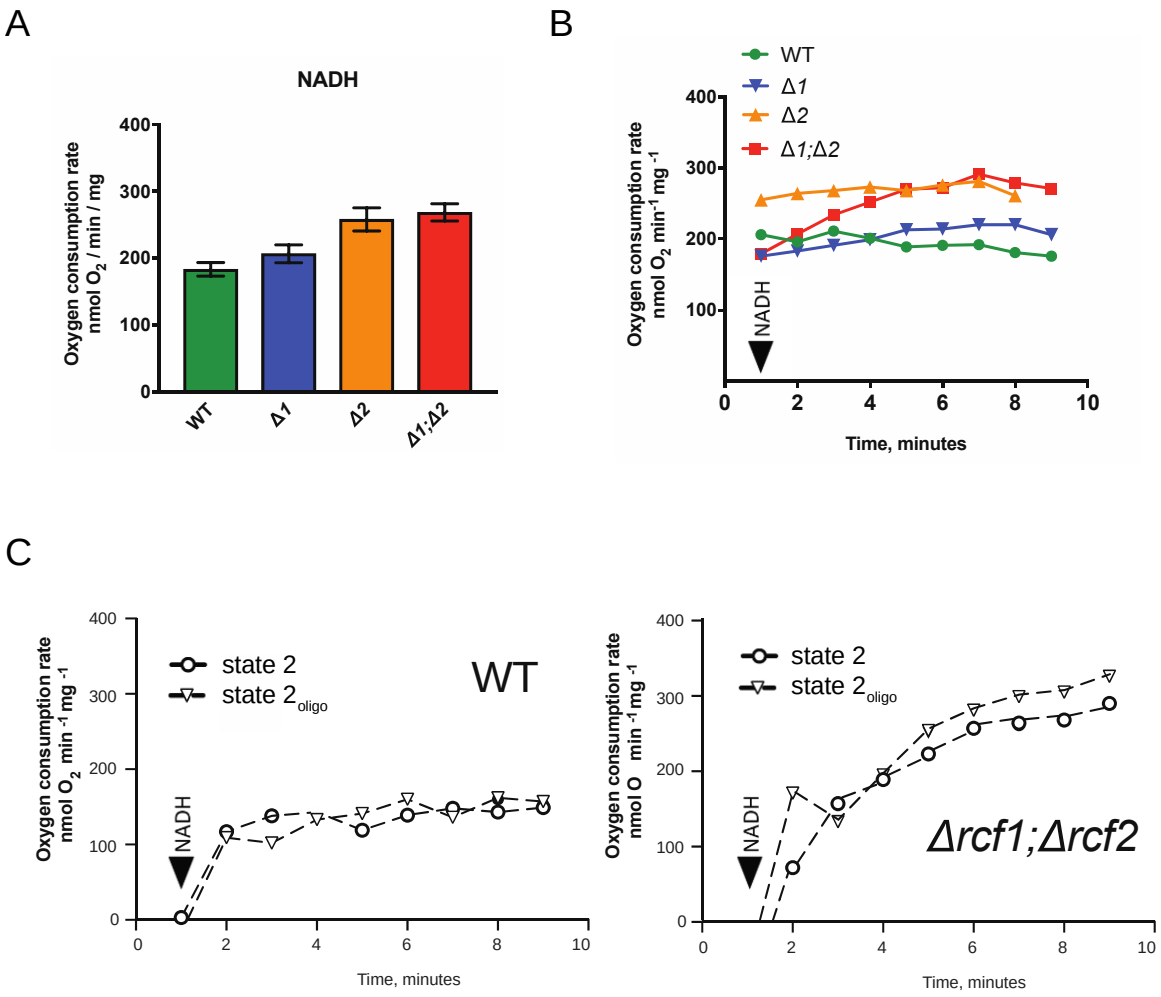

Figure 9. Deletion of Rcf1 and Rcf2 results in increased state 2 respiration. (A) State 2 respiration (oxygen consumption rate, nmol O_2 / minute / mg protein) was measured for 6-8 minutes after the addition of with NADH. Averages and SEM of at least 4 experiments are shown. **(B)** Changes in OCR with NADH (state 2 respiration) over 10 minute time period. **(C)** Effect of oligomycin on state 2 respiration in Δ*rcf1;*Δ*rcf2* mitochondria and wild type control. Mitochondria (40 µg) were added 0 minutes, immediately followed by oligomycin (state 2_{oligo}) or vehicle (DMSO, state 2) as indicated. NADH was added at 1 minute in all traces. One representative experiment is shown.

Table 7. Oxygen consumption by mitochondria from the Δ*rcf1*, Δ*rcf2*, and Δ*rcf1;*Δ*rcf2* mutants.

Mitochondria (40 µg) were isolated from indicated strains grown in YPGal at 30˚C and resuspended in buffer. OCR was recorded at 30˚C upon the addition to mitochondria of NADH (1mM) (state 2, WT (n=6), Δ*1* (n=5), Δ*2* (n=9), Δ*1*;Δ*2* (n=4)), or NADH (1mM) + ADP (200 µM) (state 3, WT (n=5), Δ*1* (n=4), Δ*2* (n=4), Δ*1*;Δ*2* (n=7)), or NADH (1mM) + CCCP (10µM) (maximal, WT (n=6), Δ*1* (n=3), Δ*2* (n=4), Δ*1*;Δ*2* (n=3)). No substrates auto-oxidation was detected without mitochondria. Average and S.E.M. values are reported, **, *p* value < 0.01; *, *p* value < 0.05.

	OCR (nmol O_2/min/mg)			+/- ADP ratio	+/- CCCP ratio
	NADH	NADH + ADP	NADH + CCCP		
WT	184 ± 10	423 ± 18	874 ± 63	2.19	4.53
Δ*rcf1*	207 ± 13	** 344 ± 22	** 398 ± 56	1.66	2.03
Δ*rcf2*	** 258 ± 17	452 ± 72	** 530 ± 40	1.75	2.05
Δ*rcf1*;Δ*rcf2*	** 269 ± 13	** 358 ± 16	** 362 ± 6	1.33	1.35

exceeded the observed increasing state 2 OCR (Figure 10B, Figure 9B). Following state 3, ADP/ATP equilibrium is restored, and PMF is reestablished, the OCR will decrease to a steady low rate again (state 4). The Δ*rcf1;*Δ*rcf2* mitochondria were unable to return to the pre-ADP OCR; Δ*rcf1;*Δ*rcf2* state 4 OCR remained higher than state 2 OCR, in contrast to wild type control. The increased state 2 OCR in the Δ*rcf1;*Δ*rcf2* mitochondria is utilizing almost all ETC capacity and leaves very little reserve (Figure 10A). To account for the state 2 differences between different mitochondrial types and illustrate the OXPHOS capacity in both the Δ*rcf1* and Δ*rcf1*;Δ*rcf2* mitochondria, the level of ADP-stimulated O_2 consumption was calculated (i.e. state 3 minus state 2 OCRs at the peak time) at 50, 100, and 200 µM ADP. The ADP-stimulated O_2 consumption

was less in Δ*rcf1*;Δ*rcf2* mitochondria than in the Δ*rcf1* at all ADP concentrations tested (Figure 10C). This was also reflected by the respiratory control ratio (RCR), the ratio of state 3 / state 2 oxygen consumption rate. RCR decreased in the absence of Rcf1 and further decreased in the absence of both Rcf1 and Rcf2 (+/- ADP, wild type = 2.19, Δ*rcf1* = 1.66, Δ*rcf2* = 1.75, Δ*rcf1;*Δ*rcf2* = 1.33, Table 7, fourth column). As a result, the bioenergetic capacity to support ATP synthesis is most compromised in the Δ*rcf1;*Δ*rcf2*.

The addition of an uncoupling ionophore such as CCCP stimulates the OCR because the ETC enzymes are no longer constrained by the PMF (maximal OCR. Maximal OCR measured in the Δ*rcf1*, Δ*rcf2*, and Δ*rcf1;*Δ*rcf2* mitochondria with NADH as a substrate was decreased (Table 7). The absolute OCR in presence of CCCP obtained with different ETC substrates is not the same. This is illustrated by the smaller maximal OCR with NADH as a substrate (Figure 10A, Table 7) than with the TMPD/Ascorbate (Figure 8E, Table 6). TMPD supports a higher maximal OCR because the electrons directly reduce complex IV via endogenous cytochrome *c* and bypass the upstream ETC enzymes, NADH dehydrogenase and complex III. With NADH as the substrate, the CCCP stimulation was smaller in the absence of Rcf1 or Rcf2 compared to wild type control (Table 7). Smaller CCCP-dependent stimulation of oxygen consumption by the mutant mitochondria supports the conclusion that PMF maintenance is impaired in mitochondria lacking Rcf1 and/or Rcf2.

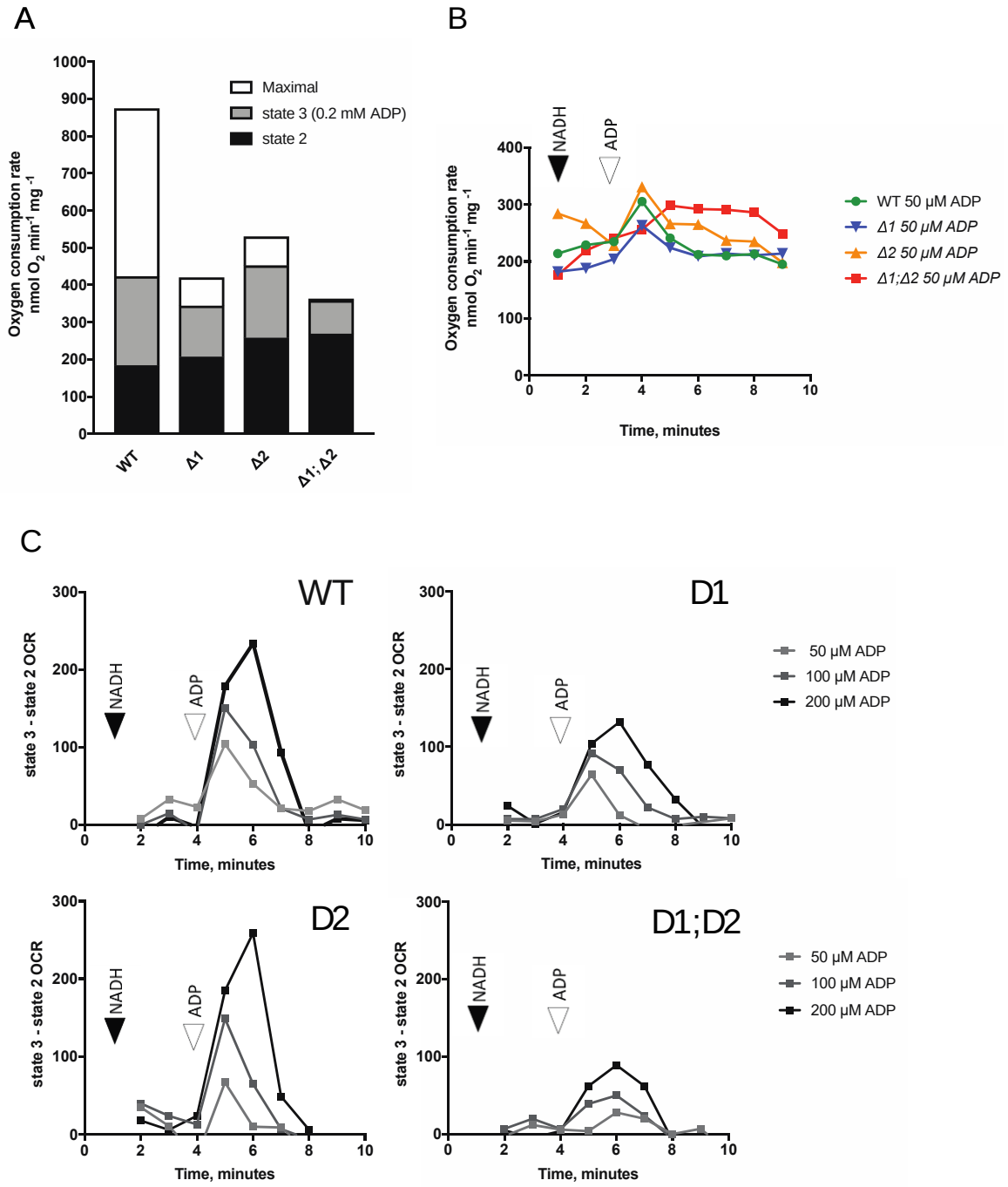

Figure 10. Lower ATP synthesis associated respiration indicates that Rcf1 and Rcf2 deletion decreased OXPHOS coupling. (A) Comparison of the OCR with NADH (state 2), NADH + 0.2 mM ADP (state 3), and NADH + CCCP (Maximal). Averages of at least 4 experiments are shown. **(B)** Changes in OCR with NADH (state 3 respiration). Arrows indicate NADH (1 mM) and ADP (50 μM) additions. **(C)** State 3 - state 2 respiration indicates the OCR stimulation associated with ATP synthesis. Arrows indicate NADH (1 mM) and ADP (50-200 μM) additions. Averages of at least 4 experiments is shown.

Previous experiments already established decreased complex IV levels and the electron transport capacity of complex IV and the electron transport chain in the absence of Rcf1 and to a lesser extent in the absence of Rcf2. The deletion of both Rcf1 and Rcf2 did not lead to greater decrease in the complex IV levels and electron transport activity than the deletion of Rcf1 alone. However, the respiration profiling indicates that deletion of both Rcf1 and Rcf2 was additive with the respect to the OXPHOS coupling, and resulted in a more severe impairment than the deletion of Rcf1 alone.

3.7. Rcf1 and Rcf2 promote optimal mitochondrial PMF.

The mitochondrial PMF driving the protons from the IMS into the matrix is a combination of both the mitochondrial membrane potential (Δψ, a charge or electrical gradient) and the mitochondrial pH gradient (ΔpH). Typical PMF values range from 180 to 220 mV, with Δψ contributing 150-180 mV, and ΔpH of 0.5-1.0 units contributing the remaining 30-60 mV (Nicholls and Ferguson, 2013).

To directly investigate the ability of the Δ*rcf1;*Δ*rcf2* mitochondria to establish and maintain PMF during state 2, state 3 depolarization, and state 4 repolarization, Δψ measurements in isolated mitochondria were performed using the lipophilic, cationic dye Rhodamine-123 (R123). R123 dye accumulates within mitochondria forming aggregates, which quenches some of its fluorescent emission. Under these conditions, once the dye is loaded into the mitochondria, a subsequent depolarization releases some of the dye, unquenching the loaded

dye, and transiently increasing the fluorescent signal. On the other hand, a repolarization will cause more dye to enter the mitochondria and cause a relative decrease in a fluorescent signal. R123 is sensitive to mitochondrial charge (Δψ) and does not measure pH specifically (Perry *et al.*, 2011). However, respiring mitochondria maintain constant PMF, thus the changes in Δψ parallel the changes in ΔpH, while different in magnitude.

Isolated mitochondria were resuspended in a buffer containing R123 and placed in a fluorimeter (S. Saddar, PhD dissertation). In wild type mitochondria, stable quenching of R123 fluorescence signal was achieved during state 2 respiration when NADH was used as a substrate. Upon the addition of ADP to drive state 3 respiration, a peak in R123 fluorescence signal was observed, corresponding to a transient loss of mitochondrial quenching of the dye fluorescence due to transient state 3 depolarization (Figure 11A). The depolarization indicates the entry of protons through the ATP synthase, which lowers both pH and charge components of the PMF. This fast depolarization was followed by somewhat slower repolarization due to ETC-dependent proton translocation. At the end of repolarization, mitochondria re-establish state 4 membrane potential comparable to state 2 prior to ADP addition, and R123 fluorescence quenching. Complex III and IV regenerate ΔpH to maintain state 4 PMF. At the end of each experiment, the PMF was dissipated by addition of an uncoupler, CCCP. CCCP addition completely depolarizes mitochondria, results in some dye molecules exiting the mitochondria, and the fluorescence signal of the loaded dye increases, observed as unquenching. The magnitude of R123 fluorescence after CCCP addition was

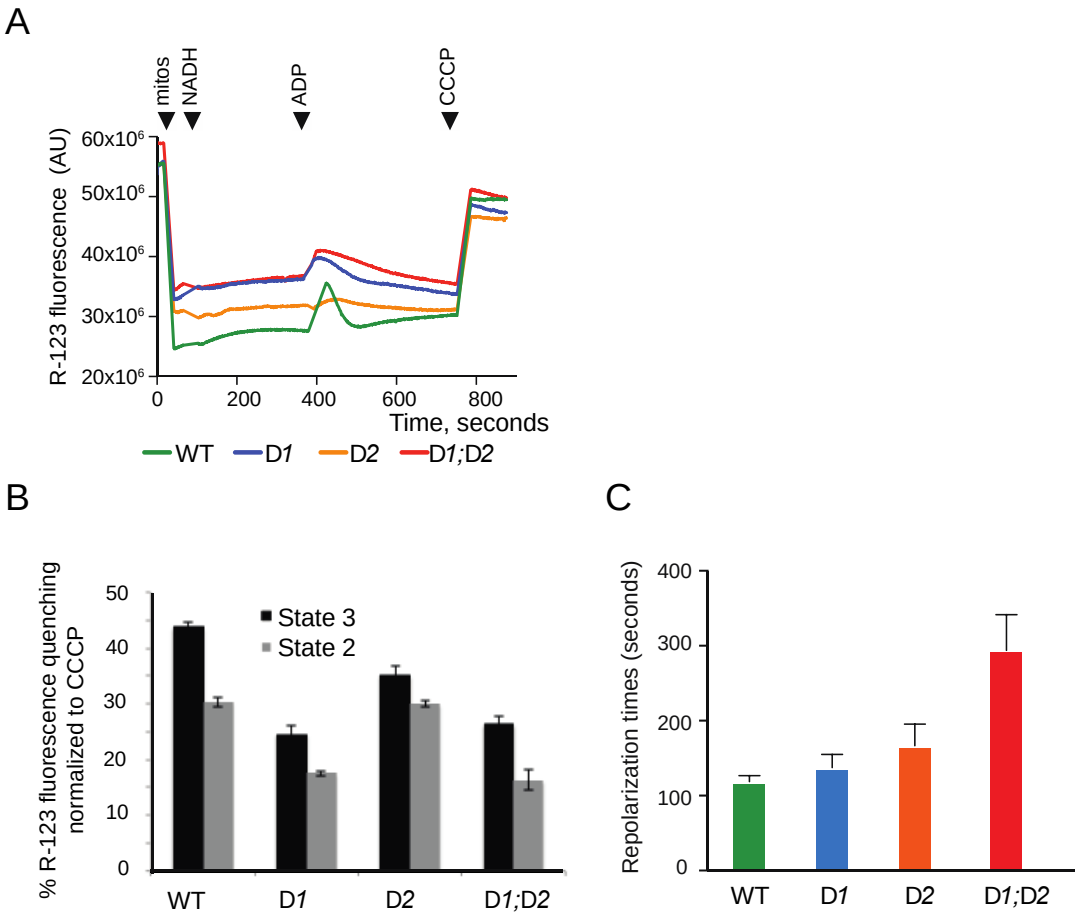

Figure 11. Changes in state 2 and state 3 membrane potential in mitochondria from the Δ*rcf1*, Δ*rcf2*, and Δ*rcf1;*Δ*rcf2* mutants. (A) Representative R-123 fluorescence traces. Mitochondria (150 µg) were resuspended in 2 ml buffer containing 0.5 µM R-123 (in methanol); additions were NADH (2 mM), ADP (45 µM), CCCP (10 µM). **(B)** Membrane potential (% R123 fluorescence quenching) was calculated as a % difference in signal in the presence between NADH and NADH+CCCP (state 2, black bars) or NADH+ADP and NADH+CCCP (state 3, gray bars). The average and SEM are shown (WT (n=3), Δ*1* (n=2), Δ*2* (n=3), Δ*1*;Δ*2* (n=3)). **(C)** Average time after the addition of ADP to achieve state 4 membrane potential. The average and SEM are shown (WT (n=3), Δ*1* (n=2), Δ*2* (n=3), Δ*1*;Δ*2* (n=3)).

set to 100% and R123 fluorescence levels during state 2 and state 3 quenching were expressed as % change from that value. The time required to repolarize after the addition of ADP was monitored and interpreted to be an indication of the capacity of proton pumping by complex IV (as well as proton translocation by complex III) to offset dissipation of membrane potential required for ATP synthesis.

All mutants established lesser state 2 membrane potential with NADH than the wild type. When energized with NADH substrate (state 2), wild type mitochondria quenched ~45% of R123 fluorescence, while Δ*rcf2* mitochondria had ~35% quenching, indicating that these mitochondria have reduced capacity to generate PMF. Quenching was similar (~25%) in Δ*rcf1* and Δ*rcf1;*Δ*rcf2* (Figure 11B). State 3 respiration was induced by the addition of 45 µM ADP. Wild type mitochondria R123 signal changed from ~45% quenched to ~30% quenched during peak depolarization. Lesser depolarization (smaller state 3 peak) was observed in Δ*rcf1* (from ~25% to ~17%) and Δ*rcf1;*Δ*rcf2* mitochondria (from ~26% to 16%) showed than the wild type (Figures 11A and 11B). State 3 depolarization was minimal in Δ*rcf2* (from ~35% to ~30%). This indicates decreased rate of ATP synthesis / entry of protons through the F_1F_O ATP synthase in the absence of Rcf1 and/or Rcf2, possibly because the capacity to regenerate ΔpH needed for ATP synthesis is inadequate.

Repolarization time was increased in Δ*rcf2* (168 seconds) and Δ*rcf1;*Δ*rcf2* mitochondria (295 seconds); Δ*rcf1;*Δ*rcf2* mitochondria took twice the time to re-establish state 4 PMF compared to wild type mitochondria (119 seconds) (Figure

11C). More severe repolarization delay was associated with the absence of Rcf2 (Δ*rcf2* repolarization times were significantly longer than wild type, and Δ*rcf1;*Δ*rcf2* were significantly longer than Δ*rcf1*). These findings suggest that in the absence of Rcf2 the ΔpH component of the PMF is limiting, indicating an impaired proton translocation during state 3, despite elevated OCR. Further lengthening of repolarization time in Δ*rcf1;*Δ*rcf2* mitochondria indicate that their capacity to generate and maintain ΔpH is more severely compromised compared to the Δ*rcf1* and Δ*rcf2* single mutants.

3.8. Deletion of *RCF2* sensitized respiratory growth to nigericin.

Evidence presented so far indicates that the mitochondria become uncoupled, i.e. unable to generate and/or maintain an optimal PMF, in the absence of Rcf1 and Rcf2. To test whether uncoupling through dissipation of ΔpH affects respiration-based growth in the absence of Rcf1 or Rcf2, growth assays were done in the presence of low concentration of PMF uncoupler nigericin. Nigericin is an electroneutral K^+/H^+ antiporter which dissipates ΔpH, the mitochondrial proton gradient, and diverts the ETC from supporting ATP synthesis. Nigericin does not dissipate membrane potential Δψ dependent on the exchange of other charged ions, including potassium, across the mitochondrial inner membrane. Nigericin action in the cell is specific to mitochondrial membrane, and therefore it is suitable for whole cell growth assays (Kovac *et al.*; 1982, Kucejova *et al.*, 2005). When the wild type control cells were grown on

1µM nigericin, their respiration-based ability to grow on galactose and glycerol was compromised but not completely inhibited, indicating that this level of nigericin was subtoxic for OXPHOS-based growth. The growth of Δ*rcf2* on galactose displayed a heightened sensitivity to nigericin (Figure 12). Thus, despite its normal growth on glycerol media (compared to wild type control) the increased nigericin sensitivity of the Δ*rcf2* mutant indicates its reduced capacity to establish/maintain a sufficient PMF, an observation consistent with the elevated O_2 consumption rate of this mutant. Sensitivity to nigericin in galactose media was observed in the Δ*rcf1*;Δ*rcf2* mutant, but not in the Δ*rcf1* (Figure 12).

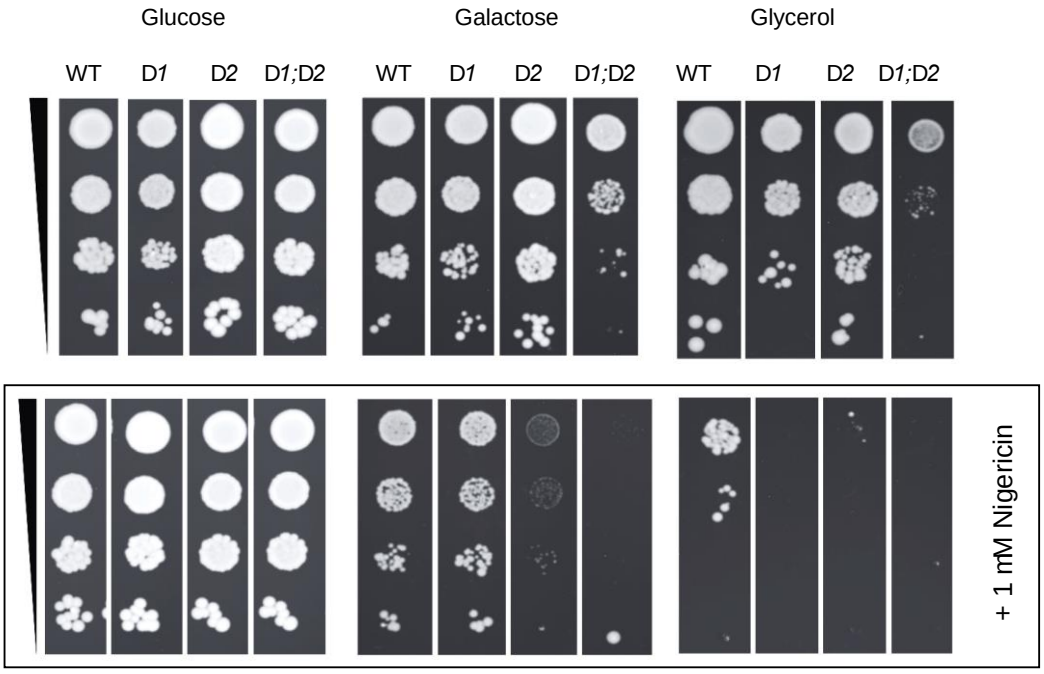

Figure 12. Sensitivity of Δ*rcf1*, Δ*rcf2*, and the Δ*rcf1*;Δ*rcf2* respiratory growth to an uncoupler nigericin. Serial dilutions of wild type (WT), Δ*rcf1* (Δ*1*), Δ*rcf2* (Δ*2*), and the Δ*rcf1;*Δ*rcf2* (Δ*1*;Δ*2*) cultures were spotted on YP agar containing 2% glucose, 2% galactose, or 3% glycerol, with or without 1 µM nigericin, as indicated. The relative cell concentration is indicated by the black wedges.

Nigericin inhibited the growth of Δ*rcf2*, Δ*rcf1*, and Δ*rcf1*;Δ*rcf2* on glycerol media (Figure 12).

Summary

This study of the consequences of Rcf1 and Rcf2 deletion for the mitochondrial bioenergetic energy conversion demonstrated the importance of coupling proton pumping to oxygen consumption, and preventing proton leak during the electron transport, known as OXPHOS coupling . ETC complex III and complex IV enzymes both generate PMF, which is necessary for the ATP synthesis by the F_1F_O ATP synthase and other essential processes driven by the ΔpH-dependent proton current. Decreased OXPHOS coupling and PMF may indicate altered complex IV proton pumping stoichiometry or proton back-leak through the enzyme, resulting in chronic sustained decreased PMF generation. Additinally, the phenomenon of acute instability of PMF or proton leak indicates proton leak that may be mediated by complex IV or other sources of proton leak.

The objective of this research was to better understand the common and distinct functions of Rcf1 and Rcf2 and explain the impaired respiration-based growth of the Δ*rcf1*;Δ*rcf2* mutant, as deletion of *RCF1* and *RCF2* individually does not strongly impair respiratory growth. Deletion of *RCF1*, more so than deletion of *RCF2*, lead to decreased complex IV steady state levels and electron transport activity (Figure 7, Figure 8), consistent with cytochrome oxidation

activity reported by others (Rydström Lundin *et al.,* 2016). In Δ*rcf2* mitochondria, complex IV content and electron transport from cytochrome *c* to oxygen were somewhat decreased, to 70% of the wild type control. Thus, Rcf2 plays a minor role, if at all, in complex IV assembly or stability. With respect to complex IV levels and electron transport activity, deletion of *RCF1* was epistatic to deletion of *RCF2* as these were not statistically different between Δ*rcf1* and Δ*rcf1*;Δ*rcf2* mutants.

Of note, cytochrome *c* oxidation assay in this study utilized titrated cytochrome *c* reductant (dithiothreitol) to avoid extra reductant remaining in the assay, and a detergent (dodecylmaltoside instead of deoxycholate) considered to be optimal for complex IV activity assays (Thompson and Ferguson-Miller 1983, Rosevear *et al.,* 1980). As a result, cytochrome *c* oxidase activity reported here differs quantitatively from our previously published results obtained using a different cytochrome *c* reduction method (with sodium dithionite) prone to artifacts due to excess of the reductant (our previous values were 70% of the wild type activity in Δ*rcf1*, 95% of the wild type activity in in Δ*rcf2*, and 20% of the wild type activity in in Δ*rcf1*;Δ*rcf2*) (Strogolova *et al.,* 2012). Importantly, cytochrome *c* oxidase activities obtained in all subsequent experiments were not statistically different between Δ*rcf1* and Δ*rcf1*;Δ*rcf2* mutants.

Deletion of *RCF2* led to reduced respiration-based growth in spite of elevated oxygen consumption rate. This is consistent with decreased respiratory coupling in the absence of Rcf2. Corroborating these phenotypes, increased sensitivity of Δ*rcf2* respiration-based growth to uncoupler nigericin and lower

PMF was observed in Δ*rcf2* mitochondria despite the elevated oxygen consumption. Therefore, respiratory coupling during PMF generation appears to be a function distinctly supported by Rcf2, likely by regulation of complex IV proton pumping activity.

The effect of Rcf1 and Rcf2 deletion on the OXPHOS coupling was cumulative. Increasing state 2 OCR (NADH) indicated an enhanced and progressive proton leak in the Δ*rcf1;*Δ*rcf2* mitochondria. Interestingly, Δ*rcf1* and Δ*rcf1;*Δ*rcf2* mitochondria achieved similar state 2 membrane potential, indicating that the progressive increase in ETC activity was temporarily able to counteract proton leak in Δ*rcf1;*Δ*rcf2* in the absence of ATP synthesis. Yet monitoring PMF return to state 4 after ADP addition revealed that re-polarization is also affected by the deletion of Rcf2: Δ*rcf1* mitochondria repolarized with kinetics similar to wild type, whereas Δ*rcf1;*Δ*rcf2* and Δ*rcf2* mitochondria repolarized more slowly. These membrane potential measurements were consistent with state 3 OCR measurements and demonstrated greater OXPHOS coupling defect in Δ*rcf1;*Δ*rcf2* mitochondria than in the Δ*rcf1* mitochondria. Decreased ETC activity in response to ADP is predicted to limit the ATP synthesis rate. ATP synthesis, as well as additional PMF-dependent mitochondrial functions: ADP/ATP exchange, mitochondrial translation and morphology, are adressed in Chapter 4.

The results presented in this chapter suggest that Rcf1 and Rcf2 operate through complex IV yet exhibit functional differentiation: Rcf1 plays a more prominent role than Rcf2 in assembly or stability of complex IV and electron transport capacity from cytochrome *c* to oxygen. However, Rcf2 alone can

maintain PMF and ATP synthesis at this level of ETC activity as demonstrated by Δ*rcf1* respiratory growth capacity. Membrane potential measurements indicate that Δ*rcf1* mitochondria maintained somewhat low state 2 PMF, yet retained capacity to stimulate proton-pumping activity under state 3 conditions and re-establish state 4 membrane potential with kinetics similar to the wild type control. Deletion of Rcf2 appears to increase oxygen consumption without corresponding increase in membrane potential, or PMF. Results presented here suggest that Δ*rcf1*;Δ*rcf2* suffers from combined lower complex IV levels and lower proton pumping of the remaining complex IV. This complex IV pumping defect resulting in OXPHOS uncoupling is consistent with the previously proposed role fore HIGD proteins in modulating complex IV proton pathways (Hayashi *et al*., 2015) and redox potential (Schäfer *et al*., 2018) and will be discussed more in chapter 5.

.

CHAPTER 4. Rcf1 and Rcf2 deletion affects PMF-dependent mitochondrial pathways and several lipid-binding OXPHOS proteins

Introduction

As shown in Chapter 3, Rcf1 and Rcf2 support complex IV ability to establish protonmotive force (PMF). The PMF is necessary for many functions including mitochondrial protein import and translocation across the inner membrane (IM) and outer membrane (OM) of mitochondria. A loss of PMF can impair maturation and proteolytic degradation of newly synthesized and misfolded proteins by a variety of mitochondrial proteases and peptidases (Schleyer *et al.,* 1982, Clarkson and Poyton, 1989, Baker and Schatz, 1991, Martin *et al*., 1991, Herrmann *et al.,* 1995, Geissler *et al.,* 2000, Fox 2012). In this chapter, mitochondrial protein synthesis and processing of mitochondrial and nuclear encoded proteins in the absence of Rcf1 and Rcf2 were examined and some changes consistent with lower PMF (ΔpH) are reported.

PMF is also essential for ATP synthesis by the F_1F_O ATP synthase (complex V) and the activity of metabolite carriers which provide the substrates for ATP synthesis, most notably ADP/ATP carrier (AAC) and phosphate carrier (PIC). In this chapter, the steady-state levels of F_1F_O ATP synthase, PIC and AAC were evaluated. Activity of AAC (mitochondrial ADP/ATP exchange) and F_1F_O ATP synthase (ATP synthesis and hydrolysis rates) were assayed in the absence of Rcf1 and/or Rcf2. Evidence is presented in this chapter that AAC molecular environment is altered in the absence of Rcf1. However, AAC-

mediated adenine nucleotide exchange function appears to remain normal in the absence of Rcf1 and Rcf2. PMF-dependent ATP synthesis rate by F_1F_O ATP synthase is decreased in the absence of Rcf1 and Rcf2. Additionally, steady-state levels of some of the F_1F_O ATP synthase protein subunits, and PMF-independent ATP hydrolysis and oligomycin sensitivity of this enzyme were also decreased. Rcf1 is proposed to be a lipid chaperone of Cox3 (Strogolova *et al.,* 2012, Garlich *et al.,* 2017), and may influence lipid composition of a wider range of OXPHOS proteins. Lipids are essential for stability and function of F_1F_O ATP synthase, AAC, and PIC. It is possible that Rcf1 and Rcf2 as lipid chaperones support stability and function of these enzymes in a PMF-independent manner.

In addition to OXPHOS enzyme activity, PMF regulates mitochondrial network morphology. Loss of membrane potential in individual organelles triggers mitochondrial network fragmentation. Mitochondrial network in YPGal growing WT, Δ*rcf1*, Δ*rcf2*, Δ*rcf1*;Δ*rcf2* cells was examined. The Δ*rcf1;*Δ*rcf2* mitochondrial networks are not more fragmented than the wild type mitochondrial networks. Yet, Δ*rcf1*;Δ*rcf2* mitochondrial networks have a unique appearance, characterized by decreased surface area and uneven fluorescent signal distribution of a mitochondrially-targeted GFP molecule.

Results

4.1. Mitochondrial translation and protein processing in the absence of Rcf1 and Rcf2.

Mitochondrial membrane potential is not required for synthesis of proteins encoded in the mitochondrial genome (Fox 2012), but it supports the maturation of mitochondrially synthesized protein Cox2 after translation (Clarkson and Poyton, 1989, Herrmann *et al*., 1995). Mitochondrial membrane potential also controls import and maturation of many nuclear-encoded mitochondrial preproteins into the mitochondria (Schleyer *et al.,* 1982, Baker and Schatz, 1991, Martin *et al*., 1991, Geissler *et al.,* 2000).

Mitochondrial translation is a key part of mitochondrial protein synthesis essential for the assembly of OXPHOS enzymes. Mitochondrial translation supplies subunits of respiratory supercomplexes III (cytochrome *b*), IV (Cox1, Cox2, and Cox3), and V (Atp6, Atp8 and Atp9) as well as Var1, a component of small subunit of the mitochondrial ribosome.

To test whether altered PMF in the absence of Rcf1 and/or Rcf2 influenced the synthesis of mitochondrially encoded subunits, mitochondrial translation in energized mitochondria was assessed in the presence of [^{35}S]-methionine. [^{35}S]-labeled translation products were analyzed using SDS-PAGE, Western blotting, and autoradiography. The Δ*rcf1*, Δ*rcf2*, and Δ*rcf1;*Δ*rcf2* mitochondria were capable of translation, although the amount of translated products was lowered in Δ*rcf2* (Figure 13). However, the mitochondrial translation pattern was altered compared to that of the wild-type control. Specifically, the translation of Var1, Cox2, and Cox3 increased in Δ*rcf1* mitochondria; translation of Cox1, Cox3, Cyt*b* and Atp8 was decreased in the

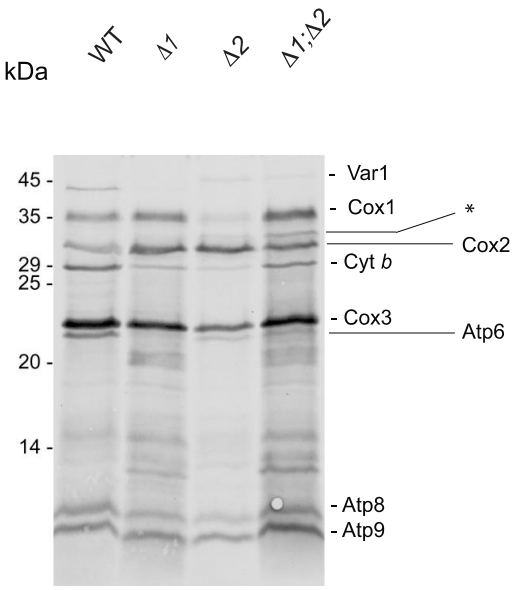

Figure 13. Deletion of Rcf1 and Rcf2 alters mitochondrial translation profile and leads to accumulation of Cox2 precursor. *In organello* translation was performed as described in Materials and Methods and products assessed by SDS-PAGE and autoradiography. The positions of the molecular mass standards and mitochondria-encoded proteins, Var1, Cox1, Cox2, cytochrome *b* (Cyt*b*), Cox3, Atp6, Atp8, and Atp9, are indicated. Asterisk (*) indicates Cox2 precursor.

Δ*rcf2* mitochondria; and the presence of some Cox2 precursor (Cox2p) was observed in Δ*rcf1* and Δ*rcf1;*Δ*rcf2* mitochondria (Figure 13, marked with an asterisk).

The Cox2 N-terminal signal sequence is translocated from the matrix where Cox2p translation takes place into the IMS, where the signal sequence is proteolytically removed by the Imp1 protease on the IMS side of the IM (Clarkson

and Poyton, 1989, Herrmann *et al*., 1995). The translocation is supported by both the Δψ and ΔpH (Herrmann *et al*., 1995). Membrane potential is also required for translocation of C-terminus of Cox2 to the IMS and proper insertion of mature Cox2 into the IM in N_{out}-C_{out} orientation (Herrmann *et al*., 1995).

Accumulation of Cox2p is indicative of lower Δψ and/or ΔpH or impaired Imp1 function in Δ*rcf1* and Δ*rcf1;*Δ*rcf2* mitochondria. To test Imp1 function, processing of other substrates cytochrome b_2 (Cyb2) and NADH-cytochrome b_5 reductase (Mcr1) were analyzed (Figure 14). Both Cyb2 and Mcr1 are nuclear-encoded proteins that are imported into the mitochondria in a Δψ-dependent manner (Geissler *et al.*, 2000, Schneider *et al.*, 1991). Mcr1 is a 34-kDa protein that can be delivered to two locations: OM (where full-length Mcr1 is present, $Mcr1_{34}$) and IM (where Mcr1 is processed to a smaller, soluble form ($Mcr1_{32}$) by Imp1 protease). Mcr1 import into the IM is Δψ-dependent (Hahne *et al*., 1994, Haucke *et al.,* 1997). Similarly, Cyb2 precursor is imported into the IM in Δψ-dependent manner and Imp1 processing of IM-inserted Cyb2 releases mature Cyb2 as soluble IMS protein. The steady-state levels of processed Mcr1 ($Mcr1_{32}$) were not decreased and even slightly elevated in Δ*rcf1* and Δ*rcf1;*Δ*rcf2* mitochondria, resulting in increased ratio of $Mcr1_{32}$:$Mcr1_{34}$ This ratio difference may indicate increased Δψ. No inhibition of Imp1 processing of Cyb2 was observed, which indicates that Imp1 proteolytic activity is not impaired in the absence of Rcf1 and Rcf2 (Figure 14B). Therefore, we conclude that Cox2p maturation protease Imp1 activity is not impaired in the absence of Rcf1 and Rcf2, and the Cox2p maturation was impaired due to decreased ΔpH component of the PMF.

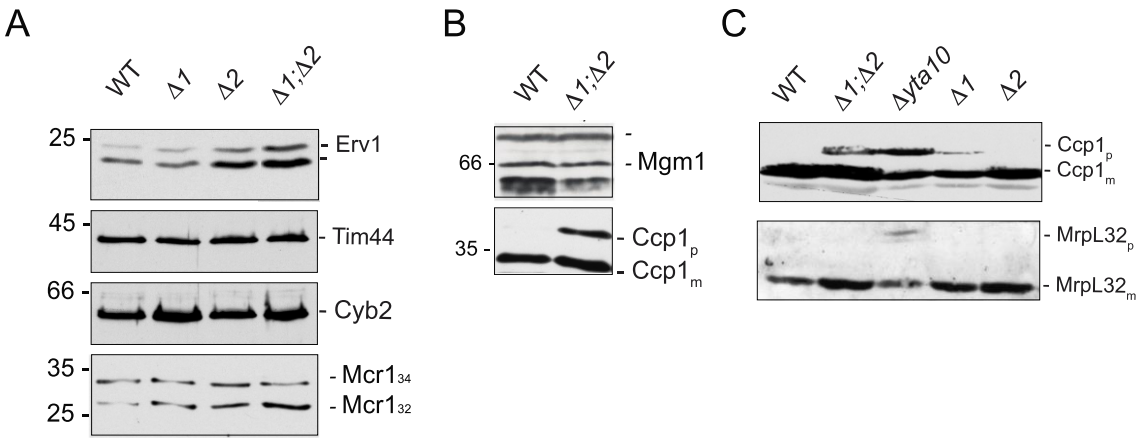

Figure 14. Changes in protein processing observed in the absence of Rcf1 and Rcf2. Steady state levels of non-OXPHOS proteins in wild type (WT) and Δ*rcf1*;Δ*rcf2* (Δ*1*;Δ*2*) evaluated using SDS-PAGE and Western blotting. **(A)** Steady-state levels of IMS protein Erv1, IMS protein cytochrome b_2 (Cyb2) and Mcr1, which is distributed from the IM to the IMS by proteolytic processing. Tim44 was used as a loading control. **(B)** Proteolytic processing of Pcp1 substrate Mgm1 and Pcp1/i-AAA substrate Ccp1. **(C)** Processing of i-AAA substrate MrpL32 and Pcp1/i-AAA substrate Ccp1. Mitochondria from Δ*yta10* strain (lacking i-AAA protease) were used as a reference. (p, precursor protein; m, mature protein).

Import of another nuclear encoded protein into the IMS, Erv1, is not PMF-dependent; rather, its import into the IMS is mediated by mediated by chaperone Mia40. Erv1 levels were increased in in Δ*rcf2* and in Δ*rcf1;*Δ*rcf2* mitochondria, indicating that PMF-independent protein import is not decreased, and is even increased (Figure 14B).

In the course of another experiment, we observed accumulation of some precursor form of cytochrome *c* peroxidase (Ccp1) in the absence of Rcf1 and

Rcf2, suggesting a protein control defect. Ccp1p processing requires m-AAA protease (Yta10/Yta12), which pulls Ccp1 precursor, Ccp1p, out of the IM into the IMS. The pulling by m-AAA protease requires ATP hydrolysis and is impaired in mutants deficient in Yta10 (Δ*yta10*) (Tatsuta *et al*., 2007, Michaelis *et al*., 2005). The m-AAA protease also processes another substrate, MrpL32, which does not depend on ATP hydrolysis (Nolden *et al*., 2005, Schmidt *et al*., 2011). Processing of MrpL32 precursor was normal in the absence of Rcf1 and Rcf2 (Figure 14C). This indicates that pulling activity of the m-AAA protease, but not its proteolytic activity, is affected in the Δ*rcf1;*Δ*rcf2* mitochondria, likely related to lower ATP synthesis or an altered membrane environment in this mutant. ATP-dependent surveillance proteases - i-AAA and m-AAA proteases - are involved in the protein control of the IMS and matrix, where they monitor and remove non-assembled and misfolded membrane proteins such as Ccp1p, Cox2p and Erv1 (Schreiner *et al*., 2012). However, pCox2 was not detectable in mitochondria isolated from Δ*rcf1;*Δ*rcf2* cells, indicating that *in vivo* it is turned over and does not accumulate.

In summary, the protein processing defects observed in Δ*rcf1,* and to a greater extent in Δ*rcf1;*Δ*rcf2* mitochondria indicate that Rcf1 and Rcf2 indirectly support ΔpH-dependent and ATP-dependent protein translocation.

4.2. F_1F_O ATP synthase.

The PMF is the driving force for the ATP synthesis by mitochondrial F_1F_O ATP synthase. This enzyme is composed of F_1, F_O, and stator sectors which are assembled separately and join to form F_1F_O ATP synthase (complex V). Transmembrane F_O sector of the F_1F_O ATP synthase is a proton channel largely composed of an oligomeric ring of Atp9 subunits. The F_O sector interacts with Atp6 and Atp8 subunits and a number of other nuclear encoded transmembrane proteins; a linker (stator) joins F_O and F_1 sector coupling their rotation. Proton translocation from the IMS to the matrix through Atp6-Atp9 oligomer of the F_O sector rotates the enzyme, driving ATP synthesis from ADP and phosphate in the catalytic sites of the matrix F_1 sector. If PMF is dissipated, F_1F_O ATP synthase can reverse its direction, operating as a secondary proton pump. In this case, protons are translocated from the matrix to the IMS powered by ATP hydrolysis catalyzed by F_1 producing ADP and phosphate. Both ATP synthesis and ATP hydrolysis can be inhibited by oligomycin, which binds to a conserved Glu59 of Atp9 subunit and blocks the F_O proton channel (Symersky *et al*., 2012).

Similar to other membrane proteins, the position of F_1F_O ATP synthase (complex V) in the IM is sealed by interactions with membrane lipids (Mehdipour and Hummer, 2016). Complex V is found at cristae rims, where it normally forms dimeric supercomplexes, V_2, which are compatible with highly curved phospholipid environment. Specific, yet intermittent (on and off), interactions of cardiolipin (CL) with a conserved Lys43 of the Atp9 subunit promote assembly, stability, and smooth rotation of the ATP synthase required for its catalytic function (Duncan *et al*., 2016).

4.2.a. F_1F_O ATP synthase levels in the absence of Rcf1/2.

The levels of the F_1F_o ATP synthase complex were initially examined using BN-PAGE, SDS-PAGE, and Western blotting. BN-PAGE / Western blotting indicated that the levels of the roughly 700-kDa F_1F_O ATP synthase complex were similar in wild-type, Δ*rcf1*, Δ*rcf2*, and Δ*rcf1;*Δ*rcf2* mitochondria (Figure 15A). Similarly, SDS-PAGE and Western blotting indicated that the levels of the Atp4 (stator subunit) were nor changed. However, steady-state levels of Atp9 were decreased in the absence of Rcf1 and Rcf2 (Figure 15B). Atp9 protein self-oligomerizes even in presence of SDS, so it was detected following TCA precipitation. Possibly, Atp9 self-oligomers are structurally different and more difficult to break in Δ*rcf1;*Δ*rcf2* mitochondria. Additionally, the levels of F_1 subunit Atp1 and peripheral subunit e (Sue) essential for complex V stability and dimerization, were decreased in Δ*rcf1;*Δ*rcf2* mitochondria (Figure 15B). The decreased detection of F_1F_o ATP synthase subunits may indicate moderate decrease in stability of the enzyme or assembly defects (e.g., decreased stoichiometry of Atp9 oligomers) in the absence of Rcf1 and Rcf2 which was not detected on a BN-PAGE.

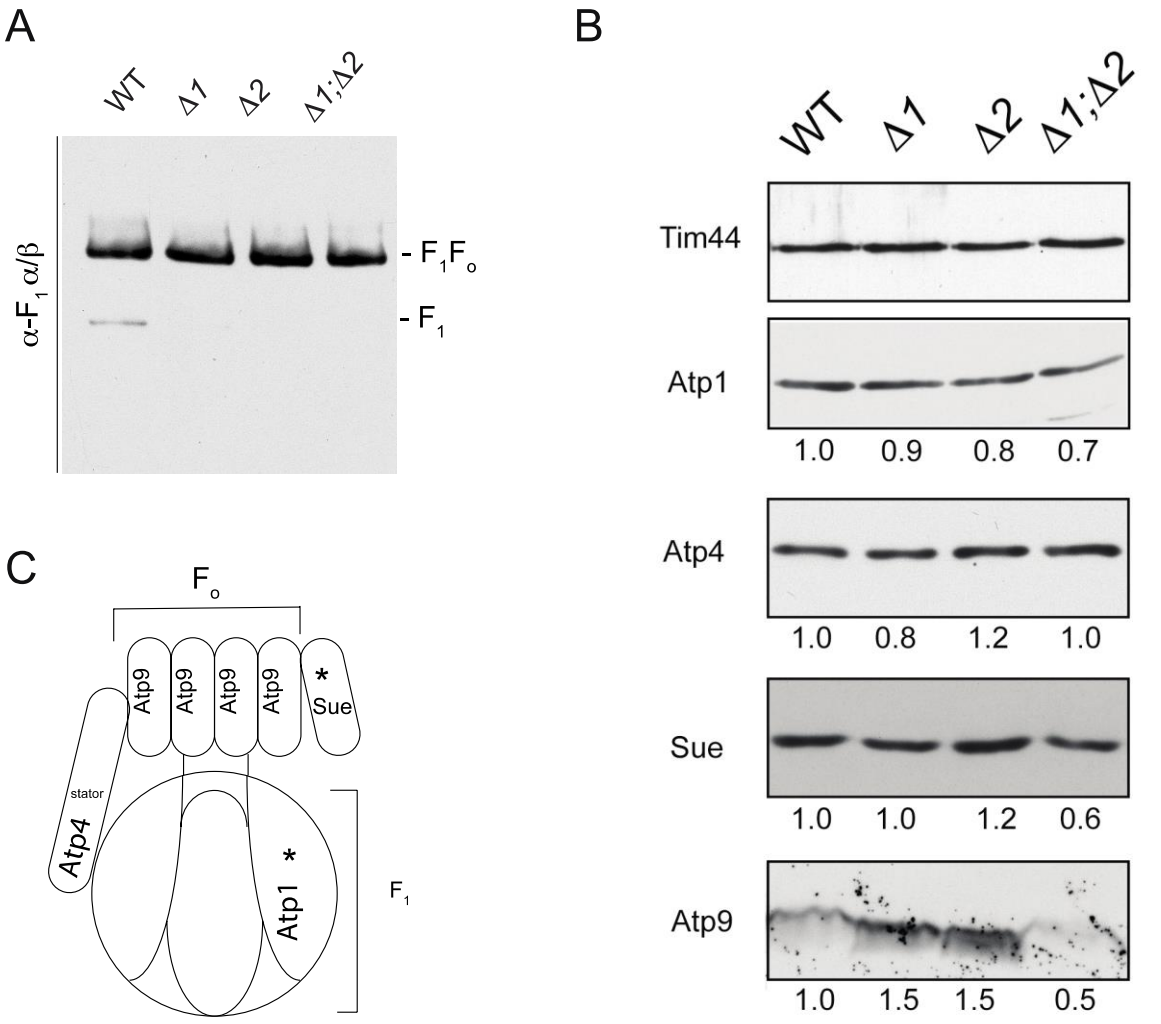

Figure 15. F_1F_O ATP synthase subunit Atp9 levels are altered in absence of Rcf1 and Rcf2, while the levels of the assembled F_1F_O ATP synthase are unchanged. (A) Mitochondria (30 µg protein) isolated from wild-type (WT), Δ*rcf1*, Δ*rcf2,* and the Δ*rcf1;*Δ*rcf2* strains were solubilized in 0.6% DDM and subjected to BN-PAGE analysis, Western blotting, and immunodecoration with antibodies to F_1 sector of ATP synthase (F_1 α/β). **(B)** Steady-state levels of F_1F_O ATP synthase subunits. Mitochondria (25 µg protein) from wild-type (WT), Δ*rcf1*, Δ*rcf2*, and the Δ*rcf1;*Δ*rcf2* strains were subjected to SDS-PAGE, Western blotting and immunodecoration with the antibodies to Atp1 (F_1 sector subunit), Atp4 (stator subunit), subunit e (Sue) (peripheral transmembrane subunit), Atp9 (F_o sector subunit). To detect Atp9, mitochondrial proteins were TCA-precipitated before SDS-PAGE, because Atp9 oligomer can be SDS-resistant. Tim44 was used as a loading control. **(C)** A diagram indicates relative position of the subunits analyzed.

4.2.b. F_1F_O ATP synthase activity in the absence of Rcf1/2.

Oligomycin-sensitive ATP synthesis by the F_1F_O ATP synthase was measured using hexokinase/glucose-6-phosphatase coupled end point assay (Materials and Methods). ATP synthesized and exported (by ADP/ATP exchange via AAC) by wild type, Δ*rcf1,* Δ*rcf2,* and Δ*rcf1;*Δ*rcf2* mitochondria when fueled with ADP and ethanol as a ETC substrate, was measured. Oligomycin-sensitive ATP synthesis was found to be decreased in mitochondria lacking Rcf1 and Rcf2 (Δ*rcf1*=69%, Δ*rcf2*=84%, and Δ*rcf1;*Δ*rcf2*=45% of wild-type) (Table 8 third column). The decrease was greatest in Δ*rcf1;*Δ*rcf2* mitochondria. To confirm that the ATP export from the mitochondria reflected total ATP synthesis, a similar experiment was conducted, except that the mitochondria were solubilized with detergent to quantify total ATP before and after ATP synthesis. In this experiment, oligomycin-sensitive ATP synthesis by Δ*rcf1;*Δ*rcf2* mitochondria was measured to be 46% of the wild-type (Table 9 third column), providing support for the extent of the ATP synthesis impairment detected by the oligomycin-sensitive ATP export assay. Such decrease in ATP synthesis in Δ*rcf1;*Δ*rcf2* mitochondria is consistent with the inability to maintain optimal PMF during state 3 respiration in the absence of Rcf1 and Rcf2.

Table 8. ATP synthesis and export decreased in the absence of Rcf1 and/or Rcf2.

Mitochondria (40 µg) were resuspended in ATP detection buffer containing ethanol (ETC substrate) with oligomycin (1 µM) (+ Oligo) or DMSO (- Oligo). Reaction was started by addition of ADP (100 nmol), incubated for 5 minutes at 30˚C. Mitochondria were pelleted through centrifugation, and supernatant collected. ATP in supernatant was measured with ATP detection enzymes, as described in Materials and Methods. The amount of ATP synthesized was calculated by subtracting the amount of ATP in a control reaction (no ethanol, 1.0 µM oligomycin, 100 nmol ADP; i.e., pre-existing mitochondrial ATP). Wild type, Δ*rcf1*, Δ*rcf2* and Δ*rcf1;*Δ*rcf2* oligomycin-sensitive ATP synthesis (calculated by subtracting second column from first column, and expressed as % of wild-type (WT)) is reported in third column; statistically significant values ($p<0.05$) are indicated by an asterisk. ATP synthase sensitivity to oligomycin, calculated by comparing ATP synthesis in presence and absence of oligomycin, is reported in last column. Average and S.E.M. values (WT (n=6), Δ*1* (n=4), Δ*2* (n=4), Δ*1*;Δ*2* (n=6)); **, *p* value < 0.01.

	ATP synthesis			
	- oligomycin nmol ATP	+ oligomycin nmol ATP	oligomycin sensitive % of WT	Sensitivity to oligomycin % inhibition
WT	46.9 ± 0.5	1.9 ± 1.3	100%	96%
Δ*rcf1*	34.2 ± 2.2	3.3 ± 0.4	**69%	90%
Δ*rcf2*	42.6 ± 1.5	4.8 ± 2.2	**84%	89%
Δ*rcf1*;Δ*rcf2*	24.8 ± 1.2	4.7 ± 0.8	**45%	81%

Table 9. Total ATP synthesis is decreased in absence of Rcf1 and Rcf2.

Mitochondria (40 µg) were resuspended in ATP detection buffer containing succinate (ETC substrate) and oligomycin (20 µM) or DMSO. Reaction was started by addition of ADP (200 nmol) and incubated for 3 minutes at 30˚C. Mitochondrial membranes were solubilized with deoxycholate (0.2%) for 5 minutes, and the total ATP in the sample was measured with ATP detection enzymes.

	Total ATP		
	- oligomycin nmol ATP	+ oligomycin nmol ATP	oligomycin-sensitive % of WT
WT	49.07	24.7	100%
Δ*rcf1*;Δ*rcf2*	31.07	19.79	46%

4.2.c. Sensitivity of F_1F_O ATP synthase to oligomycin.

ATP synthesis in oligomycin-treated Δ*rcf1,* Δ*rcf2,* and Δ*rcf1;*Δ*rcf2* mitochondria was observed to be greater than in wild type mitochondria (Table 8, second column). Oligomycin sensitivity is calculated as ATP synthesis in oligomycin-treated sample relative to ATP synthesis in absence of oligomycin. In addition to the decreased ATP synthesis rate, sensitivity of ATP synthesis to oligomycin was somewhat decreased in Δ*rcf1,* Δ*rcf2,* and Δ*rcf1;*Δ*rcf2* mitochondria (Table 8, last column). Sensitivity of ATP synthesis to oligomycin was not measured when mitochondria were solubilized with detergent since the ATP present in oligomycin treated mitochondria likely reflected total mitochondrial ATP, and not ATP synthesis (Table 9, second column).

To further explore oligomycin sensitive ATP synthesis, the concentration of oligomycin in the assay was titrated (0.5 µM and 0.1 µM). Wild type mitochondria were equally sensitive to 1.0 µM and 0.5 µM oligomycin concentration, which inhibited 89% and 88% of ATP synthesis, respectively. In contrast, Δ*rcf1* and Δ*rcf1*;Δ*rcf2* mitochondria were less sensitive to 0.5 µM oligomycin concentration, which inhibited 78% and 68% of ATP synthesis, respectively (Table 10). Oligomycin sensitivity was not decreased in Δ*rcf2* mitochondria. The 0.1 µM oligomycin concentration inhibited 50% or less ATP synthesis in wild type, Δ*rcf1* and Δ*rcf1*;Δ*rcf2* mitochondria.

Table 10. Oligomycin sensitivity of ATP synthase in the absence of Rcf1/Rcf2.

Mitochondria (40 µg) were resuspended in ATP detection buffer (0.5 ml) containing ethanol and oligomycin (1.0 µM, 0.5 µM, 0.1 µM) or DMSO (no oligomycin) (-). Reaction was started by addition of ADP (100 nmol), incubated for 5 minutes at 30˚C, mitochondria were pelleted, and supernatant collected. ATP in supernatant was measured. The amount of ATP synthesized was calculated by subtracting ATP in a control reaction (no ethanol, 1.0 µM oligomycin, 100 nmol ADP, i.e. pre-existing mitochondrial ATP). ATP synthesis is reported in the upper table (n=2 for every condition). ATP synthesis inhibition (% sensitivity) relative to ATP synthesis in absence of oligomycin, is reported in the lower table.

	ATP synthesis [nmol]			
[oligomycin], µM	**0**	**0.1**	**0.5**	**1.0**
WT	47.8 ± 0.2	27.1 ± 1.2	6.0 ± 0.0	5.2 ± 0.4
Δ*rcf1*	31.9 ± 4.1	19.1 ± 0.5	7.1 ± 0.4	2.8 ± 0.5
Δ*rcf2*	44.7 ± 2.2	18.2 ± 1.8	2.2 ± 0.2	3.3 ± 1.0
Δ*rcf1*;Δ*rcf2*	23.1 ± 2.7	12.8 ± 0.1	7.3 ± 1.0	2.4 ± 0.5

	% inhibition by oligomycin		
[oligomycin], µM	**0.1**	**0.5**	**1.0**
WT	43%	88%	89%
Δ*rcf1*	40%	78%	91%
Δ*rcf2*	59%	95%	93%
Δ*rcf1*;Δ*rcf2*	45%	68%	90%

To determine whether lower sensitivity of OXPHOS ATP synthesis to oligomycin was observed not only in isolated mitochondria, but also in cells lacking Rcf1 and Rcf2, the effect of oligomycin on respiratory growth was evaluated. When oligomycin concentration in the growth media was titrated to the threshold of inhibiting respiratory growth of wild-type cells (0.1-0.3 mg/L), the respiratory growth of the Δ*rcf1* and Δ*rcf1*;Δ*rcf2* mutant was not inihibted by this concentration of oligomycin (Figure 16A, third panel). Greater concentration of oligomycin (1.0 mg/L) was needed to inhibit respiratory growth of these mutants (Figure 16A, last panel). We conclude that these experiments show a decreased sensitivity to oligomycin in the absence of Rcf1.

Some mutations trigger mitochondrial signaling pathway (called retrograde response) resulting in expression of multidrug resistance transporter genes such as *PDR5*, which confer resistance to oligomycin and other drugs, e.g. cycloheximide (Katzmann *et al*., 1995). To test whether Δ*rcf1*;Δ*rcf2* cells were multidrug resistant, growth on cycloheximide containing media was evaluated (Figure 16B). The Δ*rcf1*;Δ*rcf2* cells did not display decreased sensitivity to cycloheximide on glucose or glycerol media. These results lead us to conclude that changes in oligomycin binding to F_1F_O ATP synthase, not the expression of multidrug resistance pumps, confers the oligomycin resistant growth to the Δ*rcf1* and Δ*rcf1*;Δ*rcf2* strains. Alternatively, an increased level of mitochondrial substrate level phosphorylation may explain increased ATP synthesis in presence of oligomycin.

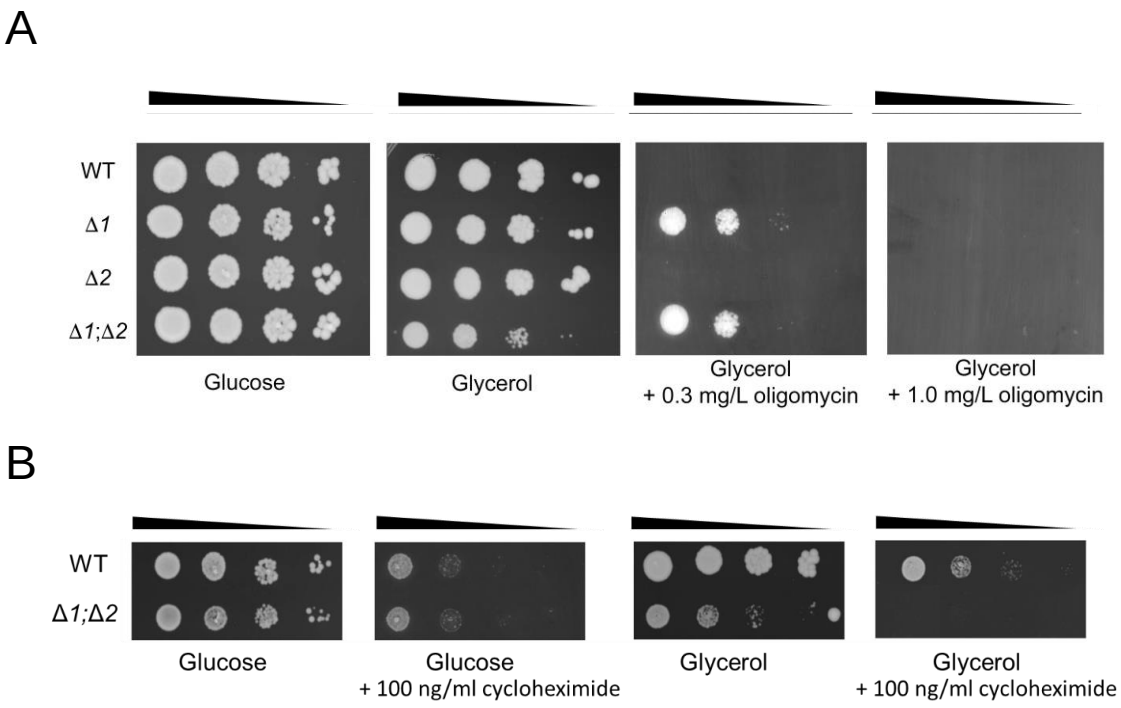

Figure 16. Decreased inhibition of respiratory growth by oligomycin in the absence of Rcf1. (A) Serial dilutions wild type, Δ*rcf1*, Δ*rcf2*, and Δ*rcf1;*Δ*rcf2* cultures were spotted on rich (YP) agar containing glucose (2%) or glycerol 3% containing low (0.3 mg/L) or high concentration (1.0 ml/L) of oligomycin and incubated for 3 days (Glucose) or 6 days (glycerol) at 30˚C. **(B)** Serial dilutions were performed as in **(A)** on agar containing no or 100 ng/ml cycloheximide and incubated for 5 days at 30˚C.

Oligomycin partitions to lipid-water interface and binds Atp9; rotation of the F_1F_O-ATP synthase F_O sector brings oligomycin deeper into the transmembrane region where it stalls the rotation at the site of Atp9 interaction with subunit a, and therefore blocks the passage of protons (Zhou and Faraldo-Gómez, 2018). Decreased inhibition of ATP synthase by oligomycin is consistent with altered conformation of Atp9 or its affinity for oligomycin in the absence of Rcf1.

4.2.d. F_1F_O ATPase activity in the absence of Rcf1/2.

When PMF is dissipated, the rotation of F_1F_O ATP synthase can be reversed, resulting in ATP hydrolysis (ATPase) activity (Bustos *et al*., 2005). ATPase activity was initially measured in mitochondria solubilized with Triton X-100 (0.0375%). The reaction was carried out for 2 minutes and stopped by the addition of trichloroacetic acid (TCA) to denature proteins; phosphate in the supernatant was measured. Oligomycin-sensitive ATP hydrolysis by detergent-solubilized Δ*rcf2* mitochondria was similar to the wild-type; and in Δ*rcf1* and Δ*rcf1;*Δ*rcf2* mitochondria ATP hydrolysis was decreased, to 73% and 77% of the wild-type ATP hydrolysis rate, respectively (Table 11). Decreased ATP hydrolysis was consistent with decreased Atp9 content in the Δ*rcf1;*Δ*rcf2* mitochondria, but contrasts with elevated Atp9 levels detected in Δ*rcf1* mitochondria (Figure 15B), indicating altered assembly or stability of F_1F_o ATP synthase.

Detergent solubilization of mitochondria can sometimes disturb the interaction of membrane-embedded F_o sector of ATP synthase with the F_1 sector. Free F_1 sector can still hydrolyze ATP but is not sensitive to oligomycin because is no longer associated with F_o sector. Therefore, sensitivity of ATP hydrolysis to oligomycin in this assay does not accurately reflect oligomycin sensitivity of intact enzyme, and it was low in wild type mitochondria (66%, Table 11 last column). ATP hydrolysis in presence of oligomycin in Δ*rcf1* and Δ*rcf2* mitochondria was greater than in wild-type mitochondria (Table 11 second column); this was consistent with the increased Atp9 levels detected (Figure 15B) and indicates

Table 11. ATP hydrolysis in mitochondrial lysate. Mitochondria (50 µg) was solubilized in buffer (0.9 ml, 0.2 M KCl, 3 mM $MgCl_2$, 0.0375% TritonX-100, 10 mM Tris-HCl, pH 8.4) at 30˚C in presence or absence of oligomycin (20 µM). Reaction was started by addition of 5 mM ATP and stopped with TCA after 2 minutes, followed by centrifugation for 10 minutes at 10000 rpm. Phosphate concentration in supernatant was measured using ammonium molybdate-ferrous sulfate colorimetric assay. Average and S.E.M. values are reported (WT (n=27), Δ*1* (n=7), Δ*2* (n=9), Δ*1*;Δ*2* (n=19)).

	Triton X-100 ATP hydrolysis [µmol Pi/mg]		Oligomycin-sensitive ATPase % of WT	Oligomycin sensitivity
	- Oligo	+ Oligo		
WT	5.32 ± 0.51	1.80 ± 0.45	100%	66%
Δ*rcf1*	4.47 ± 0.61	1.89 ± 0.49	73%	58%
Δ*rcf2*	5.80 ± 1.02	2.22 ± 0.58	101%	62%
Δ*rcf1*;Δ*rcf2*	3.68 ± 0.34	0.95 ± 0.59	77%	74%

Table 12. ATP hydrolysis in intact mitochondria. Mitochondria (50 µg) was resuspended in buffer (0.9 ml, 0.2 M KCl, 3 mM $MgCl_2$, 10 mM Tris-HCl, pH 8.4) at 30˚C in presence or absence of oligomycin (20 µM). Reaction was started by addition of 5 mM ATP and stopped with TCA after 2 minutes, followed by centrifugation for 10 minutes at 10000 rpm. Phosphate concentration in supernatant was measured using ammonium molybdate-ferrous sulfate colorimetric assay. Average and S.E.M. values are reported (WT (n=7), Δ*1* (n=5), Δ*2* (n=5), Δ*1*;Δ*2* (n=7)).

	No detergent ATP hydrolysis [µmol Pi/mg]		Oligomycin-sensitive ATPase % of WT	Oligomycin sensitivity
	- Oligo	+ Oligo		
WT	3.04 ± 0.15	0.47 ± 0.04	100%	85%
Δ*rcf1*	3.17 ± 0.45	0.51 ± 0.18	104%	84%
Δ*rcf2*	2.09 ± 0.42	0.45 ± 0.15	64%	79%
Δ*rcf1*;Δ*rcf2*	1.73 ± 0.14	0.39 ± 0.09	52%	78%

decreased stability of F_1F_O ATP synthase in these mitochondria.

ATP hydrolysis was next measured in intact mitochondria (without detergent) (Dienhart *et al.,* 2002). ATP hydrolysis in intact mitochondria was slower than in detergent solubilized mitochondria (similarly for wild type and mutant samples), reflecting the limitation posed by the rate of ATP import into the mitochondrial matrix, which is catalyzed by the ADP/ATP carrier (AAC). Also, ATP hydrolysis was more sensitive to oligomycin in intact mitochondria than in detergent mitochondria, reflecting that the association of F_1 and F_O sectors of ATP synthase was not disturbed. ATP hydrolysis activity in intact Δ*rcf1* and was similar to that of the wild type mitochondria. This contrasted with the ATP hydrolysis in detergent solubilized Δ*rcf1* mitochondria. We were unable to determine why ATP hydrolysis in detergent solubilized, but not in intact Δ*rcf1* mitochondria, was impaired. ATP hydrolysis activity in Δ*rcf2* and Δ*rcf1;*Δ*rcf2* mitochondria was decreased. Oligomycin-sensitive ATP hydrolysis in Δ*rcf2* and Δ*rcf1;*Δ*rcf2* was measured to be 64% and 52% of the wild-type ATP hydrolysis rate, respectively (Table 12). Sensitivity of ATP hydrolysis to olifomycin was not significantly different in the absence of Rcf1 or Rcf2 (Table 12, last column).

ATP hydrolysis activity in intact mitochondria normally pumps the protons out of the matrix and can sustain membrane potential, although at a lower level than the PMF generated by the electron transport chain (ETC) (Wang *et al*., 2007). The capacity of the ATP synthase to reverse its direction and establish the PMF upon inhibition of ETC was measured in intact mitochondria using membrane potential indicator, Rhodamine-123 (R-123) and in collaboration with

Dr. David Mueller (Rosalind Franklin University, Chicago, IL), using previously established methods (S. Saddar, PhD dissertation). The ATPase (F_1F_O ATP synthase reversal) activity generated the membrane potential (Table 13) in Δ*rcf1*, Δ*rcf2*, and Δ*rcf1;*Δ*rcf2* mitochondria and similar to the wild type mitochondria, indicating that F_1F_O ATP synthase retained proton pumping capacity through the F_o sector. However, the membrane potential was only monitored for 1 minute and it is possible that membrane potential was not maintained for a long period of time.

Table 13. Capacity of ATPase to establish mitochondrial membrane potential upon inhibition of ETC. Mitochondrial membrane potential generated by ATP hydrolysis was measured using Rhodamine-123 (R-123) as described in Materials and Methods. Membrane potential established by ATPase (% fluorescence quenching) was calculated as a % difference in signal with 2 mM ATP, 1 mM $MgCl_2$ and signal following depolarization (oligomycin and CCCP addition).The average and SEM are shown (WT (n=4), Δ*1* (n=4), Δ*2* (n=2), Δ*1*;Δ*2* (n=4)).

	ATP hydrolysis associated fluorescence quenching,
WT	19 ± 1%
Δ*rcf1*	26 ± 1%
Δ*rcf2*	17 ± 6%
Δ*rcf1*;Δ*rcf2*	20 ± 1%

The inconsistencies observed between the normal levels of F_1F_o ATP synthase complex on a BN-PAGE, increased Atp9 subunit levels on an SDS-

PAGE, and different ATP synthesis and ATP hydrolysis rates in the in Δ*rcf1* and Δ*rcf2* mitochondria, are without a comprehensive explanation.

The ATP hydrolysis in the Δ*rcf1;*Δ*rcf2* mitochondria was consistently decreased. We conclude that not only decreased PMF generation by the ETC, but also decreased ATP synthase levels and/or stability contributed to the decreased ATP synthesis in the absence of Rcf1 and Rcf2.

4.3. ADP/ATP carrier (AAC)

4.3.a. Stability and environment of AAC in the absence of Rcf1/2.

Exchange of metabolites across the IM is mediated by metabolite carrier proteins of the mitochondrial carrier family (MCF). Critical MCF proteins AAC and PIC preferentially import ADP and phosphate, respectively, into the mitochondrial matrix. AAC catalyzes exchange of ADP^{3-} for ATP^{4-} (Nicholls and Ferguson, 2013). The directionality of the AAC transport that is driven by the Δψ maintains the ATP/ADP ratio in the mitochondrial matrix hundreds of times lower than the ATP/ADP ratio in the cytoplasm (Gout *et al*., 2014). PIC catalyzes $H_2PO_4^-/H^+$ symport that is driven by ΔpH (Nicholls and Ferguson, 2013). Due to the action of PIC, the phosphate concentration in mitochondrial matrix is 3 times greater than in the cytoplasm. The decrease in PMF in the Δ*rcf1*;Δ*rcf2* mitochondria may therefore be limiting for ADP/ATP exchange or phosphate import.

To test whether deletion of Rcf1 and Rcf2 influenced AAC and PIC, steady-state levels of these proteins were assessed by Western blotting. The AAC and PIC levels were not adversely affected in the absence of Rcf2 compared to the wild-type control, while PIC levels were even higher in the absence of Rcf1 (Figure 17A).

AAC is found in association with the III-IV and TIM23 supercomplexes, yet AAC interaction with Rcf1 is independent of complex III and IV (Strogolova *et al*., 2012). Factors that influence AAC interaction with the supercomplexes are largely unexplored. To test whether removal of Rcf1 and/or Rcf2 would alter AAC association with the III-IV and TIM23 supercomplexes, His-tagged Aac2p was expressed in wild-type and Δ*rcf1*;Δ*rcf2* cells and mitochondria were isolated and solubilized in 0.6% digitonin, which preserves AAC association with the supercomplexes (Dienhart and Stuart, 2008). ^{HIS}Aac2 was subjected to affinity purification (Ni-NTA pull-down) assay. Affinity co-purification of complex IV component Cox3 and TIM23 complex component Tim17 with a ^{HIS}Aac2 isoform was detected in wild-type mitochondria. ^{HIS}Aac2 co-purified Tim17 and Cox3 in Δ*rcf1*;Δ*rcf2* mitochondria; less Cox3 was affinity purified with Aac2, reflecting decreased levels of complex IV in Δ*rcf1*;Δ*rcf2* mitochondria (Figure 17B). We conclude that AAC association with the supercomplexes does not require Rcf1 and Rcf2.

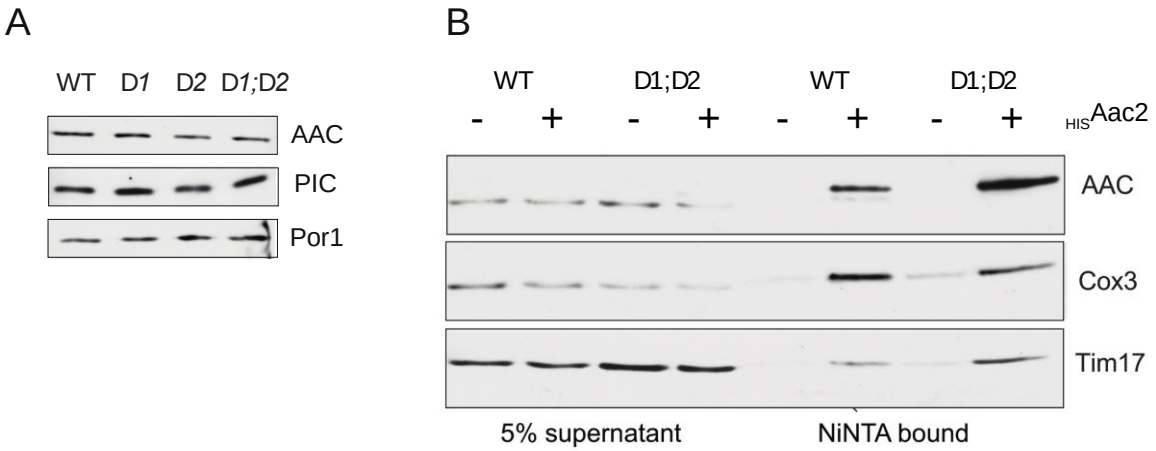

Figure 17. AAC steady state levels and environment in the absence of Rcf1 and Rcf2. (A) Steady-state levels of MFC carriers AAC and PIC. Mitochondria (25 µg protein) from wild-type, Δ*rcf1,* Δ*rcf2*, and the Δ*rcf1;*Δ*rcf2* strains were subjected to SDS-PAGE, Western blotting and immunodecoration with antibodies to AAC, PIC, Por1. Outer mitochondrial membrane porin Por1 was used as a loading control. **(B)** AAC association with III-IV and TIM23 supercomplexes. Mitochondria (30 µg) from WT or Δ*rcf1;*Δ*rcf2* strains expressing $_{HIS}$Aac2 were solubilized in digitonin (0.6%) and subjected to Ni-NTA affinity purification. Mitochondrial sample (5% supernatant) and NiNTA bound material were subjected to SDS-PAGE, Western blotting and immunodecoration with antibodies to AAC, Cox3, or Tim17.

AAC is a source of considerable proton leak and its misfolding can lower membrane potential (Brand *et al*., 2005, Liu *et al*., 2015). While the AAC proteins are thought to operate as monomers, they are present as dimers in the membrane, which are partially stable following detergent extraction. In order to evaluate AAC dimerization and possible misfolding/aggregation in the absence of Rcf1 and Rcf2, AAC monomers and oligomers were resolved in a non-denaturing native gel (BN-PAGE). Previously our lab observed that immunodetection of AAC monomers and oligomers in their native form on non-denaturing gel was impaired

in Δ*rcf1*;Δ*rcf2* mitochondria in spite of close to wild type AAC levels on an SDS-PAGE (J. Garlich, PhD dissertation and Figure 18A, compare with Figure 17A). Decreased immunodetection of non-denatured AAC molecules may be attributed to differential accessibility of the antigenic epitopes in AAC native form, and suggests that either AAC conformation or associated lipids are altered in the absence of Rcf1 and Rcf2. AAC detection was restored when first dimension non-denaturing gel electrophoresis was followed by second dimension denaturing SDS-PAGE. In addition, a shift in mobility was observed, the AAC dimer and monomer had faster mobility in the absence of Rcf1 and Rcf2, and the AAC dimer was decreased in proportion to AAC monomer (Figure 17B). Faster migration of AAC on a native gel may indicate decreased association or absence of one or more CL molecules from the carrier protein (Jiang *et al.,* 2000).

Overall, these results indicate that AAC association with the supercomplex III_2IV_{1-2} was retained in the absence of Rcf1 and Rcf2. However, AAC dimerization was reduced and gel mobility of AAC monomer was faster, possibly indicating a loss of one or more CL molecules. We conclude that the absence Rcf1 and Rcf2 impairs AAC association with lipid molecules.

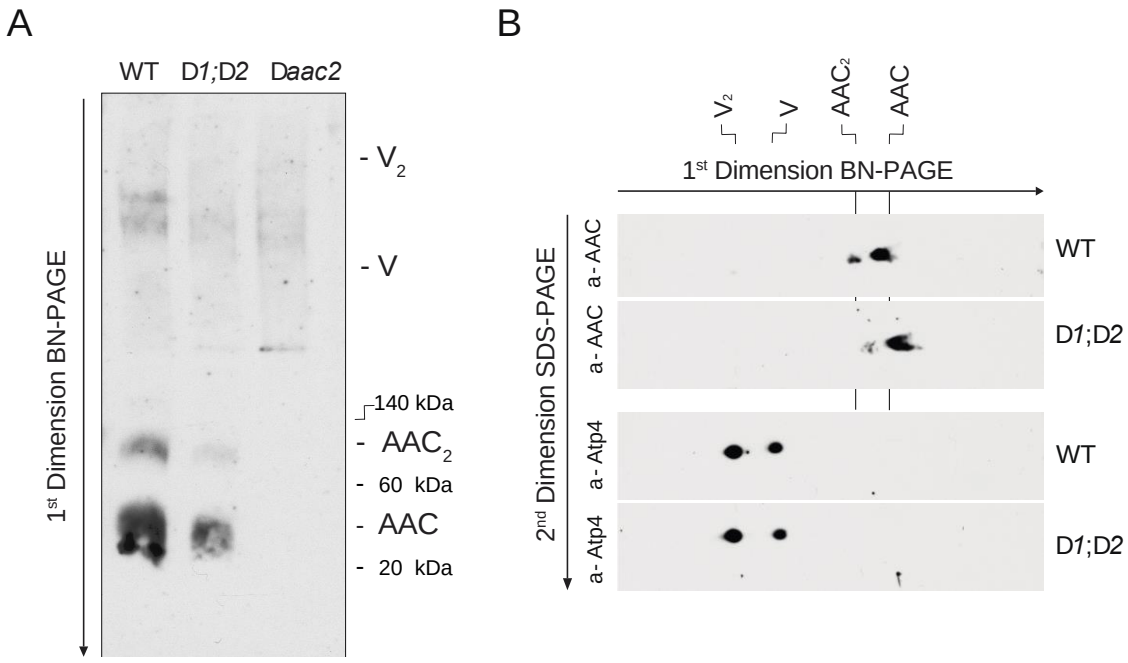

Figure 18. AAC molecular environment in the absence of Rcf1 and Rcf2. (A) Altered detection of AAC on a BN-PAGE in Δ*rcf1*;Δ*rcf2* mutant. Mitochondria (30 µg protein) from wild-type, Δ*rcf1*;Δ*rcf2* and Δ*aac2* strains were solubilized in 0.2% digitonin (Jiang *et al*., 2000) and subjected to BN-PAGE and Western blotting with α-AAC antibody. The positions of molecular mass markers and the dimeric and monomeric ATP synthase (V_2, approximately 1000 kDa, V, approximately 500 kDa) are indicated. **(B)** Two-dimension analysis of the AAC monomer and dimer mobility. Mitochondria (30 µg) from WT or Δ*rcf1*;Δ*rcf2* (Δ*1*;Δ*2*) strains were solubilized in digitonin (1%) and subjected to BN-PAGE (1st dimension), then the two gel lanes were excised and subjected to SDS-PAGE (2nd dimension), followed by Western blotting, and decoration with antibodies to AAC or to Atp4 subunit of ATP synthase, as indicated.

4.3.b. Deletion of RCF1/2 did not impair AAC-mediated adenine nucleotide exchange.

Changes in AAC-associated lipids or its surrounding proteins observed in the absence of Rcf1 and Rcf2 may impact adenine nucleotide exchange or alter this protein's inherent propensity for proton leak. To test whether Rcf1 or Rcf2 alter the adenine nucleotide exchange activity of the AAC, ATP export rate concomitant with ADP import was measured in WT, Δ*rcf1*, Δ*rcf2*, and Δ*rcf1*;Δ*rcf2* mitochondria. To this end, the rate of preexisting ATP release stimulated by the addition of ADP in the absence of ATP synthesis (in presence of 20 µM oligomycin) in isolated mitochondria was measured. The rate of ATP release was determined using a coupled hexokinase/glucose-6-phosphatase assay converting ATP to NADPH and measuring the increase in NADPH fluorescence in the supernatant over time. This assay is sensitive and suitable to measure the ATP export rate by AAC isoforms *in organello* (Hamazaki *et al.,* 2011, De Marcos Lousa *et al.,* 2002). In absence of ADP, ATP release was minimal (Table 14, first and second column). When ADP and succinate were added, the ATP release rate was greater, reflecting release of pre-existing and newly synthesized mitochondrial ATP. In presence of oligomycin, the rate of ATP release was decreased, consistent with the inhibition of the ATP synthesis. The rate of ATP release in presence of oligomycin, ADP, and substrate, was used to estimate the AAC-dependent ATP export. The AAC-dependent ATP export in Δ*rcf1* and Δ*rcf1*;Δ*rcf2* mitochondria was similar to the wild-type, while Δ*rcf2* was a little

decreased (Table 14, last column). We conclude that AAC adenine nucleotide exchange activity is not impaired in Δ*rcf1*;Δ*rcf2* mitochondria.

Table 14. AAC-dependent ATP export activity.

Mitochondria (40 µg) were resuspended in ATP detection buffer (Materials and Methods) containing ETC substrate succinate (10 mM, where indicated), oligomycin (20 µM, where indicated), and ATP detection enzymes. Reaction was started by addition of 14 nmol ADP (where indicated) and monitored for 3 minutes at room temperature. AAC activity (ATP export rate in presence of ADP, succinate, and oligomycin) is reported in lower table. Average and S.E.M. values are reported (WT (n=15), Δ*1* (n=9), Δ*2* (n=6), Δ*1*;Δ*2* (n=15)).

	ATP export [nmol Pi/min/mg]				
ADP	-	-	+	+	+
Succinate	-	+	-	+	+
Oligomycin	-	-	-	-	+
WT	3.72 ± 1.07	6.04 ± 0.18	67.45 ± 5.06	107.1 ± 4.14	34.08 ± 1.81
Δ*rcf1*	7.62 ± 1.98	6.13 ± 0.83	41.55 ± 7.95	84.52 ± 2.75	35.49 ± 3.19
Δ*rcf2*	3.90 ± 0.57	ND	65.51 ± 2.69	70.06 ± 2.44	28.16 ± 0.59
Δ*rcf1*;Δ*rcf2*	2.80 ± 0.28	4.40 ± 1.56	45.82 ± 3.01	80.09 ± 5.84	34.94 ± 1.97

	AAC activity % of WT
WT	100%
Δ*rcf1*	104%
Δ*rcf2*	83%
Δ*rcf1*;Δ*rcf2*	103%

In summary, while AAC exhibited altered mobility due to decrease association of lipid molecules in the absence of Rcf1 and Rcf2, the ADP/ATP exchange function of the carrier was not impaired. It remains possible that these changes increased AAC non-specific proton leak.

4.4. Mitochondrial network morphology in the absence of Rcf1/2.

The number of individual mitochondria in the cell is variable, because mitochondria frequently undergo fission(division) and fusion. Mitochondrial fusion connects individual mitochondrial inner and outer membranes and leads to a mixing of their contents. Multiple fused mitochondria contain multiple mitochondrial DNA molecules extend into moving and dynamic mitochondrial network. Morphology of mitochondrial network within the cell is incredibly dynamic and changes in response to the changes in respiratory activity and PMF (Egner *et al*., 2002, Lackner, 2014, Rafelski *et al*., 2012, Rafelski, 2013). Specifically, depletion of mitochondrial membrane potential(e.g. by the addition of an uncoupler CCCP) causes fragmentation in the mitochondrial network (Legros *et al*., 2002, Vowinckel *et al.*, 2015, Jones *et al*., 2017). However, the relevance of mitochondrial morphology for organelle function is not completely understood; although some proteins are known to modulate both respiratory function and mitochondrial architecture (Harner *et al.*, 2014). Many respiratory deficient mutants have apparently normal mitochondrial network morphology (Rafelski *et al*., 2012). Emerging evidence indicates that respiration and, specifically, PMF controls mitochondrial volume. Mitochondrial swelling is observed *in vivo* after mitochondrial depolarization (Safiulina *et al*., 2006, Kaasik *et al*., 2007, Miyazono *et al*., 2018).

We hypothesized that the mitochondrial network may be altered in the absence of Rcf1 and Rcf2, reflecting decreased PMF and possibly contributing to

the respiratory growth defect. In order to visualize the mitochondrial network, 3D images were collected of YPGal grown WT, Δ*rcf1*, Δ*rcf2*, and Δ*rcf1*;Δ*rcf2* cells expressing mitochondrially targeted GFP (mtGFP) protein (n=86 WT cells, n=132 Δ*rcf1* cells, n=121 Δ*rcf2* cells, n=94 Δ*rcf1*;Δ*rcf2* cells). The mitochondrial networks were evaluated by manual observation and manual scoring and the Δ*rcf1*;Δ*rcf2* mitochondrial networks appeared fragmented compared to wild-type control (Figure 19A). 3D images were analyzed in ImageJ software using the software plugin Yeast_MitoMap (Vowinckel *et al*., 2015), which automatically processes 3D images, and identifies the individual mitochondrial networks in each cell and calculates volume, surface area, and other shape descriptive parameters. The fragmentation index *f,* defined as a sum of relative fragment volumes that individually constitute less than 20% of the mitochondrial network volume, was then calculated for each cell (Table 15 second column). Mitochondrial fragmentation index *f* tended to be higher in cells lacking Rcf1 but the increase was not statistically significant (p=0.141), and in Δ*rcf2* and Δ*rcf1*;Δ*rcf2* cells, *f* was not higher than the wild-type. The uneven mtGFP signal in the Δ*rcf1*;Δ*rcf2* mitochondrial network appears to have caused the discrepancy between manual and automatic scoring results. The automatic processing of mitochondria had utilized a lower threshold than that of a human eye when distinguishing mtGFP signal from the background. On the other hand, the interspersed regions with weaker mtGFP signal within a continuous network visually (to a human eye) appeared as distinct mitochondria. The distinct, ragged morphology of Δ*rcf1*;Δ*rcf2* appeared fragmented (Figure 19A, last panel).

Other parameters were used to characterize the shape of the main mitochondrial network (main network comprising 20% or more of the total mitochondrial volume of each cell) – volume (V), surface area (SA), SA:V ratio (Vowinckel *et al*., 2015) (Table 15). Deleting Rcf1, but not Rcf2, decreased mitochondrial network volume. This was likely because smaller mitochondrial fragments were more numerous in Δ*rcf1* cells, decreasing the main network volume. Deleting Rcf2 increased mitochondrial network volume and increased surface area. Deleting both Rcf1 and Rcf2 increased mitochondrial network volume and decreased surface area. Although the changes in SA and V were not statistically significant due to large variation in mitochondrial size corresponding to variations in the cell size, SA:V ratio was calculated for each cell individually and provided normalization for the variation caused by the cell size; the SA:V ratio of mitochondrial networks in Δ*rcf1*;Δ*rcf2* cells was significantly decreased (Figure 19B). SA:V ratio is a simple shape descriptor. An inflated balloon is characterized by lower SA:V ratio than the same balloon, deflated. A decreased SA:V ratio indicates that Δ*rcf1*;Δ*rcf2* mitochondria appear thicker, more inflated than wild-type mitochondria. Such changes may reflect increased swelling of the Δ*rcf1*;Δ*rcf2* mitochondria.

A decreased SA:V ratio can be the result of changes in the mitochondrial architecture, which was addressed using electron microscopy approach. Preliminary electron microscopy (EM) imaging of wild-type and mutant cells was performed in collaboration with Dr. Benedikt Westermann and Dr. Till Klecker (Universitaet Bayreuth, Germany) according to standard protocols (Unger *et al*.,

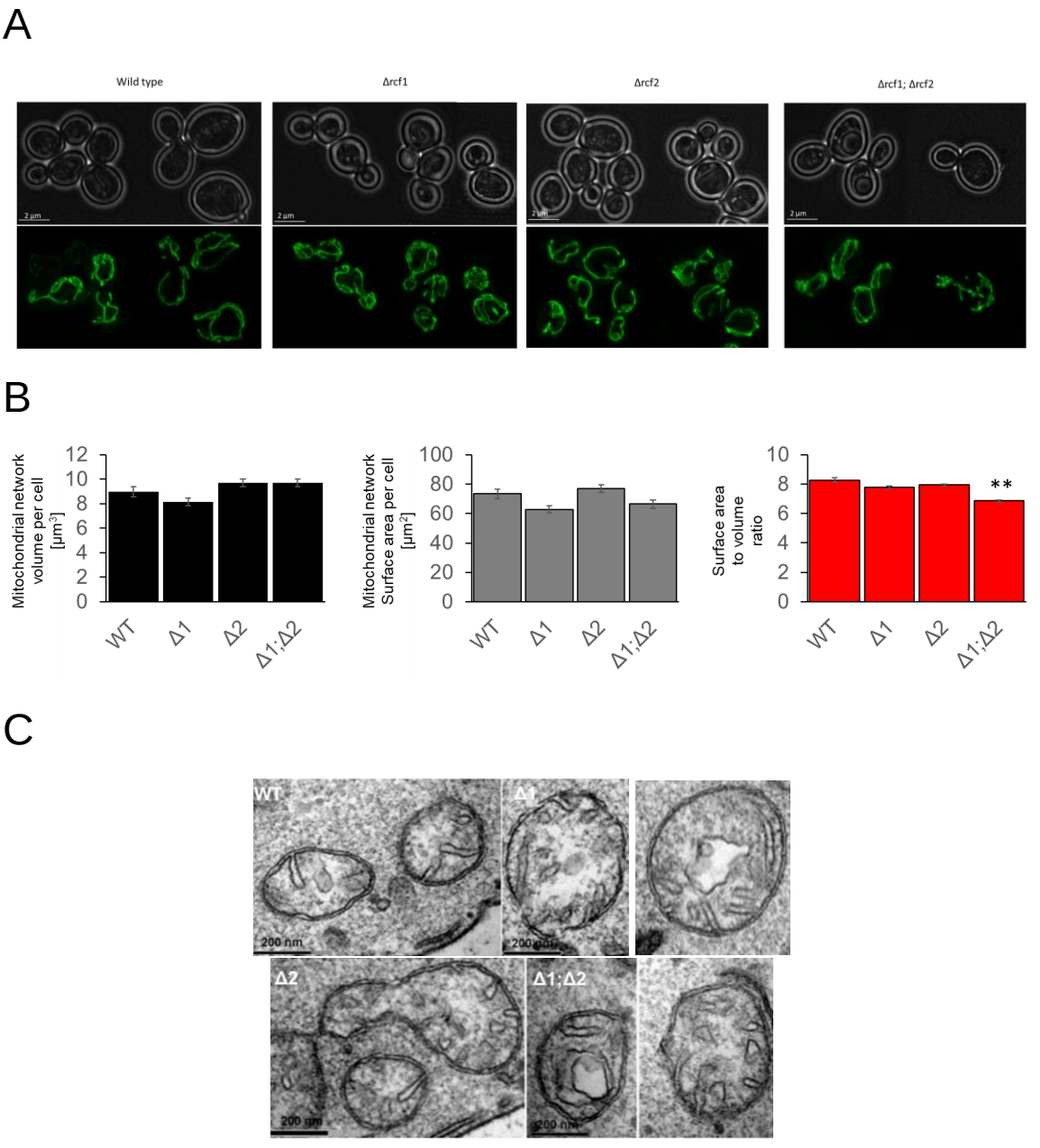

Figure 19. Mitochondrial network morphology in the mutants. (A) Representative images of the YP-Gal grown yeast cells (brightfield images, top panel) mitochondrial network visualized with mtGFP (GFP, bottom panel). **(B)** Wild type, Δ*rcf1*, Δ*rcf2*, and the Δ*rcf1;*Δ*rcf2* mtGFP images were analyzed using Yeast_MitoMap plugin. Surface area (SA), volume (V), and SA:V ratio calculated for every cellular mitochondrial network. Average +/- SEM is shown; ** indicate statistically significant difference (Student's t-test p<0.01). **(C)** Wild type (WT), Δ*rcf1* (Δ*1*), Δ*rcf2* (Δ*2*), and the Δ*rcf1;*Δ*rcf2* (Δ*1*;Δ*2*) mitochondrial morphology was visualized using electron microscopy (EM) in collaboration with Dr. Benedikt Westermann and Dr. Till Klecker (Universitaet Bayreuth, Germany). Two representative mitochondrial cross-sections from each strain are shown.

Table 15. Mitochondrial shape parameters.

Wild type (WT), Δ*rcf1* (Δ*1*), Δ*rcf2* (Δ*2*), and the Δ*rcf1;*Δ*rcf2* (Δ*1*;Δ*2*) mtGFP images were analyzed using Yeast_MitoMap plugin. Fragmentation index, *f*, mitochondrial shape parameters (volume, surface area, SA:V ratio, compactness, distribution isotropy, sphericity, radius variance) calculated for every cellular mitochondrial network. Average +/- SEM are shown; statistically significant values are denotes by * ($p<0.05$) and ** ($p<0.01$).

	number of cells, n	fragmentation index, *f*	Volume [µm^3]	Surface area [um^2]	SA:V
WT	86	3.7 ± 0.9	8.96 ± 0.42	73.4 ± 3.4	8.27 ± 0.14
Δ1	132	5.8 ± 1.0	8.14 ± 0.29	62.9 ± 2.3	7.79 ± 0.08 *
Δ2	121	2.2 ± 0.4	9.70 ± 0.30	77.1 ± 2.6	7.94 ± 0.08 *
Δ1;Δ2	94	3.1 ± 0.7	9.7 0 ± 0.30	66.4 ± 2.9	6.86 ± 0.08 **

	Compactness	Distribution isotropy	Isoperimetric quotient	Sphericity	Radius Variance
WT	0.108	0.62	0.31	0.44	0.16
Δ1	0.100	0.60	0.36	0.49	0.12
Δ2	0.129	0.63	0.30	0.43	0.18
Δ1;Δ2	0.089	0.61	0.33	0.47	0.19

Table 16. EM analysis of mitochondrial cristae. Wild type (WT), Δ*rcf1* (Δ*1*), Δ*rcf2* (Δ*2*), and the Δ*rcf1;*Δ*rcf2* (Δ*1*;Δ*2*) cells grown to exponential phase in YPGal, chemically fixed, embedded and cryo-sectioned for electron microscopy (EM) in collaboration with Dr. Benedikt Westermann and Dr. Till Klecker (Universitaet Bayreuth, Germany) to analyze mitochondrial architecture. Mitochondrial cross-sections were manually analyzed to identify cristae morphology (Harner *et al*., 2016). Normal cristae shapes (lamellae and tubules) were recorded and counted. Abnormal cristae shapes (septa, which completely cross the matrix space, onion-like morphology, or stacked sheets of cristae membrane) were recorded and counted. Mitochondrial cross-section diameter was measured for all mitochondria observed on the EM images.

	WT	*Δ1*	*Δ2*	*Δ1;Δ2*
# cells analyzed	16	14	14	14
# mitochondria analyzed	66	54	65	49
# mitochondria / cell	4.13	4.15	4.64	3.50
# cristae / mitochondria	3.76	5.46	3.29	4.38
# abnormal cristae	1	7	4	7
% mitochondria w. cristae abnormalities	2%	13%	6%	14%
average mitochondrial diameter, nm	402 +/- 12	427 +/- 14	383 +/- 13 *	426 +/- 13 *

2017). Yeast cells were grown to exponential phase in YPGal, chemically fixed, embedded and cryo-sectioned (Griffith *et al*., 2008). Mitochondrial cross-sections were manually scored. In the absence of Rcf1 and Rcf2 a weak cristae phenotype was observed (Table 16) characterized by abnormal cristae in some Δ*rcf1*;Δ*rcf2* mitochondria (representative images in Figure 19C demonstrates one mitochondrion exhibiting abnormal stacked or onion-shaped cristae), while the majority of organelles look similar to the wild type mitochondria. The diameter of the mitochondrial cross-sections was measured and average diameter of Δ*rcf1*;Δ*rcf2* mitochondria found to be modestly but significantly increased compared to wild-type (Table 16), supporting the observation that the branches of mitochondrial network in Δ*rcf1*;Δ*rcf2* cells are wider than the WT mitochondria. Increased diameter of mitochondrial cross-sections may be due to mitochondrial swelling due to ion homeostasis defect. Increased swelling and widening of the mitochondrial compartment may result in more diffuse mtGFP signal.

To summarize, neither increased mitochondrial fragmentation nor severe mitochondrial cristae defects was observed in the absence of Rcf1 and/or Rcf2. However, modest changes in mitochondrial size (branch diameter and SA:V ratio) were detected, resembling the swelling of depolarized mitochondria. There are few detailed characterizations of mitochondrial morphology of respiratory deficient mutants. Further study is needed to characterize mitochondrial morphology and dynamics in the absence of Rcf1 and Rcf2 and to determine whether the morphology is the consequence of the respiratory chain / PMF defects and/or contributes to them.

Summary

The mitochondrial PMF drives ATP synthesis by F_1F_O ATP synthase. As expected from the decreased PMF observed in mitochondria lacking Rcf1 and Rcf2, the level of ATP synthesis in these mitochondria is decreased as well. Consistent with a more severe defect in PMF maintenance, the impairment of ATP synthesis is more severe in the double Δ*rcf1*;Δ*rcf2* mutant compared to the single mutants.

F_1F_O ATP synthase complex levels appeared similar, but levels of certain subunits were altered in the absence of Rcf1 and Rcf2. The level of cardiolipin-binding, F_O ring forming Atp9 subunit was increased in Δ*rcf1* and Δ*rcf2*, yet decreased in Δ*rcf1*;Δ*rcf2* mitochondria relative to Tim44 protein in comparison to the wild type control. Additionally, decreased F_1F_O ATP synthase reverse activity (ATP hydrolysis) and sensitivity of ATP synthase to oligomycin, the inhibitor which binds to Atp9 at the membrane interface, were observed in the absence of Rcf1 and Rcf2. This is consistent with altered stoichiometry or conformation of the Atp9 subunit in the absence of Rcf1 and Rcf2. Altered oligomycin sensitivity of ATP synthase was confirmed by respiratory growth of the Δ*rcf1* and Δ*rcf1*;Δ*rcf2* cells which was resistant to sub-inhibitory doses of oligomycin, compared to the wild-type control.

PMF also supports the activity of AAC and PIC. Deletion of Rcf1 and Rcf2 did not impair AAC-mediated ATP export. PIC mediated import, while not measured, could have contributed to ATP synthesis impairment.

Additionally, changes in AAC BN-PAGE mobility consistent with impaired lipid binding to AAC were observed in Δ*rcf1*;Δ*rcf2* mitochondria. Specific, CL dependent interaction of Rcf1 with AAC was detected by Rcf1-AAC crosslinking (J. Garlich, PhD dissertation). AAC mobility in Δ*rcf1*;Δ*rcf2* mitochondria is consistent with Rcf1 and Rcf2 role supporting AAC-associated CL molecules. Decreased PMF generation by the ETC does not provide explanation for all of these pleiotropic phenotypes, some of which may be related to altered mitochondrial lipid distribution among OXPHOS proteins.

Consistent with the decreased PMF in the absence of Rcf1 and Rcf2, processing of newly translated Cox2 precursor (pCox2) was defective in Δ*rcf1*;Δ*rcf2* mitochondria. Membrane translocation of pCox2 is PMF-dependent, as is translocation of many nuclear encoded proteins; an altered processing of Mcr1 was also observed in the absence of Rcf1 and Rcf2. Unexpectedly, Mcr1 processing was increased, indicating increased Δψ. The explanation for this observation is unclear. The absence of Rcf1 and Rcf2 was not associated with defects in activity of any specific protease.

Analysis of morphology of mitochondrial network and mitochondrial ultrastructure (i.e. cristae) of Δ*rcf1*;Δ*rcf2* mitochondria does not indicate network fragmentation or strong cristae abnormalities. However, measurement of mitochondrial surface area and volume indicates that the mitochondrial networks are more swollen, results which are consistent with impaired mitochondrial PMF maintenance and lower ATP synthesis in the absence of Rcf1 and Rcf2.

CHAPTER 5. DISCUSSION

Introduction.

Mitochondrial electron transport chain (ETC) enzymes establish and maintain proton-motive force (PMF) by transporting protons against the concentration gradient. The efficient conversion of oxidation energy into the PMF depends on ETC complex IV, cytochrome *c* oxidase, harnessing the energy of electron transport to pump protons (complex IV coupling). The PMF powers the synthesis of ATP by the F_1F_O ATP synthase. PMF also supports protein translocases and metabolite carriers, and is dissipated by proton leaks. The yield of ATP synthesis relative to oxygen consumption reflects the coupling of oxidation and phosphorylation (OXPHOS coupling). Mitochondrial ATP synthesis relative to oxygen consumption in respiring cells and tissues is also referred to as respiration efficiency. OXPHOS coupling is variable; it is influenced by many factors including ETC activity, proton leak, ATP demand, and expression of tissue-specific and condition-specific OXPHOS enzyme isoforms (Kadenbach and Merle, 1989, Gouspillou *et al.,* 2011, Liu and Barrientos, 2013, Sinkler *et al.,* 2017, Salin *et al.,* 2018). Improved respiration efficiency can promote hypoxic survival of cells and tissues and provide a competitive advantage to organisms. Thus, the OXPHOS coupling in isolated mitochondria and on a cellular level is relevant and contributes to the fitness of multicellular organisms.

5.1. The role of Rcf1 and Rcf2 in respiratory efficiency.

5.1.a. The role of Rcf1 and Rcf2 in respiratory growth.

Respiration inefficiency in the yeast *Saccharomyces cerevisiae* is detected by slower or absent growth on non-fermentable carbon sources (e.g. glycerol, ethanol). Yeast mutants with defective OXPHOS capacities can be analyzed without losing viability on fermentable non-repressing carbon sources, such as galactose.

Yeast Rcf1 and Rcf2 are both needed to support optimal respiratory growth, which has previously been interpreted as evidence of the overlapping function(s) of these proteins (Strogolova *et al*., 2012). A more complete characterization of the functions of these proteins represents the goal of this study. Respiration-based growth of single Δ*rcf1*, Δ*rcf2*, and double Δ*rcf1*;Δ*rcf2* mutants was compared, with the goal of characterizing which aspects of OXPHOS function, if any, were affected in the absence of Rcf1 and/or Rcf2.

Genetic deletion of Rcf1 in the W303 background strongly decreased complex IV protein levels, yet Δ*rcf1* strain displayed almost normal growth on non-fermentable carbon sources under optimal aerobic growth conditions (30˚C, 21% O_2) on agar and in liquid media. Despite having less complex IV, the rate of cellular oxygen consumption was not strongly decreased in the Δ*rcf1* mutant, and the Δ*rcf1* mitochondria exhibited basal (state 2) oxygen consumption rates (OCR) similar to those of the wild-type mitochondria. Kinetic analysis of state 2

respiration however indicated that the OCR slightly increased over time, suggesting that the IM may have a proton leak when ETC function was induced in the absence of Rcf1. The respiration-based growth of the Δ*rcf1* strain was not more sensitive than wild type strain to nigericin, a H^+ ionophore that dissipates PMF ΔpH component and uncouples OXPHOS. The growth of Δ*rcf1* strain was sensitive to suboptimal oxygen and temperature conditions (21˚C, 21% O_2; 37˚C, 21% O_2; and 21˚C, 2% O_2). This observation is consistent with previous reports (Vukotic *et al.*, 2012, Strogolova *et al*., 2012) and indicates an OXPHOS defect that does not strongly limit respiration-based growth.

We report here that genetic deletion of Rcf2 moderately decreased complex IV protein levels and had no noticeable impact on respiratory growth under optimal conditions. Respiration-based growth of Δ*rcf2* mutant was, however, slowed down when performed in liquid media or under limiting oxygen concentration, or in presence of low concentration of nigericin. To compensate for partial dissipation of ΔpH component of PMF by nigericin, the ETC has to pump more protons, so that ΔpH is quickly converted to Δψ by activity of electroneutral H^+/ion transporters, and PMF increases (Lambert and Brand, 2004). Defective proton pumping is expected to cause nigericin sensitivity. Furthermore, despite having almost normal levels of complex IV, Δ*rcf2* cells exhibited significantly elevated rate of cellular oxygen consumption which, in contrast to the Δ*rcf1* mitochondria, was stable over time. A similar increase in basal respiration was also observed in isolated Δ*rcf2* mitochondria. These results

reveal that deletion of Rcf2, similar to Rcf1, causes sub-threshold OXPHOS defect, apparently resulting in respiratory uncoupling *in vivo*.

The Δ*rcf1;*Δ*rcf2* mutant displays a stronger respiratory growth defect than either of the single mutants. Our lab was the first to characterize the Δ*rcf1;*Δ*rcf2* mutant and to demonstrate the adverse effect of deleting both Rcf1 and Rcf2 (Strogolova *et al*., 2012). The work presented in this dissertation continues the characterization of this yeast mutant lacking both Rcf1 and Rcf2. Deletion of Rcf2 in Δ*rcf1* background severely impaired the respiration-based growth. However, it did not further decrease complex IV levels and the electron transport; they were found to be decreased to a similar extent in the isolated Δ*rcf1* and Δ*rcf1;*Δ*rcf2* mitochondria. As shown here, Δ*rcf1;*Δ*rcf2* cellular oxygen consumption was similar to that of the Δ*rcf1*, however, an enhanced instability of state 2 OCR was observed relative to that described earlier for the Δ*rcf1* mitochondria. The results presented in this dissertation indicate that the growth defect of the Δ*rcf1;*Δ*rcf2* mutant cannot be solely attributed to a decreased content of complex IV or decreased electron transport activity.

5.1.b. Rcf1 and Rcf2 promote efficient OXPHOS coupling

Mitochondrial ETC and ATP synthesis activities are interdependent and coupled by the PMF. OXPHOS coupling is defined as optimal stoichiometry of the oxidation and phosphorylation activities.

As reported here, Δ*rcf1* and Δ*rcf1;*Δ*rcf2* mitochondria were similar in the levels of ETC enzymes complex III and complex IV. Electron transport activity of complex III in the Δ*rcf1;*Δ*rcf2* mitochondria was not adversely affected; complex III activity was even increased in the absence of Rcf1 and Rcf2 proteins. How is the observed respiratory growth defect observed in the Δ*rcf1;*Δ*rcf2* strain, but not in the Δ*rcf1* strain explained? Multiple lines of evidence indicate that the OXPHOS coupling and PMF generation were decreased in Δ*rcf1,* Δ*rcf2,* and Δ*rcf1;*Δ*rcf2* mitochondria. First, complex IV activity, which is constrained by the PMF, appeared less constrained in Δ*rcf1,* Δ*rcf2,* and Δ*rcf1;*Δ*rcf2* mitochondria. This was evidenced by decreased stimulation of OCR by the PMF-dissipating uncoupler, CCCP. Indeed, direct measurements of membrane potential component of the PMF indicate it was reduced in Δ*rcf1,* Δ*rcf2,* and Δ*rcf1;*Δ*rcf2* mitochondria compared to wild-type control. Reduced PMF is less able to constrain complex IV oxygen consumption and explains elevated basal oxygen consumption in the absence of Rcf1 and Rcf2, relative to their complex IV aa_3 content.

Furthermore, uncoupling was progressive as electron transfer was occurring in Δ*rcf1;*Δ*rcf2* mitochondria, as demonstrated by the continuous increase in state 2 OCR over time when NADH was used as a substrate (as mentioned earlier, a similar but less prominent trend was observed in Δ*rcf1* state 2 OCR). Increasing state 2 OCR over incubation time indicates either increasing proton leak and/or an inability of proton pumping to counteract it, indicating that the absence of Rcf1 may be correlated with a proton leak of the IM. The OCR

remained elevated and PMF remained low in Δ*rcf1;*Δ*rcf2* mitochondria for a significantly extended time after the ADP addition (delayed state 4), relative to the wild type control. The finding that the instability of state 2 OCR was more pronounced when Rcf2 deletion was combined with Rcf1 deletion, suggests that the effect of Rcf1 and Rcf2 deletion is cumulative, consistent with a proton leak observed in the absence of Rcf1 combined with reduced proton-pumping ability of complex IV in the absence of Rcf2 is absent.

This study is the first time that a role of Rcf1 and Rcf2 in mitochondrial PMF homeostasis has been described. Consistent with the decreased PMF, ATP synthesis was impaired in Δ*rcf1,* Δ*rcf2* and Δ*rcf1;*Δ*rcf2* mitochondria. The addition of increasing concentrations of ADP to the Δ*rcf1;*Δ*rcf2* mitochondria minimally stimulated the OCR (ETC) activity. Compared to Δ*rcf1* or Δ*rcf2* mitochondria, the Δ*rcf1;*Δ*rcf2* mitochondria had the largest ATP synthesis defect (45% of WT). This defect was apparent when 100 µM ADP was added, below physiological levels of ADP in the mitochondria, estimated to be >200 µM (Gout *et al*., 2014). The cumulative effect of Rcf1 and Rcf2 deletion on the PMF and ATP synthesis may explain why Δ*rcf1;*Δ*rcf2* strain unlike the Δ*rcf1* strain, exhibits a respiration-based growth defect.

The pH component of the PMF is influenced by cytoplasmic pH and ATP. ATP generated by glycolysis and fermentation can support mitochondrial membrane potential in OXPHOS deficient cells (reference). The interplay of cytosolic and mitochondrial pH is important for cellular pH homeostasis; this is evidenced by the connection between vacuolar pH and mitochondrial function

(Hughes and Gottschling, 2012). Future work is needed to evaluate the effect of Rcf1 and Rcf2 deletion on mitochondrial PMF *in vivo* and address the consequences of respiration-based deficiency caused by Rcf1 and Rcf2 deficiency on cellular pH homeostasis, for example during growth in basic or acidic media.

5.1.c. Rcf1 and Rcf2 support CL binding proteins AAC and Atp9

In addition to PMF-dependent phenotypes, some of the differences observed in Δ*rcf1;*Δ*rcf2* mitochondria (altered native AAC gel mobility, decreased F_1F_o ATP hydrolysis levels, lower sensitivity of respiratory growth to oligomycin) do not appear to be directly related to lower PMF. All of OXPHOS enzymes have lipids as integral components, including F_1F_o ATP synthase and AAC, which bind cardiolipin (CL) and other lipids. These differences may be due to a more general role of Rcf1 and Rcf2 in the delivery of phospholipids to OXPHOS proteins. Although total mitochondrial lipid composition is not altered by the absence of Rcf1 and Rcf2 (Garlich *et al*., 2017), these proteins may play a role in lipid association with transmembrane proteins, such as Cox3 or AAC, or lipid distribution between protein complexes of the IM. The Arg67 and Trp68 residues within the QRRQ motif resemble the Arg433 and Trp434 residues of the mitochondrial IM protein Mic60, which have been shown to be critical for Mic60's lipid binding properties (Hessenberger *et al.,* 2017). Rcf1 and Rcf2 propensity for lipid binding has not been examined to date; however, their interactome (Cox3,

Cytc_1, Qcr6, AAC) contains almost exclusively lipid binding (specifically cardiolipin (CL) binding) proteins (Strogolova *et al*., 2012, Garlich *et al*., 2017, J. Garlich, PhD dissertation). A number of phenotypes have been observed in RCF-deficient yeast mitochondria: lower detection of ATP synthase Atp9 subunit, decreased rate of F_1F_o-ATP hydrolysis, decreased sensitivity of ATP synthase to oligomycin, altered AAC mobility on BN-PAGE consistent with loss of CL molecules. These varied phenotypes in absence of RCF proteins could possibly be related to altered lipid composition of the F_1F_O ATP synthase and AAC complexes.

Like Cox3, Atp9 subunit of the F_o sector of the F_1F_o-ATP synthase is a mitochondrially encoded lipid-binding OXPHOS subunit that binds CL. Although we did not detect Atp9-Rcf1/2 interaction, we report here that Atp9 steady state levels were decreased in Δ*rcf1;*Δ*rcf2* mitochondria. However, a corresponding decrease in the assembled F_1F_o-ATP synthase (on a BN-PAGE) was not detected. This may be due to altered solubilization or oligomerization stoichiometry of Atp9 preventing its detection by SDS-PAGE (Atp9 forms a homooligomeric ring of the F_o sector and thus an altered stoichiometry of Atp9 within the F_o sector in principle is possible). Atp9 is the site of F_1F_o-ATP synthase oligomycin binding and inhibition (Symersky *et al*., 2012). As reported here, Δ*rcf1* and Δ*rcf1;*Δ*rcf2* mutants exhibited decreased senstivity to oligomycin, which may be attributable to altered Atp9 conformation or CL binding, or to an increase in F_1F_O ATP synthase independent ATP synthesis. Interestingly, interaction of Atp9 with complex IV assembly intermediates containing also Rcf1 (McStay *et al*.,

2012, Su *et al*., 2014) was reported recently, and proposed to accelerate Atp9 ring formation. These observations raise the possibility that Rcf1 may interact with Atp9 and possibly influence Atp9 CL binding.

CL molecules are critical to mitochondrial function. Lipid-protein interactions “seal” the transmembrane OXPHOS enzymes and mediate lateral proton currents between supercomplex III-IV and ATP synthase (Haines and Dencher, 2002, Mehdipour and Hummer, 2016, Sjöholm *et al*., 2017), supporting ΔpH homeostasis. CL is important for complex IV stability and proton pumping (discussed in more detail in the section 5.1.e); and association of CL with ATP synthase is important to support its rotation in the IM and prevent proton leak (Duncan *et al*., 2016). Therefore, altering CL distribution and/or tight association with protein complexes interferes with OXPHOS and with PMF generation. Notably, screening of yeast deletion library for nigericin hypersensitive mutants indicated that deletion of *CRD1* (CL synthase) confers hypersensitivity to nigericin (Jakubkova *et al.*, 2016), a phenotype which we also observed in the Δ*rcf2* strain. Genetic deletion of CL synthase decreases OXPHOS coupling, characterized by increased state 2 OCR and lower Δψ (Baile *et al*., 2013); removal of cardiolipin (CL) also destabilizes complex IV (Sedlák and Robinson, 2015). OXPHOS de-coupling and specifically sensitivity of Δ*rcf2* to nigericin reported in this dissertation study may be related to an altered CL distribution between OXPHOS complexes.

Interestingly, recent therapeutic use of cell-penetrating aromatic-cationic peptides containing just a few amino acids, that selectively target cardiolipin and

increase coupling efficiency, and reportedly promote tissue regeneration (Szeto and Schiller, 2011, Szeto and Liu, 2018). These short peptides (Szeto-Schiller peptides) are proposed to bind CL and prevent its peroxidation, which plays a role in CL loss with age and ensuing mitochondrial dysfunctions. Intriguing possibility that Rcf1 and Rcf2 may bind CL raise a possibility for a similar role for Rcf1 and Rcf2 in yeast mitochondria. Future experiments are needed to explore possible Rcf1 and Rcf2 lipid-binding properties, and may utilize Rcf1 or Rcf2 truncations, including perhaps an extreme truncation, QRRQ motif alone.

5.1.d. Rcf1 and Rcf2 influence PMF dependent protein translocation

In addition to decreased ATP synthesis, PMF is essential for the import of nuclear-encoded and insertion of mitochondrially-encoded OXPHOS proteins into the inner membrane (IM). Results presented here indicate that reduced PMF in the absence of Rcf1 and Rcf2 interferes with these processes.

We looked at the proteolytic processing state of a number of mitochondrial proteins, because for many proteins, these maturation events are supported through the mitochondrial PMF. We first detected two forms of Mcr1, which is sorted into an outer membrane (OM) anchored larger form (Mcr_{34}) or an IMS localized smaller form (Mcr_{32}) which is proteolytically matured by Imp1 peptidase at the IM surface (Schneider et al., 1991). Formation of Mcr_{32} requires import of the N-terminal region of the protein across the IM in a $\Delta\psi$ dependent manner (Hahne et al., 1994, Haucke et al., 1997). In the absence of Rcf1 and Rcf2,

formation of Mcr_{32} was not impaired, rather, it was even increased in Δ*rcf1;*Δ*rcf2* mitochondria relative to the wild type control.

Another protein, Ccp1, also displayed altered proteolytic maturation when Rcf1 was missing. Ccp1 is matured by Pcp1 peptidase in a manner which involves the activities of the Yta10/12 proteins, which are thought to dislocate cleavage site of the Ccp1 from the lipid environment of the IM to a soluble environment of the peptidase (Tatsuta et al., 2007). This process was adversely affected in the absence of Rcf1.

Finally, the maturation of the mitochondrially encoded Cox2 precursor (pCox2) was also partially impaired in the absence of Rcf1/Rcf2. Cleavage of the N-terminal presequence of pCox2 by Imp1 requires export of N-terminus to the IMS, a process supported by both Δψ and ΔpH (Herrmann *et al.,* 1995).

Collectively, whether these various processing defects are indications of a lowered PMF or an imbalance of Δψ and ΔpH, is unknown. Yet, these observed defects serve to further illustrate the pleiotropic nature of the defects caused by the absence of Rcf1 and Rcf2.

5.1.e. Possible complex IV proton pumping defect.

How could Rcf1 and Rcf2 support PMF maintenance? The results presented in this dissertation study indicate that, in the absence of Rcf1 and Rcf2, not only complex IV protein content but also its ability to transfer protons was impaired. Complex IV is the primary proton pump (there is no complex I in

yeast mitochondria; complex III is not a proton pump and contributes to PMF generation via a redox loop mechanism with constant stoichiometry). The data presented here indicate that Δ*rcf1* mitochondria had lower PMF; the decrease could be attributed to the decreased complex IV levels. However, the Δ*rcf2* mitochondria had complex IV levels similar to wild type mitochondria and elevated oxygen consumption; yet Δ*rcf2* mitochondria exhibited lower PMF than wild type mitochondria. The comparison of Δ*rcf1* and Δ*rcf1;*Δ*rcf2* mitochondria show that the removal of Rcf2 resulted in progressive OXPHOS uncoupling and inability to repolarize after ADP addition, without noticeable changes in complex IV levels and electron transport activity. Thus, Rcf2 plays an important role in PMF maintenance and repolarization, possibly regulating complex IV proton pumping. This hypothesis is corroborated by the findings of our collaborators (Ngoc Hoang and Jonathan Hosler at the University of Mississippi Medical Center). Using TMPD/ascorbate to simultaneously measure OCR and membrane potential generated by bioenergetically isolated complex IV, they confirmed a complex IV proton translocation defect in intact Δ*rcf2* and Δ*rcf1;*Δ*rcf2* mitochondria, indicating that the proton pumping capacity of complex IV is impaired when Rcf2 is absent (Strogolova *et al.,* manuscript in preparation).

Complex IV proton pumping can be de-coupled from electron transport and oxygen consumption. Proton pumping is driven by the redox energy released during the transport of electrons and is constrained by the PMF (Nicholls and Ferguson, 2013). However, at least under some conditions, complex IV can consume oxygen without pumping protons. Such de-coupling was reported in

purified bacterial cytochrome *c* oxidase and in mammalian tissues (Brzezinski and Johansson, 2010; Kadenbach, 2003). One mechanism for de-coupling could be a proton back-leak pathway identified in the bovine complex IV enzyme (Muramoto *et al.,* 2010). This pathway is postulated to be conformationally gated, and similar slipping of protons was reported in the homologous *E.coli* enzyme cytochrome bo_3 (Li *et al* 2015).

Loss of proton pumping in a catalytically active cytochrome *c* oxidase is a hallmark of the suicide inactivation phenomenon (Bratton *et al*., 1999, Gilderson *et al*., 2003, Hosler, 2004). This phenomenon was first characterized in the purified bacterial enzyme and was attributed to a loss of subunit 3 (Cox3) (Bratton *et al*., 1999). Suicide inactivation is a sequence of events initiated by structural changes in the binuclear center (BNC) formed by heme a_3 and copper Cu_B physically associated with the Cox1 subunit. These changes lower the redox potential of the BNC, resulting in a loss of proton pumping, followed by the loss of copper Cu_B and inactivation of electron transport. Although Cox3 does not directly participate in electron transport, it is intimately associated with and influences the activity of Cox1. Cox3 displays sequence conservation as high as that of the catalytic subunit Cox1, indicating that it is likely to be highly important for facilitating proton uptake and pumping (Penttilä 1983, Varanasi and Hosler 2012). Cox3's interaction with Cox1 is supported by phospholipid molecules (CL and phosphatidylglycerol) (Bratton *et al*., 1999). These lipids are essential for complex IV structural stability (Musatov and Robinson, 2012, Musatov and Robinson, 2014) and are suggested to play a role in channeling oxygen to the

catalytic center of the enzyme (Penttilä 1983, Mills and Hosler 2005, Varanasi and Hosler 2012). Suicide inactivation of cytochrome *c* oxidase may thus involve changes in Cox3's position relative to Cox1 and associated lipids.

Rcf1 and Rcf2 associate with a subpopulation of complex IV in the mitochondria and likely are regulating its conformational dynamics. Evidence for heterogeneity of complex IV, i.e. that two or more distinct subpopulations of complex IV exist in mitochondria, has been published (Moody *et al*., 1991, Rydström Lundin *et al*., 2016). These complex IV subpopulations display differences in EPR spectra, cyanide binding, CO binding, and dithionite reduction kinetics. In the absence of Rcf1 or Rcf2, the heterogeneity of complex IV is reported to increase, shifting the balance to a greater proportion of a minor subpopulation with a lower redox potential of the BNC (Rydström Lundin et al., 2016, Rydström Lundin and Brzezinski 2017, Schäfer *et al*., 2018), and redox potential of the BNC determines proton pumping capacity of the enzyme (Sharma and Wikström, 2014). Therefore, it is likely that a subpopulation of complex IV that does not pump protons becomes more abundant in the absence of Rcf1 or Rcf2. Rcf1 and Rcf2 proteins may serve to influence complex IV enzyme proton pumping function and/or acting to counteract complex IV instability, which may lead to the suicide inactivation of the enzyme.

5.2. Model: Rcf1 and Rcf2 repair or remodel complex IV to increase complex IV proton-pumping efficiency.

We propose that Rcf1 and Rcf2 regulate complex IV proton pumping ability by ensuring the correct conformation of Cox3 subunit and/or associated lipid (CL) molecules and this may play an active role in repairing the complex IV enzyme to prevent it's premature and irreversible suicide inactivation. While many assembly chaperones of Cox1 and Cox2 are known, Rcf1 was the first protein to act as an assembly partner of Cox3 (Strogolova *et al*., 2012). Additionally, we propose that Rcf1 through its Arg65 and Trp66 residues located within its conserved QRRQ motif at the turn between the two transmembrane helices may bind lipid head groups near the membrane interface. Rcf1 transmembrane helices flanking the QRRQ motif structurally resemble the lipid binding cleft of Cox3 (Zhou *et al*., 2018, J. Hosler, personal communication). Rcf1 is proposed to mediate Cox3 lipidation and correct assembly into the complex IV enzyme (Figure 20). Consistent with its participation in the complex IV assembly and/or restructuring, Rcf1-associated complex IV is missing late assembling subunits Cox12 and Cox13 (Garlich *et al*., 2017).

We further propose that Rcf1 and Rcf2 play a role in repair of partially inactivated complex IV subpopulation (i.e. possibly undergoing suicide inactivation) as a consequence of normal catalytic activity (Figure 20). As discussed earlier, data to indicate the existence of a partially inactive complex IV subpopulation (i.e. that does not pump protons) that is naturally present in mitochondria and is increased in the absence of Rcf1 or Rcf2, has been published (Rydström Lundin et al., 2016, Rydström Lundin and Brzezinski 2017, Schäfer *et al*., 2018). Partial inactivation of complex IV may result in its

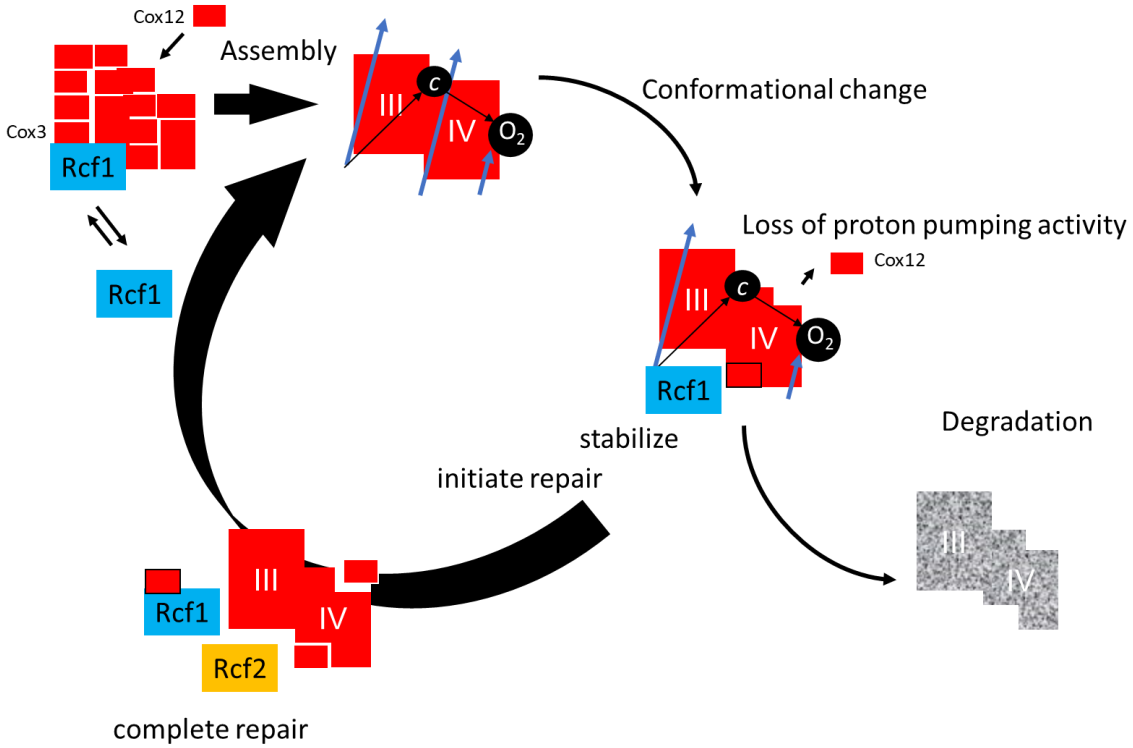

Figure 20. Proposed function of Rcf1 and Rcf2 in complex IV (cytochrome *c* oxidase) repair/remodeling. Assembly of complex III and IV subunits (red) together to form a supercomplex III_2IV_{1-2} is completed by joining of peripheral subunits (e.g. Cox12). For simplicity,only complex III and complex IV is depicted. Rcf1 (blue) assists complex IV subunit 3 (Cox3) assembly into the supercomplex. Catalytic activity or oxidative stress changes complex IV conformation (or result in damage, e.g. lipid peroxidation) which bring about changes in Cox1-Cox3 interface (black line) and loss of proton pumping activity. The loss of proton pumping activity leads to complex IV degradation. Rcf1 recognizes and interacts with the subpopulation of supercomplex with impaired proton pumping. Association of Rcf1 stabilizes complex IV, preventing its degradation. Rcf2 initiates repair/remodeling of Rcf1-associated enzymes. Rcf1 and Rcf2 repair the supercomplex, replacing lipids and/or changing conformation of Cox3. Complete repair restores proton pumping activity to complex IV and supports its steady state levels.

proteolytic turnover, unless it is repaired. Suicide inactivation of cytochrome *c* oxidase due to changes in Cox3 relationship with Cox1 may involve the associated lipids. Oxidative stress damage to CL (e.g. peroxidation) inactivates complex IV (Paradies *et al.*, 1998). It is unknown whether the lipids associated with Cox3 are displaced or damaged and thus need to be repositioned and/or exchanged during the natural lifespan of the complex IV enzyme. Overall, little is known about complex IV repair or remodeling (Sinkler *et al*., 2017). A previously hypothesized Rcf1 modification of complex IV lipid composition (Garlich *et al*., 2017) is proposed to support complex IV proton pumping and prevent complex IV degradation considering the aforementioned role of lipids at the Cox1-Cox3 interface, in complex IV proton pumping and stability.

A repair role for Rcf1 and Rcf2 is consistent with the dynamic nature of their interaction with complex IV and supercomplex III-IV and explains the partial inactivation of complex IV from Δ*rcf1* mitochondria previously reported (Rydström Lundin and Brzezinski, 2017). As reported here, proton-pumping activity of complex IV but not its stability in Δ*rcf2* mitochondria appears to be negatively affected. Rcf2 interaction with complex IV is less well characterized. Our lab previously reported (i) that Rcf1 and Rcf2 associate with complex IV independently; (ii) the association of Rcf1 with complex IV is stronger than Rcf2 (as indicated by its retention with complex IV when solubilized with a more stringent detergent); however, lower level of complex IV are recovered with Rcf1 than with Rcf2, and (iii) Rcf2 successfully competes with Rcf1, as the absence of Rcf2 promoted more Rcf1-complex IV interaction (Strogolova *et al* 2012). Based

on this information, we propose that Rcf2 association may complete the repair and stimulate the dissociation of Rcf1 from the enzyme (Figure 20). Consequently, when Rcf2 is absent we propose that complex IV enzyme that has defective proton pumping capacity accumulates in the mitochondria.

We speculate that both Rcf1 and Rcf2 play a role in repairing complex IV proton pumping. Rcf1 or Rcf2 alone may complete the repair process but less effectively. Rcf1 is speculated to play a role in stabilization of partially inactive complex IV (e.g. containing damaged/oxidized CL molecules). In the absence of Rcf1, the partially inactive complex IV would be proteolytically degraded, contributing to the reduced levels of complex IV in the absence of Rcf1. In the absence of Rcf2, partially inactive complex IV is stabilized and can contribute to oxygen consumption activity, albeit with reduced proton pumping capacity. The action of Rcf2 in the repair beyond promoting Rcf1 dissociation, deserves further future investigation. According to the model shown in Figure 20, when both Rcf1 and Rcf2 are removed, complex IV is not repaired, the result is lower levels of complex IV combined with a gradual loss of its proton pumping capacity.

The hypothesis that Rcf1 and Rcf2 restore the proton-pumping activity of complex IV can be tested by stimulating complex IV and CL damage with conditions known to stimulate oxidative stress or hypoxic conditions, which in mammalian mitochondria are also linked to reactive oxygen species generation and elevated oxidative damage.

Future studies by our collaborators will be focused on characterizing proton pumping of complex IV purified from Δ*rcf1;*Δ*rcf2* mitochondria. Moreover,

further studies should be done to characterize its lipid composition. Functional consequences of Rcf1 and Rcf2 deletion on other OXPHOS and non-OXPHOS processes should be explored in future experiments. For this purpose, a Δ*rcf1;*Δ*rcf2* strain lacking complex IV will be generated by deleting complex IV assembly factors (Cox10 or Cox11). Similarly, the effects of Rcf1 and Rcf2 deletion on complex IV function in absence of complex III could be studied in a similarly constructed strain lacking complex III (Δ*rcf1*;Δ*rcf2*;Δ*cor1)*.

5.3. The overall importance of HIGD proteins

We propose that yeast HIGD proteins Rcf1 and Rcf2 regulate the coupling of electron and proton transfer activity of complex IV, possibly by interaction with negatively charged CL molecules integral to complex IV enzyme. We anticipate that this function be evolutionarily conserved in homologous HIGD proteins in mammalian mitochondria and in bacteria.

Cytochrome *c* oxidase (complex IV) is an A-type enzyme of the bacterial heme copper oxidase family, postulated to have evolved later than the closely related B and C type enzymes. The evolution of heme copper oxidases corresponds to the time when oxygen concentration increased in the atmosphere, when heme copper oxidase enzyme family evolved from nitric oxide reductase family, and likely performed an oxygen scavenging function (Sharma and Wikström, 2014). Proton pumping is not central to cytochrome oxidase family; enzymes of B and C type are inefficient in proton pumping and are leaky

to protons even at a low PMF (Rauhamäki and Wikström, 2014). Evolution of proton pumping D-channel in A-type enzymes supported more efficient proton pumping and aerobic energy generation. A-type enzymes are widely phylogenetically distributed and are present in all α-proteobacteria lineages (Sousa *et al*., 2012). Proteins with homology to the HIGD are also found in bacteria and appear to be limited to α-proteobacteria. It is possible that the α-proteobacteria HIGD protein homologs function similarly to yeast Rcf1 and Rcf2 and support more efficient proton pumping of A-type cytochrome *c* oxidases and aerobic energy generation.

HIGD protein homologs in mammalian mitochondria are subdivided into constitutively expressed type 2 isoforms and stress-inducible type 1 isoforms, and classification is largely based on differences in the HIGD QRRQ motif (Figure 3A). Verification of the importance of conserved cationic amino acids of the QRRQ motif for PMF generation is beyond the scope of the current study, but should be addressed in the future, because mutations in HIGD motif sequence can strengthen or weaken association of Rcf1 with complex IV (Garlich *et al.*, 2017). Therefore, HIGD QRRQ motif sequence may be a conserved feature providing the means to influence association of HIGD proteins with complex IV and thus have an impact on coupling of electron and proton transfer activity of complex IV.

The type 2 HIGD proteins contain a canonical QRRQ motif sequence, QX3RXRX3Q, i.e. similar to the QRRQ motif of yeast Rcf1 and Rcf2. Highest level of expression of these isoforms are in heart, kidney and leukocytes tissues

(An *et al*., 2011). The functional relevance of the mammalian mitochondria type 2 HIGD proteins have not yet been studied. The QRRQ motif of the type 1 HIGD proteins displays sequence variation, this class of HIGD protein isoforms contain a V/IHLIHMRX3Q sequence. Highest level of expression of these isoforms are in brain and heart tissues (Wang *et al*., 2006, An *et al*., 2011) The mammalian type 1 HIGD proteins have been shown to associate with isolated mammalian complex IV and can accelerate electron transfer (Hayashi *et al*., 2015). The effect of these type 1 proteins on proton pumping capacity of the complex IV is, however, unknown. Yeast do not have type 1 HIGD proteins and when expressed in yeast, type 1 proteins did not associate with complex IV or support respiratory growth of the Δ*rcf1*;Δ*rcf2* mutant, suggestive of a divergent function of type 1 and type 2 proteins (Strogolova *et al.*, 2012, Garlich *et al.*, 2017, J. Garlich PhD dissertation).

We envision that the HIGD proteins in mammalian mitochondria may associate with complex IV and increase or decrease the of proton-pumping capacity. Mammalian mitochondria exhibit great physiological plasticity.This plasticity requires uncoupling, for example when stress or Ca^{2+} concentration cause PMF fluctuations, ΔpH_m increase, and associated ROS production by mammalian mitochondrial complex I enzyme (Lambert and Brand, 2004). Phenotypes observed in mammalian cells in the absence of specific HIGD isoforms – changes in mitochondrial morphology, increased cell death, sensitivity to hypoxia and oxidative stress – are all phenotypes adversely affected by alterations in PMF. Increased complex IV proton pumping counteracts proton

leak and supports OXPHOS ATP synthesis on which differentiated, respiring mammalian cells depend for survival, especially under conditions of hypoxia/ischemia. On the other hand, de-coupling of complex IV electron transport from proton pumping may also be physiologically relevant under certain metabolic and/or growth conditions, i.e. in tissues are dependent on glycolytic rather than OXPHOS metabolism. This includes undifferentiated stem cells, which depend on uncoupling of OXPHOS to preserve pluripotency (Zhang *et al*., 2012). Thus under these conditions it may be advantageous for the cell to have a mitochondrial complex IV enzyme with a disengaged proton pumping capacity. The mechanisms of uncoupling of OXPHOS in undifferentiated stem cells are unexplored and the expression and function of HIGD isoforms in stem cells have not yet been addressed.

Uncoupling of complex IV may serve to accommodate activity of non-OXPHOS intermembrane space (IMS) cytochrome *c* reducing enzymes, such as Erv1/Mia40 protein translocation disulfide relay system, cytochrome *c* peroxidase, or cytochrome b_2. The activity of these cytochrome *c* reducing enzymes is supported by the re-oxidation of their substrate cytochrome *c* by complex IV. A high PMF that inhibits complex IV and thus cytochrome *c* re-oxidation would inhibit these enzymes' activity. Decreasing the stringency of complex IV proton pumping may allow it to re-oxidize cytochrome *c* under conditions of high PMF. The Erv1/Mia40 import pathway is essential for cell viability and must occur even during OXPHOS suppression.

The work presented here indicates that the Rcf1 and Rcf2 proteins, members of the HIGD type 2 protein family, support mitochondrial PMF generation, possibly through repairing of a partially inactive complex IV. Additional evidence presented here add support to the suggestion that the function of Rcf1 and Rcf2 may be related to incorporation and/or restructuring of lipid molecules which are physically and functionally associated with components of the mitochondrial OXPHOS system. It is important to continue deciphering the function of HIGD protein family and the mechanisms underlying the protective effect of the HIGD type 1 proteins in vulnerable populations such as neurons and pancreatic cells. Recent successful use of hypoxia as a therapy for mitochondrial disease raises the possibility that the expression of HIGD proteins may be a promising therapeutic strategy as well.

BIBLIOGRAPHY

Alkhaja AK, Jans DC, Nikolov M, Vukotic M, Lytovchenko O, Ludewig F, Schliebs W, Riedel D, Urlaub H, Jakobs S, Deckers M. MINOS1 is a conserved component of mitofilin complexes and required for mitochondrial function and cristae organization. Mol Biol Cell. 2012 Jan;23(2):247-57.

Alnajjar KS, Hosler J, Prochaska L. Role of the N-terminus of subunit III in proton uptake in cytochrome *c* oxidase of *Rhodobacter sphaeroides*. Biochemistry. 2014 Jan 28;53(3):496-504.

Ameri K, Jahangiri A, Rajah AM, Tormos KV, Nagarajan R, Pekmezci M, Nguyen V, Wheeler ML, Murphy MP, Sanders TA, Jeffrey SS, Yeghiazarians Y, Rinaudo PF, Costello JF, Aghi MK, Maltepe E. HIGD1A regulates oxygen consumption, ROS production, and AMPK activity during glucose deprivation to modulate cell survival and tumor growth. Cell Rep. 2015 Feb 12. pii: S2211-1247(15)00033-9.

Ameri K, Maltepe E. HIGD1A-mediated dormancy and tumor survival. Mol Cell Oncol. 2015 Apr 14;2(4):e1030537.

An HJ, Cho G, Lee JO, Paik SG, Kim YS, Lee H. Higd-1a interacts with Opa1 and is required for the morphological and functional integrity of mitochondria. Proc Natl Acad Sci U S A. 2013 Aug 6;110(32):13014-9.

Anderson S, Bankier AT, Barrell BG, de Bruijn MH, Coulson AR, et al. Sequence and organization of the human mitochondrial genome. Nature. 1981;290:457–-65.

Arnarez C, Mazat JP, Elezgaray J, Marrink SJ, Periole X. Evidence for cardiolipin binding sites on the membrane-exposed surface of the cytochrome bc_1. J Am Chem Soc. 2013 Feb 27;135(8):3112-20.

Baile MG, Claypool SM. The power of yeast to model diseases of the powerhouse of the cell. Front Biosci (Landmark Ed). 2013 Jan 1;18:241-78.

Baile MG, Sathappa M, Lu YW, Pryce E, Whited K, McCaffery JM, Han X, Alder NN, Claypool SM. Unremodeled and remodeled cardiolipin are functionally indistinguishable in yeast. J Biol Chem. 2014 Jan 17;289(3):1768-78.

Baker KP, Schatz G. Mitochondrial proteins essential for viability mediate protein import into yeast mitochondria. Nature. 1991 Jan 17;349(6306):205-8.

Ball WB, Neff JK, Gohil VM. The role of nonbilayer phospholipids in mitochondrial structure and function. FEBS letters. 2017

Baracca A, Sgarbi G, Solaini G, Lenaz G. Rhodamine 123 as a probe of mitochondrial membrane potential: evaluation of proton flux through F(0) during ATP synthesis. Biochim Biophys Acta. 2003 Sep 30;1606(1-3):137-46.

Barrientos A. In vivo and in organelle assessment of OXPHOS activities. Methods 2002; 26:307-316.

Barrientos A, Korr D, Tzagoloff A. Shy1p is necessary for full expression of mitochondrial COX1 in the yeast model of Leigh's syndrome. EMBO J. 2002 Jan 15;21(1-2):43-52.

Barrientos A, Ugalde C. I function, therefore I am: overcoming skepticism about mitochondrial supercomplexes. Cell Metab. 2013 Aug 6;18(2):147-9.

Bashford CL, Thayer WS. Thermodynamics of the electrochemical proton gradient in bovine heart submitochondrial particles. J. Biol. Chem. 1977;252:8459–8463.

Bernardi G, Piperno G, Fonty G. The mitochondrial genome of wild-type yeast cells. I. Preparation and heterogeneity of mitochondrial DNA. J Mol Biol. 1972 Mar 28;65(2):173-89.

Björck ML, Brzezinski P. Control of transmembrane charge transfer in cytochrome *c* oxidase by the membrane potential. Nat Commun. 2018 Aug 9;9(1):3187.

Bloch D, Belevich I, Jasaitis A, Ribacka C, Puustinen A, Verkhovsky MI, Wikström M. The catalytic cycle of cytochrome *c* oxidase is not the sum of its two halves. Proc Natl Acad Sci U S A. 2004 Jan 13;101(2):529-33.

Bloch DA, Jasaitis A, Verkhovsky MI. Elevated proton leak of the intermediate OH in cytochrome *c* oxidase. Biophys J. 2009 Jun 3;96(11):4733-42.

Blomberg MR, Siegbahn PE. The mechanism for proton pumping in cytochrome *c* oxidase from an electrostatic and quantum chemical perspective. Biochim Biophys Acta. 2012 Apr;1817(4):495-505.

Bobyleva V, Bellei M, Pazienza TL, Muscatello U. Effect of cardiolipin on functional properties of isolated rat liver mitochondria. Biochem Mol Biol Int. 1997 Mar;41(3):469-80.

Bohovych I, Chan SS, Khalimonchuk O. Mitochondrial protein quality control: the mechanisms guarding mitochondrial health. Antioxid Redox Signal. 2015 Apr 20;22(12):977-94.

Brand MD, Nicholls DG. Assessing mitochondrial dysfunction in cells. Biochem J. 2011 Apr 15;435(2):297-312.

Bruder S, Reifenrath M, Thomik T, Boles E, Herzog K. Parallelised online biomass monitoring in shake flasks enables efficient strain and carbon source dependent growth characterisation of *Saccharomyces cerevisiae*. Microb Cell Fact. 2016 Jul 25;15(1):127.

Bustos DM, Velours J. The modification of the conserved GXXXG motif of the membrane-spanning segment of subunit g destabilizes the supramolecular species of yeast ATP synthase. J Biol Chem. 2005 Aug 12;280(32):29004-10.

Carlson M. Glucose repression in yeast. Curr Opin Microbiol. 1999 Apr;2(2):202-7.

Chen E, Kiebish MA, McDaniel J, Niedzwiecka K, Kucharczyk R, Ravasz D, et al. Perturbation of the yeast mitochondrial lipidome and associated membrane proteins following heterologous expression of Artemia-ANT. Sci Rep. 2018 Apr 12;8(1):5915.

Chen YC, Taylor EB, Dephoure N, Heo JM, Tonhato A, Papandreou I, et al. Identification of a protein mediating respiratory supercomplex stability. Cell Metab. 2012 Mar 7;15(3):348-60.

Chong YT, Koh JL, Friesen H, Duffy SK, Cox MJ, Moses A, Moffat J, Boone C, Andrews BJ. Yeast proteome dynamics from single cell imaging and automated analysis. Cell. 2015 Jun 4;161(6):1413-24.

Clarkson GH, Poyton RO. A role for membrane potential in the biogenesis of cytochrome *c* oxidase subunit II, a mitochondrial gene product. J Biol Chem. 1989 Jun 15;264(17):10114-8.

Cogliati S, Enriquez JA, Scorrano L. Mitochondrial cristae: where beauty meets functionality. Trends Biochem Sci. 2016 Mar;41(3):261-273.

Cortese JD, Voglino AL, Hackenbrock CR. Persistence of cytochrome *c* binding to membranes at physiological mitochondrial intermembrane space ionic strength. Biochim Biophys Acta. 1995 Mar 14;1228(2-3):216-228.

Cruciat CM, Brunner S, Baumann F, Neupert W, Stuart RA. The cytochrome bc_1 and cytochrome *c* oxidase complexes associate to form a single supracomplex in yeast mitochondria. J Biol Chem. 2000 Jun 16;275(24):18093-8.

Cui TZ, Conte A, Fox JL, Zara V, Winge DR. Modulation of the respiratory supercomplexes in yeast: enhanced formation of cytochrome oxidase increases the stability and abundance of respiratory supercomplexes. J Biol Chem. 2014 Feb 28;289(9):6133-41.

Dabir DV, Leverich EP, Kim SK, Tsai FD, Hirasawa M, Knaff DB, Koehler CM. A role for cytochrome *c* and cytochrome *c* peroxidase in electron shuttling from Erv1. EMBO J. 2007 Nov 28;26(23):4801-11.

Daum G, Gasser SM, Schatz G. Import of proteins into mitochondria. Energy-dependent, two-step processing of the intermembrane space enzyme cytochrome b_2 by isolated yeast mitochondria. J Biol Chem. 1982 Nov 10;257(21):13075-80.

De Marcos Lousa C, Trézéguet V, Dianoux AC, Brandolin G, Lauquin GJ. The human mitochondrial ADP/ATP carriers: kinetic properties and biogenesis of wild-type and mutant proteins in the yeast *S. cerevisiae*. Biochemistry. 2002 Dec 3;41(48):14412-20.

Devenish RJ, Prescott M, Roucou X, Nagley P. Insights into ATP synthase assembly and function through the molecular genetic manipulation of subunits of the yeast mitochondrial enzyme complex. Biochim Biophys Acta. 2000 May 31;1458(2-3):428-42.

Dienhart M, Pfeiffer K, Schagger H, Stuart RA. Formation of the yeast F_1F_0-ATP synthase dimeric complex does not require the ATPase inhibitor protein, Inh1. J Biol Chem. 2002 Oct 18;277(42):39289-95.

Dienhart MK, Stuart RA. The yeast Aac2 protein exists in physical association with the cytochrome bc_1-COX supercomplex and the TIM23 machinery. Mol Biol Cell. 2008 Sep;19(9):3934-43.

Dimitrov LN, Brem RB, Kruglyak L, Gottschling DE. Polymorphisms in multiple genes contribute to the spontaneous mitochondrial genome instability of *Saccharomyces cerevisiae* S288C strains. Genetics. 2009;183:365–383.

Dudkina NV, Kouril R, Peters K, Braun HP, Boekema EJ. Structure and function of mitochondrial supercomplexes. Biochim Biophys Acta. 2010 Jun-Jul;1797(6-7):664-70.

Dumke CL, Mark Davis J, Angela Murphy E, Nieman DC, Carmichael MD, Quindry JC, Travis Triplett N, Utter AC, Gross Gowin SJ, Henson DA, McAnulty SR, McAnulty LS. Successive bouts of cycling stimulates genes associated with mitochondrial biogenesis. Eur J Appl Physiol. 2009 Nov;107(4):419-27.

Dujon B, Sherman D, Fischer G, Durrens P, Casaregola S, Lafontaine I, et al. Cardiolipin binds selectively but transiently to conserved lysine residues in the rotor of metazoan ATP synthases. Proc Natl Acad Sci U S A. 2016 Aug 2;113(31):8687-92.

Egner A., Jakobs S., Hell S.W. Fast 100-nm resolution three-dimensional microscope reveals structural plasticity of mitochondria in live yeast. Proc. Natl. Acad. Sci. 2002;99:3370–3375.

Emaus RK, Grunwald R, Lemasters J. Rhodamine 123 as a probe of transmembrane potential in isolated rat liver mitochondria: spectral and metabolic properties. Biochim. Biophys. Acta, 850 (1986), pp. 436-448.

Fendt SM, Sauer U. Transcriptional regulation of respiration in yeast metabolizing differently repressive carbon substrates. BMC Syst Biol. 2010 Feb 18;4:12.

Fischer F, Filippis C, Osiewacz HD. RCF1-dependent respiratory supercomplexes are integral for lifespan-maintenance in a fungal ageing model. Sci Rep. 2015 Jul 29;5:12697.

Fontanesi F, Soto IC, Horn D, Barrientos A. Assembly of mitochondrial cytochrome *c*-oxidase, a complicated and highly regulated cellular process. Am J Physiol Cell Physiol. 2006 Dec;291(6):C1129-47.

Fox TD. Mitochondrial protein synthesis, import, and assembly. Genetics. 2012 Dec;192(4):1203-34.

Friedman JR, Mourier A, Yamada J, McCaffery JM, Nunnari J. MICOS coordinates with respiratory complexes and lipids to establish mitochondrial inner membrane architecture. Elife. 2015 Apr 28;4. doi: 10.7554/eLife.07739.

Fukuda R, Zhang H, Kim JW, Shimoda L, Dang CV, Semenza GL. HIF-1 regulates cytochrome oxidase subunits to optimize efficiency of respiration in hypoxic cells. Cell. 2007 Apr 6;129(1):111-22.

Garlich J, Strecker V, Wittig I, Stuart RA. Mutational analysis of the QRRQ motif in the yeast HIG1 type 2 protein Rcf1 reveals a regulatory role for the cytochrome *c* oxidase complex. J Biol Chem. 2017 Mar 31;292(13):5216-5226.

Gassmann M, Grenacher B, Rohde B, Vogel J. Quantifying western blots: pitfalls of densitometry. Electrophoresis 2009 (30):1845-1855

Ghaemmaghami S, Huh WK, Bower K, Howson RW, Belle A, Dephoure N, et al. Global analysis of protein expression in yeast. Nature. 2003 Oct 16;425(6959):737-41.

Ghosh A, Trivedi PP, Timbalia SA, Griffin AT, Rahn JJ, Chan SS, Gohil VM. Copper supplementation restores cytochrome *c* oxidase assembly defect in a mitochondrial disease model of COA6 deficiency. Hum Mol Genet. 2014 Jul 1;23(13):3596-606.

Gnaiger E, Lassnig B, Kuznetsov A, Rieger G, Margreiter R. Mitochondrial oxygen affinity, respiratory flux control and excess capacity of cytochrome *c* oxidase. J Exp Biol. 1998 Apr;201(Pt 8):1129-39.

Gouspillou G, Rouland R, Calmettes G, Deschodt-Arsac V, Franconi JM, Bourdel-Marchasson I, Diolez P. Accurate determination of the oxidative phosphorylation affinity for ADP in isolated mitochondria. PLoS One. 2011;6(6):e20709.

Guerra-Castellano A, Díaz-Quintana A, Pérez-Mejías G, Elena-Real CA, González-Arzola K, García-Mauriño SM, et al. Oxidative stress is tightly regulated by cytochrome *c* phosphorylation and respirasome factors in mitochondria. Proc Natl Acad Sci U S A. 2018 Jul 31;115(31):7955-7960.

Hackenbrock CR. Ultrastructural bases for metabolically linked mechanical activity in mitochondria. I. Reversible ultrastructural changes with change in metabolic steady state in isolated liver mitochondria. J Cell Biol. 1966 Aug;30(2):269-97.

Hahne K, Haucke V, Ramage L, Schatz G. Incomplete arrest in the outer membrane sorts NADH-cytochrome b_5 reductase to two different submitochondrial compartments. Cell. 1994 Dec 2;79(5):829-39.

Haines TH, Dencher NA. Cardiolipin: A proton trap for oxidative phosphorylation. FEBS Lett. 2002;528(1-3):35–39.

Hamazaki T, Leung WY, Cain BD, Ostrov DA, Thorsness PE, Terada N. Functional expression of human adenine nucleotide translocase 4 in *Saccharomyces cerevisiae*. PLoS One. 2011 Apr 21;6(4):e19250.

Harner ME, Unger AK, Geerts WJ, Mari M, Izawa T, Stenger M, et al. An evidence based hypothesis on the existence of two pathways of mitochondrial crista formation. Elife. 2016 Nov 16;5. pii: e18853.

Haucke V, Ocana CS, Hönlinger A, Tokatlidis K, Pfanner N, Schatz G. Analysis of the sorting signals directing NADH-cytochrome b_5 reductase to two locations within yeast mitochondria. Mol Cell Biol. 1997 Jul;17(7):4024-32.

Hayashi T, Asano Y, Shintani Y, Aoyama H, Kioka H, Tsukamoto O, et al. Higd1a is a positive regulator of cytochrome *c* oxidase. Proc Natl Acad Sci U S A. 2015 Feb 3;112(5):1553-8.

Helbig AO, de Groot MJ, van Gestel RA, Mohammed S, de Hulster EA, Luttik MA, et al. A three-way proteomics strategy allows differential analysis of yeast mitochondrial membrane protein complexesunder anaerobic and aerobic conditions. Proteomics. 2009 Oct;9(20):4787-98

Hell K, Tzagoloff A, Neupert W, Stuart RA. Identification of Cox20p, a novel protein involved in the maturation and assembly of cytochrome oxidase subunit 2. J Biol Chem. 2000 Feb 18;275(7):4571-8.

Herrero P, Fernández R, Moreno F. Differential sensitivities to glucose and galactose repression of gluconeogenic and respiratory enzymes from *Saccharomyces cerevisiae*. Arch Microbiol. 1985 Dec;143(3):216-9.

Herrmann JM, Koll H, Cook RA, Neupert W, Stuart RA. Topogenesis of cytochrome oxidase subunit II. Mechanisms of protein export from the mitochondrial matrix. J Biol Chem. 1995 Nov 10;270(45):27079-86.

Hess DC, Myers CL, Huttenhower C, Hibbs MA, Hayes AP, Paw J, Clore JJ, Mendoza RM, Luis BS, Nislow C, Giaever G, Costanzo M, Troyanskaya OG, Caudy AA. Computationally driven, quantitative experiments discover genes required for mitochondrial biogenesis. PLoS Genet. 2009 Mar;5(3):e1000407.

Hessenberger M, Zerbes RM, Rampelt H, Kunz S, Xavier AH, Purfürst B, Lilie H, Pfanner N, van der Laan M, Daumke O. Regulated membrane remodeling by Mic60 controls formation of mitochondrial crista junctions. Nat Commun. 2017 May 31;8:15258.

Hinkle PC. P/O ratios of mitochondrial oxidative phosphorylation. Biochim Biophys Acta. 2005 Jan 7;1706(1-2):1-11.

Hoch FL. Cardiolipins and biomembrane function. Biochim Biophys Acta. 1992 Mar 26;1113(1):71-133.

Hon T, Dodd A, Dirmeier R, Gorman N, Sinclair PR, Zhang L, Poyton RO. A mechanism of oxygen sensing in yeast. Multiple oxygen-responsive steps in the heme biosynthetic pathway affect Hap1 activity. J Biol Chem. 2003 Dec 12;278(50):50771-80.

Hosler JP, Ferguson-Miller S, Mills DA. Energy transduction: proton transfer through the respiratory complexes. Annu Rev Biochem. 2006;75:165-87.

Hughes AL, Gottschling DE. An early age increase in vacuolar pH limits mitochondrial function and lifespan in yeast. Nature. 2012 Dec 13;492(7428):261-5.

Hwang HJ, Lynn SG, Vengellur A, Saini Y, Grier EA, Ferguson-Miller SM, et al. Hypoxia inducible factors modulate mitochondrial oxygen consumption and transcriptional regulation of nuclear-encoded electron transport chain genes. Biochemistry. 2015 Jun 23;54(24):3739-48.

Ivanina AV, Nesmelova I, Leamy L, Sokolov EP, Sokolova IM. Intermittent hypoxia leads to functional reorganization of mitochondria and affects cellular bioenergetics in marine molluscs. J Exp Biol. 2016 Jun 1;219(Pt 11):1659-74.

Jain IH, Zazzeron L, Goli R, Alexa K, Schatzman-Bone S, Dhillon H, et al. Hypoxia as a therapy for mitochondrial disease. Science. 2016 Apr 1;352(6281):54-61.

Jakubkova M, Dzugasova V, Truban D, Abelovska L, Bhatia-Kissova I, Valachovic M, et al. Identification of yeast mutants exhibiting altered sensitivity to valinomycin and nigericin demonstrate pleiotropic effects of ionophores on cellular processes. PLoS One. 2016 Oct 6;11(10):e0164175.

Jastroch M, Divakaruni AS, Mookerjee S, Treberg JR, Brand MD. Mitochondrial proton and electron leaks. Essays Biochem. 2010;47:53-67.

Jelicić B, Traven A, Filić V, Sopta M. Mitochondrial dysfunction enhances Gal4-dependent transcription. FEMS Microbiol Lett. 2005 Dec 15;253(2):207-13. Epub 2005 Oct 7.

Jiang F, Ryan MT, Schlame M, Zhao M, Gu Z, Klingenberg M, et al. Absence of cardiolipin in the crd1 null mutant results in decreased mitochondrial membrane potential and reduced mitochondrial function. J Biol Chem. 2000 Jul 21;275(29):22387-94.

Jones E, Gaytan N, Garcia I, Herrera A, Ramos M, Agarwala D, Rana M, Innis-Whitehouse W, Schuenzel E, Gilkerson R. A threshold of transmembrane potential is required for mitochondrial dynamic balance mediated by DRP1 and OMA1. Cell Mol Life Sci. 2017 Apr;74(7):1347-1363.

Julienne CM, Tardieu M, Chevalier S, Pinault M, Bougnoux P, Labarthe F, et al. Cardiolipin content is involved in liver mitochondrial energy wasting associated with cancer-induced cachexia without the involvement of adenine nucleotide translocase. Biochim Biophys Acta. 2014 May;1842(5):726-33.

Kaasik A, Safiulina D, Zharkovsky A, Veksler V. Regulation of mitochondrial matrix volume. Am J Physiol Cell Physiol. 2007 Jan;292(1):C157-63.

Kadenbach B. Intrinsic and extrinsic uncoupling of oxidative phosphorylation. Biochim Biophys Acta. 2003 Jun 5;1604(2):77-94.

Kadenbach B, Hüttemann M. The subunit composition and function of mammalian cytochrome *c* oxidase. Mitochondrion. 2015 Sep;24:64-76.

Kadenbach B., Merle P. On the function of multiple subunits of cytochrome *c* oxidase from higher eukaryotes. FEBS Letters. 1981;135(1):1–11.

Kathiresan M, Martins D, English AM. Respiration triggers heme transfer from cytochrome *c* peroxidase to catalase in yeast mitochondria. Proc Natl Acad Sci U S A. 2014 Dec 9;111(49):17468-73.

Katzmann DJ, Hallstrom TC, Voet M, Wysock W, Golin J, Volckaert G, Moye-Rowley WS. Expression of an ATP-binding cassette transporter-encoding gene (YOR1) is required for oligomycin resistance in *Saccharomyces cerevisiae*. Mol Cell Biol. 1995 Dec;15(12):6875-83.

Kellis M, Birren BW, Lander ES. Proof and evolutionary analysis of ancient genome duplication in the yeast *Saccharomyces cerevisiae*. Nature. 2004 Apr 8;428(6983):617-24.

Khalifat N, Puff N, Bonneau S, Fournier JB, Angelova MI. Membrane deformation under local pH gradient: mimicking mitochondrial cristae dynamics. Biophys J. 2008 Nov 15;95(10):4924-33.

Kim N, Ripple MO, Springett R. Measurement of the mitochondrial membrane potential and pH gradient from the redox poise of the hemes of the *bc1* complex. Biophysical J 2012 Mar;102: 1194-1203.

Kjeld T, Stride N, Gudiksen A, Hansen EG, Arendrup HC, Horstmann PF, et al. Oxygen conserving mitochondrial adaptations in the skeletal muscles of breath hold divers. PLoS One. 2018 Sep 19;13(9):e0201401.

Klingenberg M. Cardiolipin and mitochondrial carriers. Biochim Biophys Acta. 2009 Oct;1788(10):2048-58

Kovác L, Böhmerová E, Butko P. Ionophores and intact cells. I. Valinomycin and nigericin act preferentially on mitochondria and not on the plasma membrane of *Saccharomyces cerevisiae*. Biochim Biophys Acta. 1982 Dec 30;721(4):341-8.

Kucejova B, Kucej M, Petrezselyova S, Abelovska L, Tomaska L. A screen for nigericin-resistant yeast mutants revealed genes controlling mitochondrial volume and mitochondrial cation homeostasis. Genetics. 2005 Oct;171(2):517-26.

Kyhse-Andersen J. Electroblotting of multiple gels: a simple apparatus without buffer tank for rapid transfer of proteins from polyacrylamide to nitrocellulose. J Biochem Biophys Methods. 1984 Dec;10(3-4):203-9.

Lackner LL. Shaping the dynamic mitochondrial network. BMC Biol. 2014 May 27;12:35. doi: 10.1186/1741-7007-12-35.

Laemmli UK. Cleavage of structural proteins during the assembly of the head of bacteriophage T4. Nature. 1970 Aug 15;227(5259):680-5.

Lagunas R. Misconceptions about the energy metabolism of *Saccharomyces cerevisiae*. Yeast. 1986 Dec;2(4):221-8.

Lambert AJ, Brand MD. Superoxide production by NADH:ubiquinone oxidoreductase (complex I) depends on the pH gradient across the mitochondrial inner membrane. Biochem J. 2004 Sep 1;382(Pt 2):511-7.

Lapuente-Brun E, Moreno-Loshuertos R, Acín-Pérez R, Latorre-Pellicer A, Colás C, Balsa E, et al. Supercomplex assembly determines electron flux in the mitochondrial electron transport chain. Science. 2013 Jun 28;340(6140):1567-70. doi: 10.1126/science.1230381.

Lenaz G, Genova ML. Structural and functional organization of the mitochondrial respiratory chain: a dynamic super-assembly. Int J Biochem Cell Biol. 2009 Oct;41(10):1750-1772.

Lesur I, Ma L, Muller H, Nicaud JM, Nikolski M, Oztas S, et al. Genome evolution in yeasts. Nature. 2004 Jul 1;430(6995):35-44.

Legros F, Lombes A, Frachon P, Rojo M. Mitochondrial fusion in human cells is efficient, requires the inner membrane potential, and is mediated by mitofusins. Mol Biol Cell. 2002;13(12):4343–4354.

Li M, Jørgensen SK, McMillan DG, Krzemiński Ł, Daskalakis NN, Partanen RH, Tutkus M, Tuma R, Stamou D, Hatzakis NS, Jeuken LJ. Single enzyme experiments reveal a long-lifetime proton leak state in a heme-copper oxidase. J Am Chem Soc. 2015 Dec 30;137(51):16055-63.

Liu J, Barrientos A. Transcriptional regulation of yeast oxidative phosphorylation hypoxic genes by oxidative stress. Antioxid Redox Signal. 2013 Dec 1;19(16):1916-27.

Martin J, Mahlke K, Pfanner N. Role of an energized inner membrane in mitochondrial protein import. Delta psi drives the movement of presequences. J Biol Chem. 1991 Sep 25;266(27):18051-7.

Martin WF, Garg S, Zimorski V. Endosymbiotic theories for eukaryote origin. Philos Trans R Soc Lond B Biol Sci. 2015 Sep 26;370(1678):20140330.

McDonald, J.H. Handbook of Biological Statistics (3rd ed.) Sparky House Publishing, Baltimore, MD. 2014.

Meeusen S, DeVay R, Block J, Cassidy-Stone A, Wayson S, McCaffery JM, Nunnari J. Mitochondrial inner-membrane fusion and crista maintenance requires the dynamin-related GTPase Mgm1. Cell. 2006 Oct 20;127(2):383-95

Mehdipour AR, Hummer G. Cardiolipin puts the seal on ATP synthase. Proc Natl Acad Sci U S A. 2016 Aug 2;113(31):8568-70.

Mills DA, Hosler JP. Slow proton transfer through the pathways for pumped protons in cytochrome *c* oxidase induces suicide inactivation of the enzyme. Biochemistry. 2005 Mar 29;44(12):4656-66.

Mitchell P. Coupling of phosphorylation to electron and hydrogen transfer by a chemi-osmotic type of mechanism. Nature. 1961 Jul 8;191:144-8.

Miyazono Y, Hirashima S, Ishihara N, Kusukawa J, Nakamura KI, Ohta K. Uncoupled mitochondria quickly shorten along their long axis to form indented spheroids, instead of rings, in a fission-independent manner. Sci Rep. 2018 Jan 10;8(1):350.

Moreno-Beltrán B, Guerra-Castellano A, Díaz-Quintana A, Del Conte R, García-Mauriño SM, Díaz-Moreno S, et al. Structural basis of mitochondrial dysfunction in response to cytochrome *c* phosphorylation at tyrosine 48. Proc Natl Acad Sci U S A. 2017 Apr 11;114(15):E3041-E3050.

Nicholls, D. G., and Ferguson, S. J. Bioenergetics. Fourth edition. Academic Press, London. 2013.

Nilsson T, Lundin CR, Nordlund G, Ädelroth P, von Ballmoos C, Brzezinski P. Lipid-mediated protein-protein interactions modulate respiration-driven ATP synthesis. Sci Rep. 2016 Apr 11;6:24113.

Nolden M, Ehses S, Koppen M, Bernacchia A, Rugarli EI, Langer T. The m-AAA protease defective in hereditary spastic paraplegia controls ribosome assembly in mitochondria. Cell. 2005 Oct 21;123(2):277-89.

Nunnari J, Suomalainen A. Mitochondria: in sickness and in health. Cell. 2012 Mar 16;148(6):1145-59.

Ocampo A, Liu J, Schroeder EA, Shadel GS, Barrientos A. Mitochondrial respiratory thresholds regulate yeast chronological life span and its extension by caloric restriction. Cell Metab. 2012 Jul 3;16(1):55-67.

Paradies G, Ruggiero FM, Petrosillo G, Quagliariello E. Peroxidative damage to cardiac mitochondria: cytochrome oxidase and cardiolipin alterations. FEBS Lett. 1998 Mar 13;424(3):155-8.

Penttilä T. Properties and reconstitution of a cytochrome oxidase deficient in subunit III. Eur J Biochem. 1983 Jun 15;133(2):355-61.

Perry SW, Norman JP, Barbieri J, Brown EB, Gelbard HA. Mitochondrial membrane potential probes and the proton gradient: a practical usage guide. Biotechniques. 2011 Feb;50(2):98-115.

Peyta L, Jarnouen K, Pinault M, Guimaraes C, Pais de Barros JP, Chevalier S, et al. Reduced cardiolipin content decreases respiratory chain capacities and increases ATP synthesis yield in the human HepaRG cells. Biochim Biophys Acta. 2016 Apr;1857(4):443-53.

Pöyry S, Cramariuc O, Postila PA, Kaszuba K, Sarewicz M, Osyczka A, et al. Atomistic simulations indicate cardiolipin to have an integral role in the structure of the cytochrome *bc*1 complex. Biochim Biophys Acta. 2013 Jun;1827(6):769-78.

Quarato G, Piccoli C, Scrima R, Capitanio N. Variation of flux control coefficient of cytochrome *c* oxidase and of the other respiratory chain complexes at different values of protonmotive force occurs by a threshold mechanism. Biochim Biophys Acta. 2011 Sep;1807(9):1114-24.

Rafelski S.M. Mitochondrial network morphology: building an integrative, geometrical view. BMC Biol. 2013;11:71

Rafelski SM, Viana MP, Zhang Y, Chan YH, Thorn KS, Yam P, et al. Mitochondrial network size scaling in budding yeast. Science. 2012 Nov 9;338(6108):822-4.

Rak M, Bénit P, Chrétien D, Bouchereau J, Schiff M, El-Khoury R, Tzagoloff A, et al. Mitochondrial cytochrome *c* oxidase deficiency. Clin Sci (Lond). 2016 Mar;130(6):393-407.

Rauhamäki V, Wikström M. The causes of reduced proton-pumping efficiency in type B and C respiratory heme-copper oxidases, and in some mutated variants of type A. Biochim Biophys Acta. 2014 Jul;1837(7):999-1003.

Rigoulet M, Aguilaniu H, Avéret N, Bunoust O, Camougrand N, Grandier-Vazeille X, et al. Organization and regulation of the cytosolic NADH metabolism in the yeast *Saccharomyces cerevisiae*. Mol Cell Biochem. 2004 Jan-Feb;256-257(1-2):73-81.

Römpler K, Müller T, Juris L, Wissel M, Vukotic M, Hofmann K, Deckers M. Overlapping role of respiratory supercomplex factor Rcf2 and Its N-terminal homolog Rcf3 in *Saccharomyces cerevisiae*. J Biol Chem. 2016 Nov 4;291(45):23769-23778.

Rosevear P, VanAken T, Baxter J, Ferguson-Miller S. Alkyl glycoside detergents: a simpler synthesis and their effects on kinetic and physical properties of cytochrome *c* oxidase. Biochemistry. 1980 Aug 19;19(17):4108-15.

Russell AP, Foletta VC, Snow RJ, Wadley GD. Skeletal muscle mitochondria: a major player in exercise, health and disease. Biochim Biophys Acta. 2014 Apr;1840(4):1276-84.

Rydström Lundin C, Brzezinski P. Modulation of O(2) reduction in *Saccharomyces cerevisiae* mitochondria. FEBS Lett. 2017 Dec;591(24):4049-4055.

Rydström Lundin C, von Ballmoos C, Ott M, Ädelroth P, Brzezinski P. Regulatory role of the respiratory supercomplex factors in *Saccharomyces cerevisiae*. Proc Natl Acad Sci U S A. 2016 Aug 2;113(31):E4476-85.

Safiulina D, Veksler V, Zharkovsky A, Kaasik A. Loss of mitochondrial membrane potential is associated with increase in mitochondrial volume: physiological role in neurones. J Cell Physiol. 2006 Feb;206(2):347-53.

Salin K, Villasevil EM, Auer SK, Anderson GJ, Selman C, Metcalfe NB, Chinopoulos C. Simultaneous measurement of mitochondrial respiration and ATP production in tissue homogenates and calculation of effective P/O ratios. Physiol Rep. 2016 Oct;4(20). pii: e13007.

Salin K, Villasevil EM, Anderson GJ, Selman C, Chinopoulos C, Metcalfe NB. The RCR and ATP/O indices can give contradictory messages about mitochondrial efficiency. Integr Comp Biol. 2018 Jul 5.

Sambrook J, Fritsch EF, Maniatis T. Molecular cloning: a laboratory manual. Cold Spring Harbor Laboratory Press, New York. 1989.

Saraste M. Oxidative phosphorylation at the fin de siècle. Science. 1999 Mar 5;283(5407):1488-93.

Schäfer J, Dawitz H, Ott M, Ädelroth P, Brzezinski P. Regulation of cytochrome *c* oxidase activity by modulation of the catalytic site. Sci Rep. 2018 Jul 30;8(1):11397.

Schäfer A, Zick M, Kief J, Steger M, Heide H, Duvezin-Caubet S, Neupert W, Reichert AS. Intramembrane proteolysis of Mgm1 by the mitochondrial rhomboid protease is highly promiscuous regarding the sequence of the cleaved hydrophobic segment. J Mol Biol. 2010 Aug 13;401(2):182-93

Schägger H, Pfeiffer K. Supercomplexes in the respiratory chains of yeast and mammalian mitochondria. EMBO J. 2000 Apr 17;19(8):1777-83.

Schlame M, Greenberg ML. Biosynthesis, remodeling and turnover of mitochondrial cardiolipin. Biochim Biophys Acta. 2017 Jan;1862(1):3-7.

Schleyer M, Schmidt B, Neupert W. Requirement of a membrane potential for the posttranslational transfer of proteins into mitochondria. Eur J Biochem. 1982;125:109–116.

Schneider A, Behrens M, Scherer P, Pratje E, Michaelis G, Schatz G. Inner membrane protease I, an enzyme mediating intramitochondrial protein sorting in yeast. EMBO J. 1991 Feb;10(2):247-54.

Schmidt O, Pfanner N, Meisinger C. Mitochondrial protein import: from proteomics to functional mechanisms. Nat Rev Mol Cell Biol. 2010 Sep;11(9):655-67.

Schreiner B, Westerburg H, Forné I, Imhof A, Neupert W, Mokranjac D. Role of the AAA protease Yme1 in folding of proteins in the intermembrane space of mitochondria. Mol Biol Cell. 2012 Nov;23(22):4335-46.

Scott GR, Schulte PM, Egginton S, Scott AL, Richards JG, Milsom WK. Molecular evolution of cytochrome *c* oxidase underlies high-altitude adaptation in the bar-headed goose. Mol Biol Evol. 2011 Jan;28(1):351-63.

Sharma V, Wikström M. The role of the K-channel and the active-site tyrosine in the catalytic mechanism of cytochrome *c* oxidase. Biochim Biophys Acta. 2016 Aug;1857(8):1111-1115.

Shimada S, Shinzawa-Itoh K, Baba J, Aoe S, Shimada A, Yamashita E, et al. Complex structure of cytochrome *c* - cytochrome *c* oxidase reveals a novel protein-protein interaction mode. EMBO J. 2017 Feb 1;36(3):291-300.

Shinzawa-Itoh K, Aoyama H, Muramoto K, Terada H, Kurauchi T, Tadehara Y, et al. Structures and physiological roles of 13 integral lipids of bovine heart cytochrome *c* oxidase. EMBO J. 2007 Mar 21;26(6):1713-25

Siegbahn PE, Blomberg MR. Mutations in the D-channel of cytochrome *c* oxidase causes leakage of the proton pump. FEBS Lett. 2014 Feb 14;588(4):545-8.

Sinkler CA, Kalpage H, Shay J, Lee I, Malek MH, Grossman LI, Hüttemann M. Tissue- and condition-specific isoforms of mammalian cytochrome *c* oxidase subunits: from function to human disease. Oxid Med Cell Longev. 2017;2017:1534056.

Sjöholm J, Bergstrand J, Nilsson T, Šachl R, Ballmoos CV, Widengren J., Brzezinski P. The lateral distance between a proton pump and ATP synthase determines the ATP-synthesis rate. Sci Rep. 2017 Jun 7;7(1):2926.

Somerville GA, Proctor RA. Cultivation conditions and the diffusion of oxygen into culture media: the rationale for the flask-to-medium ratio in microbiology. BMC Microbiol. 2013 Jan 16;13:9.

Song DH, Park J, Maurer LL, Lu W, Philbert MA, Sastry AM. Biophysical significance of the inner mitochondrial membrane structure on the electrochemical potential of mitochondria. Phys Rev E Stat Nonlin Soft Matter Phys. 2013 Dec;88(6):062723.

Soto IC, Fontanesi F, Liu J, Barrientos A. Biogenesis and assembly of eukaryotic cytochrome *c* oxidase catalytic core. Biochim Biophys Acta. 2012 Jun;1817(6):883-97.

Soubannier V, Vaillier J, Paumard P, Coulary B, Schaeffer J, Velours J. In the absence of the first membrane-spanning segment of subunit 4(b), the yeast ATP synthase is functional but does not dimerize or oligomerize. J Biol Chem. 2002 Mar 22; 277 (12):10739-45.

Sousa FL, Alves RJ, Ribeiro MA, Pereira-Leal JB, Teixeira M, Pereira MM. The superfamily of heme-copper oxygen reductases: types and evolutionary considerations. Biochim Biophys Acta. 2012 Apr;1817(4):629-37.

Stefano GB, Kream RM. Glycolytic coupling to mitochondrial energy production ensures survival in an oxygen rich environment. Med Sci Monit. 2016 Jul 20;22:2571-5.

Strogolova V, Furness A, Robb-McGrath M, Garlich J, Stuart RA. Rcf1 and Rcf2, members of the hypoxia-induced gene 1 protein family, are critical components of the mitochondrial cytochrome *bc*1-cytochrome *c* oxidase supercomplex. Mol Cell Biol. 2012 Apr;32(8):1363-73

Su CH, McStay GP, Tzagoloff A. Assembly of the rotor component of yeast mitochondrial ATP synthase is enhanced when Atp9p is supplied by Atp9p-Cox6p complexes. J Biol Chem. 2014 Nov 7;289(45):31605-16.

Su CH, McStay GP, Tzagoloff A. The Cox3p assembly module of yeast cytochrome oxidase. Mol Biol Cell. 2014 Apr;25(7):965-76.

Symersky J, Osowski D, Walters DE, Mueller DM. Oligomycin frames a common drug-binding site in the ATP synthase. Proc Natl Acad Sci U S A. 2012 Aug 8;109(35):13961-5.

Szeto HH, Liu S. Cardiolipin-targeted peptides rejuvenate mitochondrial function, remodel mitochondria, and promote tissue regeneration during aging. Arch Biochem Biophys. 2018 Oct 23;660:137-148.

Szeto HH, Schiller PW. Novel therapies targeting inner mitochondrial membrane--from discovery to clinical development. Pharm Res. 2011 Nov;28(11):2669-79.

Thompson DA, Ferguson-Miller S. Lipid and subunit III depleted cytochrome *c* oxidase purified by horse cytochrome *c* affinity chromatography in lauryl maltoside. Biochemistry. 1983 Jun 21;22(13):3178-87.

Tzagoloff A, Akai A, Needleman RB. Assembly of the mitochondrial membrane system. Characterization of nuclear mutants of *Saccharomyces cerevisiae* with defects in mitochondrial ATPase and respiratory enzymes. J Biol Chem. 1975 Oct 25;250(20):8228-35. PubMed PMID: 170284.

Unger AK, Geimer S, Harner M, Neupert W, Westermann B. Analysis of Yeast Mitochondria by Electron Microscopy. Methods Mol Biol. 2017;1567:293-314.

van der Laan M, Horvath SE, Pfanner N. Mitochondrial contact site and cristae organizing system. Curr Opin Cell Biol. 2016 Aug;41:33-42.

Varanasi L, Hosler JP. Subunit III-depleted cytochrome *c* oxidase provides insight into the process of proton uptake by proteins. Biochim Biophys Acta. 2012 Apr;1817(4):545-51.

Villani G, Greco M, Papa S, Attardi G. Low reserve of cytochrome *c* oxidase capacity in vivo in the respiratory chain of a variety of human cell types. J Biol Chem. 1998 Nov 27;273(48):31829-36.

Vowinckel J, Hartl J, Butler R, Ralser M. MitoLoc: A method for the simultaneous quantification of mitochondrial network morphology and membrane potential in single cells. Mitochondrion. 2015 Sep;24:77-86.

Vukotic M, Oeljeklaus S, Wiese S, Vögtle FN, Meisinger C, Meyer HE, et al. Rcf1 mediates cytochrome oxidase assembly and respirasome formation, revealing heterogeneity of the enzyme complex. Cell Metab. 2012 Mar 7;15(3):336-47

Wang J, Cao Y, Chen Y, Chen Y, Gardner P, Steiner DF. Pancreatic beta cells lack a low glucose and O2-inducible mitochondrial protein that augments cell survival. Proc Natl Acad Sci U S A. 2006 Jul 11;103(28):10636-41.

Wang Y, Singh U, Mueller DM. Mitochondrial genome integrity mutations uncouple the yeast *Saccharomyces cerevisiae* ATP synthase. J Biol Chem. 2007 Mar 16;282(11):8228-36.

Waterland RA, Basu A, Chance B, Poyton RO. The isoforms of yeast cytochrome *c* oxidase subunit V alter the in vivo kinetic properties of the holoenzyme. J Biol Chem. 1991 Mar 5;266(7):4180-6.

Wikstrom MK. Proton pump coupled to cytochrome *c* oxidase in mitochondria. Nature. 1977 Mar 17;266(5599):271-3.

Wikström M, Sharma V, Kaila VR, Hosler JP, Hummer G. New perspectives on proton pumping in cellular respiration. Chem Rev. 2015 Mar 11;115(5):2196-221.

Xia D, Esser L, Tang WK, Zhou F, Zhou Y, Yu L, Yu CA. Structural analysis of cytochrome *bc*1 complexes: implications to the mechanism of function. Biochim Biophys Acta. 2013 Nov-Dec;1827(11-12):1278-94.

Xu Y, Phoon CK, Berno B, D'Souza K, Hoedt E, Zhang G, et al. Loss of protein association causes cardiolipin degradation in Barth syndrome. Nat Chem Biol 2016; 12, 641–647

Yagi T, Seo BB, Nakamaru-Ogiso E, Marella M, Barber-Singh J, Yamashita T, et al. Can a single subunit yeast NADH dehydrogenase (Ndi1) remedy diseases caused by respiratory complex I defects? Rejuvenation Res. 2006 Summer;9(2):191-7.

Zaman S, Lippman SI, Zhao X, Broach JR. How *Saccharomyces* responds to nutrients. Annu Rev Genet. 2008;42:27-81.

Zhang X, Degenstein L, Cao Y, Stein J, Osei K, Wang J. β-Cells with relative low HIMP1 overexpression levels in a transgenic mouse line enhance basal insulin production and hypoxia/hypoglycemia tolerance. PLoS One. 2012;7(3):e34126.

Zhong Q, Gohil VM, Ma L, Greenberg ML. Absence of cardiolipin results in temperature sensitivity, respiratory defects, and mitochondrial DNA instability independent of pet56. J Biol Chem. 2004 Jul 30;279(31):32294-300

Zhou W, Faraldo-Gómez JD. Membrane plasticity facilitates recognition of the inhibitor oligomycin by the mitochondrial ATP synthase rotor. Biochim Biophys Acta Bioenerg. 2018 Sep;1859(9):789-796.

Zhou S, Pettersson P, Brzezinski P, Ädelroth P, Mäler L. NMR study of Rcf2 reveals an unusual dimeric topology in detergent micelles. Chembiochem. 2018 Mar 2;19(5):444-447.

Zhou S, Pettersson P, Huang J, Sjöholm J, Sjöstrand D, Pomès R, et al. Solution NMR structure of yeast Rcf1, a protein involved in respiratory supercomplex formation. Proc Natl Acad Sci U S A. 2018 Mar 5.

Ziello JE, Jovin IS, Huang Y. Hypoxia-Inducible Factor (HIF)-1 regulatory pathway and its potential for therapeutic intervention in malignancy and ischemia. Yale J Biol Med 2007 Jun; 80(2): 51-60.